Spectroscopic investigations of a luminescent conjugated polymer

Frank Feller

Abstract

This work presents experimental results and comprehensive analysis of the first electroabsorption and photocurrent measurements on the conjugated polymer poly(2,5-pyridinediyl) (PPY). In the electroabsorption experiment the change of the UV/vis absorption spectrum of disordered (spin-cast) and oriented (stretched), 100 nm thin PPY films due to the presence of a strong electric field was measured. The spectra were successfully fitted to a linear combination of the linear absorption spectrum and its first and second derivative. From the analysis of the obtained linear coefficients it is concluded that the electroabsorption spectrum is dominated by a Stark-red-shift of the first allowed optical transition at 3.2 eV and by the emergence of a normally one-photon forbidden $2A_g$ state at 3.7 eV. In addition polarised electroabsorption spectroscopy on oriented films and on films in sandwich configuration have been used to investigate the alignment of the polymer chains and the directions of the relevant transition dipole moments in PPY. The photoconductivity measurements have been carried out on thin films of PPY in the sandwich configuration of the structure ITO/PPY/semitransparent metal. Photocurrent spectra have been recorded using the four possible directions of the applied electric field and illumination directions and the dependence on temperature, film thickness and applied electric field has been investigated. The combined analysis of the experimental results shows that the photocurrent originates from the dissociation of excitons, which are photogenerated inside the polymer near the negative electrode. Finally evidence is given for the electron transporting, semiconducting properties of PPY and the photocurrent-voltage-characteristic have been successfully modelled with an Onsager-theory yielding an apparent exciton binding energy of 0.14 eV. All results of the work are compared and contrasted with those reported for other conjugated polymers.

Spectroscopic Investigations of a Luminescent Conjugated Polymer

Frank Feller

A thesis submitted to the University of Durham for the degree of Master of Science by Research and Thesis

University of Durham
Department of Physics
September 1999

Contents

Figures and Tables

Declaration

All material contained in this thesis is original and is the result of my own work except where explicit reference is made. Material from work of others has been suitably indicated.

This thesis has not been submitted in whole or in part for the award of a degree at this or any other university.

1 Introduction

Organic macromolecular compounds and polymers*) form the basis of a multifarious and fast extending range of substances and our life would be unthinkable without the applications of these materials. During this century they have penetrated more and more into the classical fields of application of metals and natural materials and have replaced them or have improved their technical properties. Plastics have rapidly establish a major role in daily life and modern technology, which is mainly due to the low weight of these materials in conjunction with excellent mechanical properties and low production costs. Although plastics have been used technically for over 100 years, the existence of macromolecules as the components of these materials was shown by Staudinger in the 1920's. Since then a variety of different polymerisation procedures have been developed and a great range of materials with most varied mechanical properties have been synthesised.

In the late 1970's it was found that some polymers possess electrically conducting properties in contrast to the normally insulating behaviour of plastics. Soon it was realised that the field of application of these substances is not restricted to their mechanical properties. The combination of the electrical and optical properties of semiconductors with the advantages of polymers promised the start of a new generation of materials that create new technological perspectives. While initial conductive polymers where highly unstable and very difficult to process, increasing knowledge in macromolecular chemistry allowed the synthesis of soluble and more stable derivatives. Today doped polymers can be processed, which exhibit conductivity in the region of copper and there are indications that this value can even be exceeded. Many polymers are not a priori conductive but show semiconductive properties. As in inorganic semiconductors, the supply of energy is necessary to generate mobile charge carriers. As a result, diode-like current-voltage behaviour, photoconductivity and photoluminescence are experimentally found in polymer films having similarities with inorganic semiconducting materials. It was recognised from systematic experimental and theoretical work that the quality of the electrical and

*) greek : polymer = composed of many parts

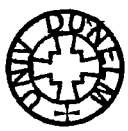

optical properties is strongly correlated to the intrinsic order in the polymer. For example, it was found that aligned polymers show far better conductivity in the direction of the polymer chain, indicating that charge carriers are able to move freely along the chain with apparently little cost of energy. On the other hand, movement in the direction perpendicular to the polymer axis was rather restricted. Through further progress in macromolecular chemistry the one-dimensional electrical and optical behaviour of certain polymers could be explained by the formation of spatially extended, band-like molecular orbitals along the polymer chain. The merging of the molecular orbitals of the single repeat units to form such bands gave rise for the term 'conjugated polymers'. Within the conjugated bands of these polymers charge carriers are considered to be delocalised enabling facile charge transport and large dipole moments in the chain direction, which are responsible for their interesting properties.

A further milestone in the history of conjugated polymer was the discovery of electroluminescence in 1990 and the fabrication of the first light emitting diode with a polymer as the active layer[1]. Since this discovery more and more research has been focused in the field of polymer LED's (PLED's) to improve their efficiency, stability and simplicity of production. The commercial interest in PLED's is due to the possibility to produce devices with very different physical properties. A working PLED can be processed with a thickness of less than two millimetres over a large area, can be bent and flexible.[2] With an applied voltage of a few volts they reach a high brightness, creating a market for all kinds of displays. Today 55 companies are involved in the development and production of PLED applications and the first fast high-resolution displays using conjugated polymers have been produced.

The aim of this work can be summarised in two points: First, electroabsorption and photocurrent measurement have been carried out on the conjugated polymer poly(2,5-pyridinediyl) and the analysis of the results has been used to obtain further insight into the nature of optical excitations in this material. Second, the established models for excitations in conjugated polymers are confronted with the results of PPY providing further arguments for or against their validity. Chapter 2 gives a brief introduction into the relevant models for the description of conjugated polymers in

general and for their electroabsorption and photocurrent response. Chapter 3 describes the fabrication of samples, explains the experimental apparatus and provides information about the measurement processes. In chapter 4 the experimental results are presented and analysed using appropriate models. The information and values obtained are discussed and compared with results of other conjugated polymers. Finally, chapter 5 summarises the work and puts the results together to form a picture of the optical excitations in PPY. In addition some suggestions for future work are given.

2 Optical Spectroscopy of Conjugated Polymers

2.1 Definition of Conjugated Polymers

The basic component of organic molecules and polymers is the carbon atom. An isolated carbon atom possess' completely filled 1s and 2s atomic orbitals and two electrons in the 2p orbital. Since 2s states and 2p states are energetically similar the orbitals are likely to hybridise when establishing chemical bonds. In unsaturated carbon compounds three of the four valence electrons of each carbon atom are accommodated in three half filled sp^2 hybrid orbitals. The sp^2 orbitals all lie in the same plane and the overlap with the orbitals of neighbouring atoms forms strong σ-bonds and determines the geometry of the molecule. The fourth electron resides in a p_z orbital, which sticks out perpendicular to the plane of the sp^2 hybrid orbitals. In an unsaturated carbon linkage the p_z-orbitals of the two carbon atoms can combine symmetrically to form bonding π-orbitals or anti-symmetrically to form antibonding, π^*-orbitals. If the molecules consist of more than one unsaturated linkages under certain conditions all π- or π^*-bonds can conjugate (overlap) to create band-like extended π- or π^*-orbitals lying above and below the plane of the molecule. One condition for the conjugation to occur is that the carbon atoms, which possess the unsaturated p_z orbitals are arranged sufficiently close to each other to enable the orbitals to overlap. Atoms with saturated bonds can prevent or break the conjugation. Conjugated polymers can be understood as the periodic arrangement of the same π-conjugated repeat unit. The π-bonds of neighbouring repeat units are then able to merge and the conjugated system extends to a large band along the polymer chain. The length of this band is known as the conjugation length and typical values are in the region of 10 repeat units.[3] Electrons in π-conjugated systems are therefore no longer localised to a parent atom but are delocalised over many repeat units along the polymer chain. Since a π^*-band forms in a similar way and the initial p_z-orbitals are half filled the whole conjugated electron system can be considered to be half filled, which enables electronic transitions between unoccupied and occupied bands.

The strong σ-bonds that determines the chain structure of the polymer and the relatively weakly bound π-conjugated system in which electrons are delocalised along the chain gives conjugated polymers their pronounced anisotropic nature. Interchain coupling is small compared to intrachain coupling which supports the picture of a one-dimensional structure. For this reason the fabrication of aligned polymer films is of experimental importance to carry out measurements using polarised light or electric fields applied in a certain angle with respect to the polymer axis.

2.2 Excitations in Conjugated Polymers

The description of excitations in conjugated polymers is the centre of focus in the discussion about possible explanations of the electrical and optical behaviour. In general an excited state is formed as a result of energy transfer from an extrinsic source into the system by light absorption or by thermal or electrical excitation, for example. An electron being promoted to an excited state can either be transferred to an extrinsic component, for instance an electrode to contribute to a current, or it can decay to the ground state radiatively or non-radiatively. In the case of the radiative decay a photon is emitted, which has an energy corresponding to the energy gap between ground and excited state. Depending on whether the electron was promoted by absorption of a photon or injected by an externally applied electric field from an electrode the effect is called either photoluminescence or electroluminescence. Two models have been established to allow a quantitative description of the excited states in conjugated polymers. The models both use elements of the well-studied physics of inorganic semiconductors. Despite being contrary in many fundamental aspects, both models are able to explain the basic experimental findings in conjugated polymers.

2.2.1 The semiconductor band model

Conjugated polymers show a number of similarities with inorganic semiconductors. Both materials consist of a periodic arrangement of a certain structure or entity. While in inorganic semiconductors this order is maintained in all three dimensions, which leads to the approximately isotropic electrical properties of a 3-D lattice, in conjugated polymers electronic coupling between neighbouring chains is weak and a 1-D lattice with highly anisotropic properties is formed. In addition, their electrical and optical properties suggest a band like energy structure in those organic materials. Hence a description of conjugated polymers in terms of a conventional semiconductor band model, which takes into account a one-dimensional structure, appears sensible. Such a theory was initiated by the works of Su, Schrieffer and Heeger[4] on the simplest conjugated polymer, polyacetylene $(CH)_x$.

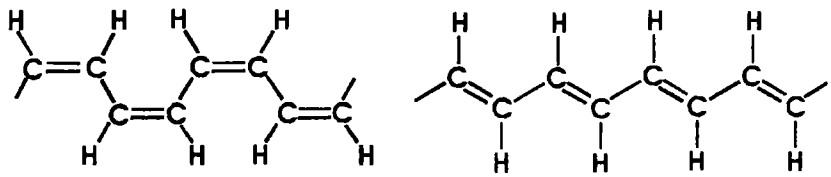

cis-polyacetylene trans-polyacetylene

Figure 2. 1 Chemical structure of polyacetylene.

Polyacetylene consists of a continuous chain of carbon atoms linked by alternating single and double bonds and occurs in two isomeric arrangements, cis-$(CH)_x$ and trans-$(CH)_x$ (Figure 2. 1). The three sp^2 hybrid orbitals of each carbon atom lie in a plane separated by 120° and form σ-bonds with the orbitals of the two neighbouring carbon atoms and the hydrogen atom. The p_z-orbital sticks out perpendicular from this plane and establishes π-bonds with the p_z-orbital of one of the two neighbouring C-atoms. Because the initial p_z-orbitals are half filled, the conjugated π-band is also expected to be half filled. However, as shown by Peierls[5] in the state of equilibrium some bonds between two carbon atoms in polyacetylene are shorter than other bonds. This deviation from the ideal structure with equal bond lengths, the Peierls distortion, increases the elastic energy of the lattice (distortion energy) but lowers the electronic energy by a greater amount. As a result the lowest

energetic state corresponds to a distorted lattice and the energy band of the π-electrons splits at the fermi-level into an occupied "valence band" and an unoccupied "conduction band".

To provide a theoretical description of the electronic structure of polyacetylene a Su-Schrieffer-Heeger-Hamiltonian was introduced. It includes two assumptions: First, only interactions between nearest neighbours are contributing (tight binding approximation) and second, no electron-electron interactions occur (free electron approximation). If u_n denotes the displacement of the n'th CH group from its equilibrium position measured along the molecular symmetry axis then the SSH-Hamiltonian is:[6]

$$H = \frac{K}{2}\sum_n (u_n - u_{n+1})^2 + \frac{M}{2}\sum_{n,s} \dot{u}_n^{\,2} - \sum_{n,s}\left[t_0 + \alpha(u_n - u_{n+1})\right]\left(c^+_{n+1,s}c_{n,s} + c^+_{n,s}c_{n+1,s}\right)$$

$c^+_{n,s}, c_{n,s}$ creation and annihilation operators of π-electrons

K spring-constant of the σ-bonds

M mass of the CH-group

t_o hopping integral for equal bond lengths

α electron-phonon coupling constant

For polyacetylene the SSH-Model predicts the co-existence of two structurally different but energetically identical phases, which means that the ground state of $(CH)_x$ is energetically degenerated. The two phases can be illustrated by an interchange of shorter double and longer single bonds (Figure 2. 2).

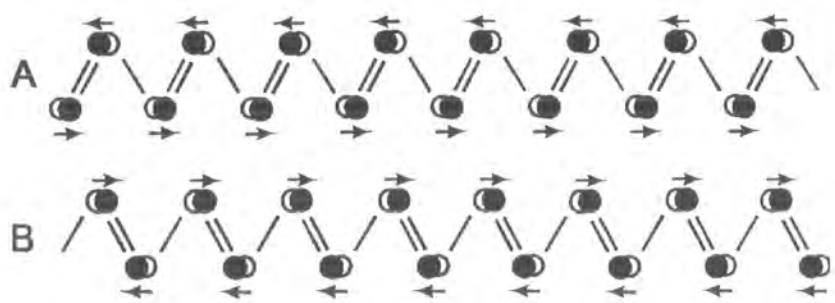

Figure 2. 2 Degenerate ground states in polyacetylene. After Ref[6]

For the excited chain the SSH-model finds certain arrangements of those two phases. If phase A and phase B occur on the same chain a bond alternation defect, or soliton, is created. These solitons are neutral. If an electron or a hole is removed they can posses either positive or negative charge. If a neutral soliton and a charged soliton occur on the same chain they attract and form positive or negative polarons. On the other hand, a pair of equally charged solitons gives rise to positive or negative bipolarons. Therefore polarons and bipolarons can be understood as spatially confined structural lattice distortions, which are able to move along the chain with little or no cost of energy (Figure 2. 3).

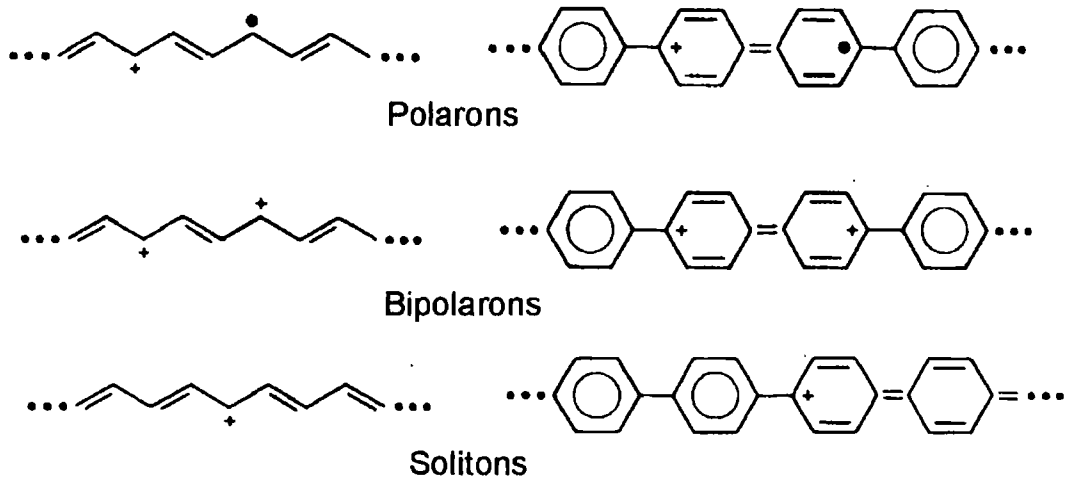

Figure 2. 3 Polarons, Bipolarons and Solitons in polyacetylene (left) and poly(p-phenylene) (right). After Ref[7].

In polymers with non-degenerated ground state solitons must be unstable because they separate two phases of different energy. Polarons and bipolarons can play an important role in polymers with nearly degenerated ground state. Poly(p-phenylene) (PPP) belongs to this group and the formation of the described topological defects is illustrated in Figure 2. 3.

2.2.2 The exciton model

Although the semiconductor band model provides conclusive explanations for many experimental findings, particularly conductivity, numerous experimental findings give rise to doubt on the validity of the assumptions on which this model is based. The exciton model respects that real polymer layers are not entirely pure and that the chains are not all perfectly aligned and rigid. Rather they contain molecular impurities and the chains are bent or twisted to a certain amount. This influences the overlap of neighbouring p_z-orbitals and leads to a breaking of the conjugated π-bands limiting the conjugation length to a few repeat units. This again means that an excited electron is no longer delocalised over the whole chain but remains under the influence of the Coulomb attraction of its correlated hole. Thus, excitation in this picture creates bound electron-hole pairs, called excitons. Depending on the distance of the electron-hole separation three types of excitons are distinguished similar to those definitions in molecular crystals: In a Frenkel exciton the electron stays in the vicinity of the hole on the same molecular unit and does not establish a permanent dipole moment. A charge transfer exciton is created when the electron (or the hole) is transferred to a neighbouring chain, which leads to a permanent dipole moment. In the extreme case of a Mott-Wannier-exciton electron and hole are separated by a distance in which Coulomb attractions are very weak The charges can move rather independently from each other and, like in Frenkel excitons, no permanent dipole moment is created.

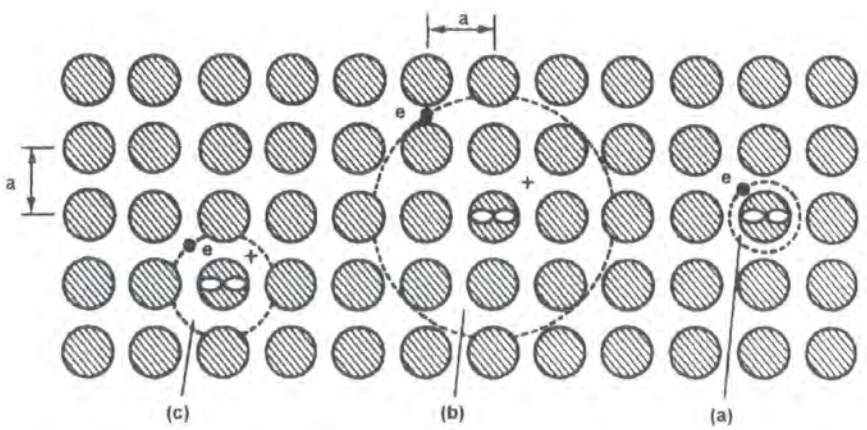

Figure 2. 4. (a) Frenkel-, (b) Mott-Wannier- and (c) Charge-transfer-excitons as defined in molecular crystals (From Ref[8]).

The energy obtained by integrating the Coulomb attractions between electron and hole from the exciton separation radius to infinity is the exciton binding energy. The determination of this energy plays a key factor in the discussion of the exciton model versus semiconductor band model. For poly(p-phenylenevinylene) (PPV), one of the best studied conjugated polymers, because of its importance in PLED's, various experimental and theoretical methods have been developed and applied and results have been reported, ranging from kT at room temperature (25 meV) up to 1 eV.[9,10,11,12,13,14,15] The values obtained have been used to argue for or against the validity of the two models. A very low exciton binding energy would imply a very high separation distance between electron and hole and would therefore support a description in the delocalised semiconductor band model. However, a remarkable number of different theoretical and experimental methods have recently agreed to a value of E_b=0.3...0.4 eV[9,11,14,15], which favours the correlated picture.

2.3 Light absorption

If light penetrates into a material that absorbs, its intensity will be reduced and at a penetration depth x its intensity becomes

$$I(x) = I(0)\exp(-\alpha x) \qquad \text{(Lambert - Beer law)},$$

with α the absorption coefficient of the material. Since α depends on the photon energy of the incident light the quantity oscillator strength is used, which is a measure of the absorption of a certain transition integrated over the spectral range:[16]

$$f = 6.25 \times 10^{-20} \cdot \int \alpha(E) dE$$

Considering the dependence of α Considering the dependence of alpha on photon energy two kinds of absorption are distinguished. First, an absorption line is obtained if the incident light gives rise to the excitation from the ground state to a certain vibrational mode of a higher energetic state. To label these states the symmetry of the molecule is considered. Most conjugated polymers posses a molecular geometry, i.e. an arrangement of the participating atoms and bonds that is

1. symmetric with respect to rotation by π around an axis perpendicular to the polymer backbone,

2. symmetric with respect to reflection at the plane in which the molecule lies and
3. symmetric with respect to inversion (point reflection) at the point where the rotation axis hits the reflection plane.

Molecules that posses these three properties are denoted to have C_{2h} symmetry[17] and their molecular orbitals fall into two groups when considering their change in sign upon the third symmetry transformations, i.e. the point inversion. Orbitals, which keep their sign - orbitals (or states) of even parity - are labeled with A_g, while B_u denotes states, which change their sign upon inversion transformation (states of odd parity). One-photon optical transitions are allowed between states of opposite parity and forbidden for states of the same parity. Then only light with a photon energy equal to this particular energy gap will be absorbed. Second, if the light excites virtually free charges, like electrons in metals, a steady absorption signal results with onset at a photon energy equal to the band gap.

As already mentioned, the disorder and imperfections in polymers lead to a distribution of the conjugation length and thus the absorption spectrum of conjugated polymers can rather be understood as an assembly of the absorption lines of every single chain. Therefore a decision whether a localised or a delocalised model is more appropriate to describe excitations in conjugated polymers can not be made only on the basis of the absorption spectrum.

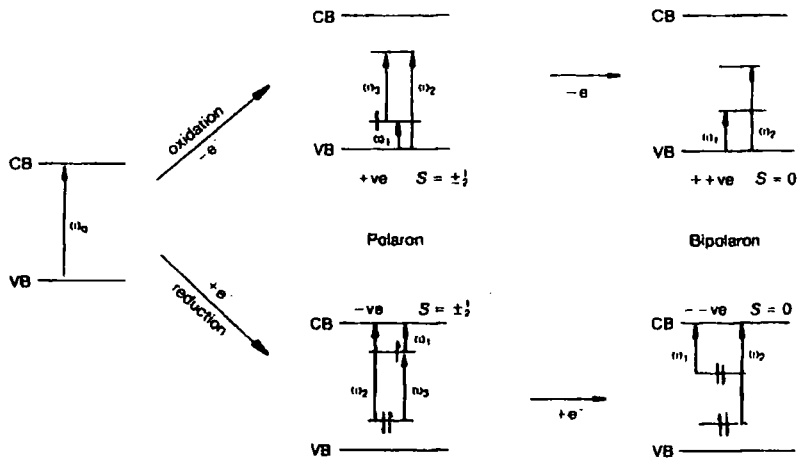

Figure 2. 5 Theoretical energy levels and allowed optical transitions in polarons and bipolarons. From Ref[18]. Experimentally the energy levels are observed to be displaced with respect to mid-gap and not all transitions are found to be allowed.

In the semiconductor band model the incident light gives rise to the formation of the mobile topological defects that are described in section 2.2.1 and to electron transitions to or from these states. As a solution of the SSH-Hamiltonian solitons are found to have an energy in the middle of the band gap. Electrons can be transferred from the ground state to a soliton state or from the (occupied) soliton state to the conduction band as long as such transition obey Pauli's exclusion principle. In polarons and bipolarons the mid-gap state splits off symmetrically allowing optical transitions as depicted in Figure 2. 5. On the other hand, in the exciton model an incident photon leads to the photogeneration of a bound electron-hole pair, an exciton. In this process the electron is initially promoted to a higher vibronic state of the exciton level and immediately starts to relax to the vibronic ground state of this level (Figure 2. 6). Such thermalised excitons can then either dissociate into independent charge carrier (with cost of energy) or undergo germinate pair recombination in a radiative or non-radiative process.

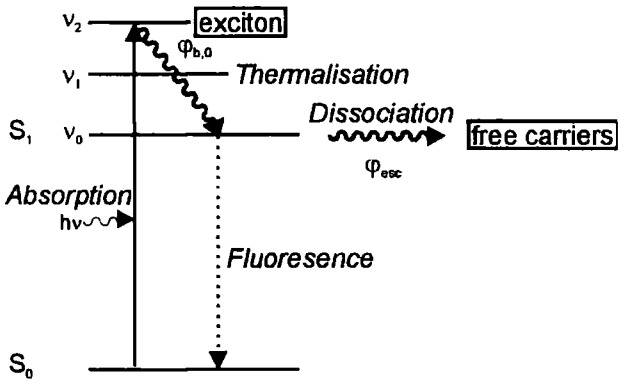

Figure 2. 6 Photogeneration, thermalisation and annihilation of excitons

The electroabsorption and photocurrent studies presented in this work, both address the process of photoexcitation. The former provides insight into the energy levels and the nature of the excited states, while the photocurrent measurements explore the photogeneration and transport mechanisms of charge carriers in the investigated polymers.

2.4 Electroabsorption

To understand the electro-optical and physical properties of conjugated polymers the determination of the energy states of the π-electron system is of great importance. In this respect electroabsorption has proved itself to be a useful tool to probe the electronic energy levels of conjugated polymers.[19,20,21,22] In an electroabsorption experiment the relative change of light absorption of a sample which is perturbed by a strong electric field is measured. There are three main effects which contribute to an electroabsorption spectrum of conjugated polymers: the Stark shift of the linear absorption signal, changes of the oscillator strengths of the participating electronic states due to a change of the selection rules for electronic transitions, which may cause the appearance of normally forbidden transitions due to the symmetry breaking effects of the applied electric field.

In an electroabsorption experiment the field induced relative change in sample transmission $\Delta T / T$ is measured, which is related to the field induced change in absorption $\Delta\alpha$ by the relationship

$$\frac{\Delta T}{T} = -d\Delta\alpha ,$$

with d the thickness of the sample. The field induced change in absorption can be understood to be the difference of the absorption of the sample, which is perturbed by the applied electric field, as compared to the absorption without an electric field applied:

$$\Delta\alpha(E) = \alpha^F(E) - \alpha(E) \qquad (2.1)$$

To achieve an expression for $\alpha^F(E)$ it is assumed that the peak-width of the transitions giving rise to the absorption band is not significantly influenced by the electric field. In this case $\alpha^F(E)$ is dominated by three effects : The Stark effect, the redistribution of oscillator strength among two neighbouring energy states and the appearance of transitions to energy states which are normal one photon forbidden. In the latter case the applied electric field breaks the symmetry of the molecular orbitals of the polymer, allowing such transitions.

The Stark effect causes an energy shift of the whole absorption band by an amount ΔE . This means that the transition energy from the ground state $1A_g$ to a given electronic state (whose absorption band is shifted) changes when applying an electric field by ΔE :

$$\Delta E = E(F) - E(0)$$

This difference is determined by the Stark effect:[23]

$$\Delta E = \Delta \mathbf{p} \cdot \mathbf{F} + \tfrac{1}{2} \mathbf{F} \cdot \Delta \tilde{\alpha} \cdot \mathbf{F} \qquad (2.2)$$

The first term describes the linear Stark effect with $\Delta \mathbf{p}$ the difference in electric dipole moment between the ground state and the exited state and usually dominates the right hand side of eq. 2. 2 when a polarised charge transfer transition occurs. In this case $\Delta \mathbf{p}$ represents the dipole moment of a polarised charge transfer exciton. The second term of eq. 2. 2 describes the non-linear Stark effect, with $\Delta \tilde{\alpha}$ a second rank tensor of the difference in polarisibility between the ground state and the exited state. In a material with randomly orientated molecules the transition dipole moments of the excited states are also randomly orientated, hence spatial average causes $\Delta \mathbf{p}$ to vanish. This is the case for Frenkel excitons, originating from the change of polarisibility in the presence of the electric field.

The redistribution of oscillator strength amongst energy states lying close to each other results in a change in the intensity of the related absorption bands. Thus the intensity of an absorption signal may be reduced when applying an electric field if there is another, forbidden transition, close to it in energy terms that becomes allowed in the presence of the field and to which therefore a certain amount of oscillator strength is shifted. According to this the field-induced change in absorption can now be written in the form:

$$\alpha^F(E) = k \cdot \alpha(E + \Delta E)$$

Using a Taylor-Expansion of $\alpha(E + \Delta E)$ up to second order of the Stark shift, and substituting in eq. 2. 1 yields

$$\Delta\alpha\ (E) = (k-1)\alpha(E) + k\Delta E \frac{d\alpha(E)}{dE} + \frac{k\Delta E^2}{2} \frac{d^2\alpha(E)}{dE^2} \qquad (2.3)$$

The electroabsorption spectrum is therefore expected to be a linear combination of the absorption describing the shift of oscillator strength to or from neighbouring states and its first and second derivative describing the Stark effect, unless a normally forbidden transition becomes allowed and contributes to the spectrum. In other words, if there is a discernible feature in the difference function of the measured field induced absorption and the fit via eq. 2. 3 then this feature can be assigned to be the absorption band of a transition to a new electronic state, formally forbidden, becoming allowed because of the symmetry breaking of the electric field. In this case, oscillator strength is shifted from the neighbouring allowed transitions towards the new transitions which means that the electric field causes a bleaching of the corresponding absorption bands indicated by a negative contribution of the absorption signal to the electroabsorption spectrum.

Therefore, to analyse the electroabsorption spectrum $\Delta\alpha(E)$ an additional accurate measurement of the absorption spectrum $\alpha(E)$ of the same film is necessary. From the curve obtained the first and second derivative can be calculated. Afterwards a least square fit calculates a linear combination of the three curves $\alpha(E)$, $d\alpha(E)/dE$ and $d^2\alpha(E)/dE^2$ that resembles the electroabsorption spectrum according to eq. 2. 3.

If the linear coefficients of eq. 2. 3 are determined by fitting to experiment the average value of the charge transfer dipole moment $\langle \Delta \mathbf{p} \rangle$ and the average over the change of components of the polarisibility tensor $\langle \Delta \ddot{\alpha} \rangle$ can be calculated using eq. 2. 2.

2.5 Photoconductivity

Photocurrent measurements have been widely used in the past to obtain information about both photogeneration[24,12] and transport mechanisms[25,26] of charge carriers, particularly to yield evidence for either the exciton model or the semiconductor band model as the most appropriate to explain the excited states and correlated phenomena in conjugated polymers. In the semiconductor band model free charge carriers are photogenerated directly via an interband transition allowing

electrons and holes to move freely and independently from each other. In contrast, in the exciton model the initial process of charge carrier generation in a photocurrent experiment is the photogeneration of a singlet exciton, a germinate electron-hole pair bound by the Coulomb attraction. In a second process the excitons have to be broken to obtain free charge carriers that can migrate in an external applied electric field to give rise to a photocurrent. This separation is aided at a heterojunction between two polymers of different carrier mobility[27] and at chemical defects, which trap electrons or holes leaving its counterpart free as mobile charge carriers[28]. However, another important source of charge carriers in real devices is the carrier injection or the carrier tunnelling from the metal electrodes into the polymer[24,29,30]. To achieve information about which of these processes contribute to the photocurrent in a certain conjugated polymer its dependence on applied electric field, temperature and incident photon energy has to be considered to form a consistent picture. In this aspect the influence of temperature on the process of charge carrier generation has been a matter of discussion. The dissociation of thermalised excitons under the influence of a external electric field is a process well described by Onsager's theory[31] that implies a characteristic field dependence and temperature activation of the photocurrent. Measurements of the temperature characteristics of the photocurrent have been carried out on relatively thick films (about 1 μm) of PPV[28] and MEH-PPV[32] showing a strong change of the photocurrent over three to four orders of magnitude. On the other hand, Moses *et al.*[33] reported measurements on thin films of MEH-PPV that show a very small temperature dependence of the photocurrent indicating that the initial process of charge carrier generation is temperature independent and that only the mobility of the free charge carriers is thermally activated. These findings were used to support the semiconductor band model. However, Albrecht, Barth and Bassler[9,34] could show that the electric field *and* temperature dependence of the photogeneration process can be explained within an exciton model, which includes structural disorder in polymers. They proposed a model that describes the photocurrent as originating from the dissociation of germinate electron hole pairs in a random hopping system under the influence of an electric field that is composed of the effective external field and the Coulomb field created by the two charges.

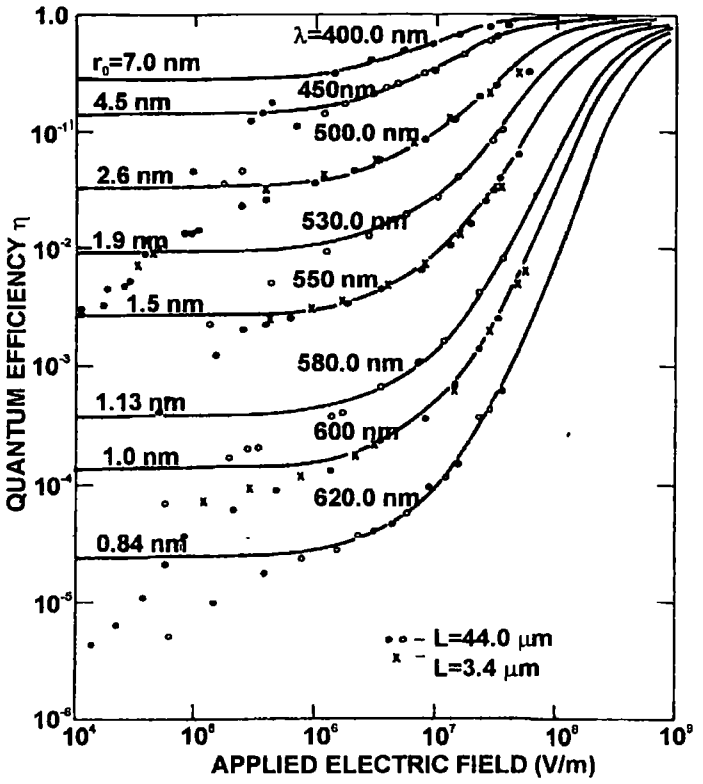

Figure 2. 7 Theoretical escape quantum yields from Onsager's theory (solid lines) and experimental data for the photoinjection of holes in amorphous selenium (symbols). From Ref[35].

Such electron hole pairs arise from thermalised excitons, which are photogenerated by the incident light. Using Monte Carlo simulation techniques, which include the structural disorder that is known to be present in conjugated polymers, the Marburg-group have successfully modelled the experimental results of photocurrent measurements on thin films. Two main results were pointed out: First, the field dependence of φ_b, the exciton dissociation yield obtained from normalising the photocurrent to the number of absorbed photons, follows the predictions of Onsager's theory. Second, disorder in conjugated polymers aids germinate pair dissociation and leads to a non-Arrhenius-like temperature dependence of φ_b. In the framework of Onsager's theory φ_b can be written as the product of the primary dissociation yield $\varphi_{b,0}$ and the quantum yield φ_{esc}, which describes the probability of the generated electron hole pair to escape germinate recombination. In the limit $T \to \infty$ the escape quantum yield is assumed to become unity, which allows the experimental determination of $\varphi_{b,0}$ via the extrapolation $\varphi_{b,0} = \varphi_b(T \to \infty)$. The field dependence of the escape quantum yield $\varphi_{esc} = \varphi_b / \varphi_{b,0}$ is then given by Onsager's theory of germinate pair dissociation using an approximation by Pai and

Enck[35]. The absolute value and the line shape of such a curve depends on the parameter r_0, the initial intra-pair distance, which corresponds to the electron-hole separation in a thermalised exciton. Therefore, using the Coulomb equation, the model allows an estimate of the exciton binding energy.

Other quantitative models have been developed or adopted from inorganic semiconductors. In a recent work, Harrison *et al.*[32] applied some of them to model the photocurrent spectrum of the conjugated polymer MEH-PPV and reports moderate fits to the experimental results. In this work the spectral dependence of the photocurrent is explained qualitatively and provides a consistent picture of the localisation of the charge generation zone, while the temperature and field dependence is analysed quantitatively in the framework of the model described above.

2.6 Poly(2,5-pyridinediyl)

2.6.1 Chemical description of PPY

The repeat unit of PPY is an aromatic carbon ring with one carbon atom being replaced by a nitrogen atom (phenzyl ring). This simple arrangement alone suggest that this polymer is of basic relevance. The p_z orbitals of the unsaturated ring carbon atoms stand perpendicular to the ring plane and establish conjugated π-bonds. The nitrogen lone pair electrons reside in an orbital, which 'sticks' out from the ring in the same plane as the polymeric chain and therefore does not contribute to the conjugated π-electron system.[36] Thus the π-electron density along the polymer chain is reduced in comparison to polyparaphenylene (PPP) making PPY more stable with respect to oxidation[37].

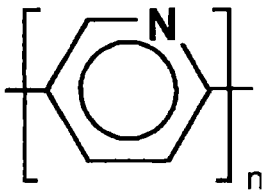

Figure 2. 8 The repeat unit of poly(2,5-pyridinediyl)

In 1994 the first chemical synthesis of PPY was reported by Yamamoto *et al.*[37] A yellow powder was produced that was soluble in formic acid allowing deposition of the polymer by simple spin casting on appropriate substrates. It was also pointed out in Yamamoto's work that the polymer chains have rigid-rod like nature. Recent X-ray powder diffraction, dynamic light scattering and ellipsometry measurements on PPY by Monkman *et al.*[38] have provided further insight into the chemical and physical structure of this material. The results indicate a relatively high degree of crystallinity and anisotropy. Bond lengths were measured and the average chain was determined to contain about 80 repeat units resulting in a total chain length of about 35 nm.

2.6.2 Characterisation and Photophysics of PPY

In the initial studies of PPY by the group of T. Yamamoto basic investigations in the optical and electronically properties included absorption and fluorescence measurements[37] showing a broad absorption band at 3.3 eV corresponding to the first allowed optical transition and weak fluorescence with maximum at about 2.3eV. From UV-photoelectron spectroscopy[39] an ionisation energy of 6.3 eV was determined. In addition, conductivity measurements of doped PPY were carried out, and n-type-conducting properties were concluded from a chemical point of view.

Shortly after this first investigations a significant contribution to the understanding of PPY were provided by the Blatchford and Epstein *et al.*[40,41,42] Among other things, the group carried out time resolved absorption and luminescence spectroscopy on PPY in solution and in thin films. In these experiments they could give strong evidence for exciton formation in PPY as the dominating excited species responsible for the optical properties. In addition, semiempirical quantum chemical calculations of four-ring oligomers of PPY were

performed by Blatchford *et al.*[42] to model the absorption spectrum and low energy polaron, bipolaron and triplet states were calculated.

Probably the most promising property of PPY is its photoluminescence. Remarkable progress has been made at the University of Durham to improve the chemical synthesis of the polymer and a quantum yield (PLQY) of 37% in the solid state has been achieved[43], while less than 10% was reported in the initial studies. Clear differences in the luminescence behaviour are found between solid state and solution: While the emission maximum of the solid PPY (e. g. when spun to a substrate) is in the green (2.2 eV) the formic acid solution emits in the blue (2.7 eV)[40] with a PLQY of only 17%.[44] The high photoluminescence quantum yield of the Durham-PPY films combined with their very high stability with respect to oxidation promises applications of this polymer for example in multi-layer light emitting diodes[45,46].

3 Experimental Techniques

3.1 Electroabsorption experiment

3.1.1 Device Fabrication

The synthesis of poly(p-pyridine-2,5-diyl) was performed by Dr. L. E. Horsburgh and the chemical procedures can be found in Ref.[43]. PPY was dissolved in formic acid using a concentration of 10 mg PPY per 1 ml formic acid. The solutions were filtered through a pipette containing a layer of glass wool followed by a layer of ultra-fine filtering sand.

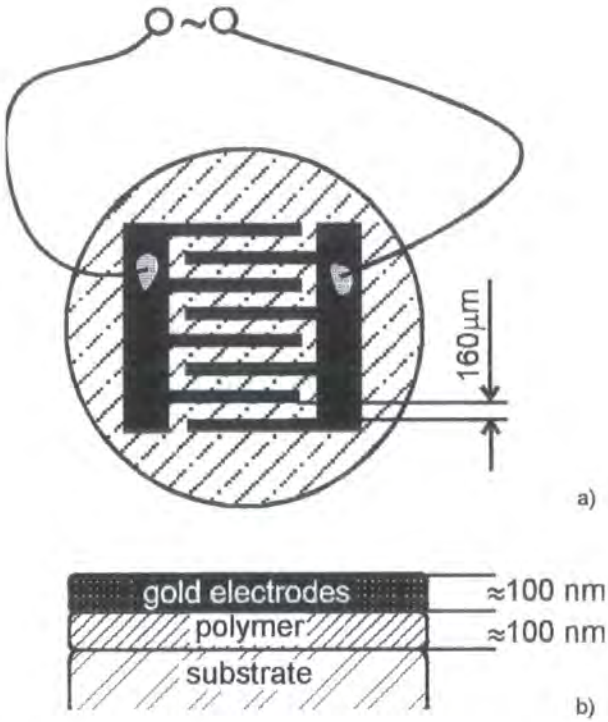

Figure 3. 1 Structure of samples used in electroabsorption measurements; a) interdigitated gold electrodes and connection, b) sample cross-section

With the filtered solutions thin films were easily spun onto suitable substrates. Sapphire discs with a diameter of 1 cm were chosen to ensure good heat conduction for low temperature measurements. Typical spinning conditions were a spin velocity of 1000 rpm for 60 seconds. This led to PPY films of about 70 nm on top of the substrate. All the formic acid is removed from the film during spinning, which means that the PPY film is not protonated[47]. Thickness measurements were carried out using

an α-step mechanical thickness meter allowing measurements with an accuracy of about 2 to 15 percent depending on the quality of the films.

In a vacuum evaporator gold electrodes were evaporated trough a shadow mask on top of the polymer film at a pressure of about 1×10^{-5} mbar. The ≈100 nm thick interdigitated electrode layer has an electrode spacing of 160 um (Figure 3. 1) and allows the application of electric fields up to 65 kV/cm. Connections to the electric circuit were established using thin copper wires (50 μm) attached to the electrodes by conducting silver paint as demonstrated in Figure 3. 1 a. Samples were then placed into a closed loop helium cryostat, so the sample could be held under vacuum and at temperatures down to 10 K during the measurements. Special care was taken to ensure good heat-conducting connections between the sapphire substrate and the copper sample holder of the cryostat.

3.1.2 Experimental Set-up

For electroabsorption measurements an experimental set-up arranged by S. Pomfret[48] was used and extended appropriately (Figure 3. 2).

A 150 W Xe-arc lamp was chosen to provide light in the visible and UV region from 2.5 eV to about 5 eV. The light was monochromated by a grating monochromator consisting of two gratings and appropriate filters to cut off second order light. An adjustable entrance slit, controlled by computer, always kept the amount of light hitting the sample within the desired region to avoid saturation of the silicon photo detector. After passing the monochromator the beam was focused by a quartz lens to bring it to the appropriate size on the sample. Behind the sample another quartz lens focused the transmitted light onto the silicon photo detector. Care was taken to ensure that the detector collects all light that is transmitted through the active sample area. The high voltage electric field was supplied by a Trek 10/10 amplifier which amplifies the sinusoidal output signal (f=173 Hz) of the internal oscillator of a lock-in amplifier. Bearing in mind the magnitude of the sample layers the application of voltages up to 1000 V needs special care to achieve stable results.

Therefore low temperatures and good vacuum is necessary before the voltage can be tuned very slowly to such high values.

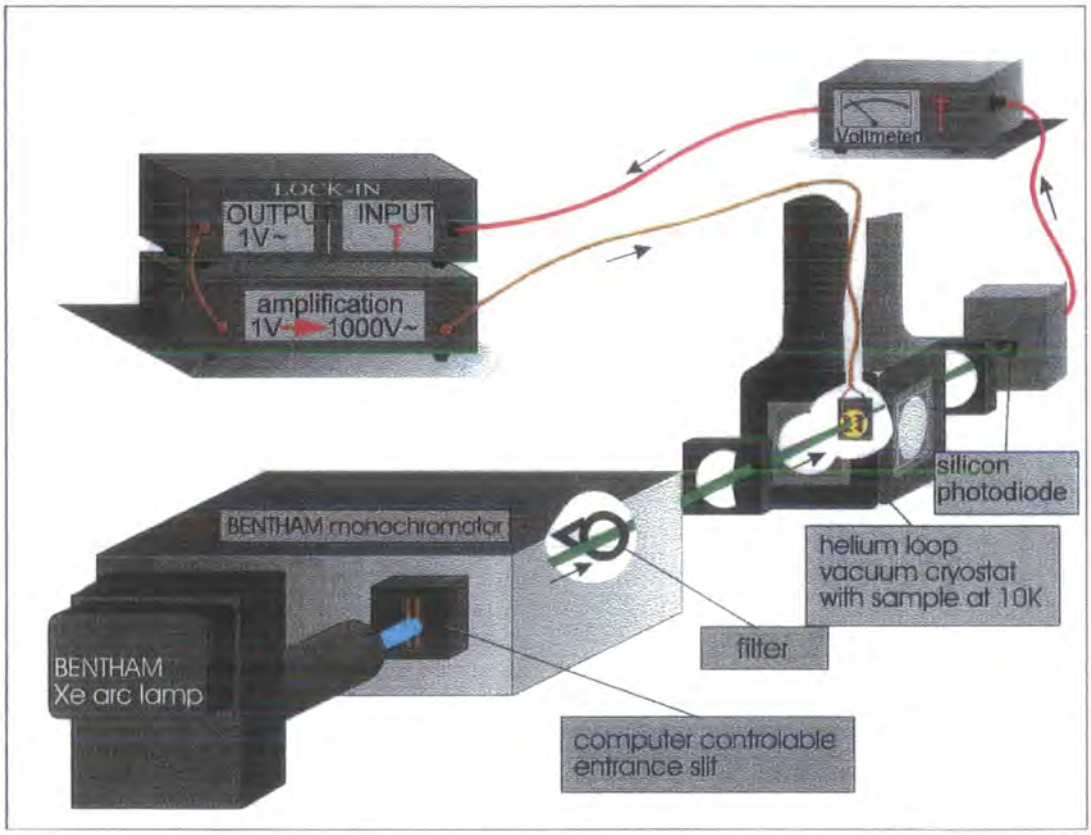

Figure 3. 2 Experimental set-up for electroabsorption measurements. The brown cable contains two wires and applies the high voltage to the sample, the red cable transmits the signal of the photodetector to the lock-in measurement unit.

The digital lock-in amplifier also measures the signal detected by the photodiode with a frequency of 2f. Thereby the field induced change in sample transmission, ΔT, is obtained, while the linear transmission of the unperturbed sample T is recorded by a digital voltmeter simultaneously. In this way the energy dispersion of $\Delta T / T$ can be obtained.

The measurement of the electroabsorption spectrum was controlled by PC. Typical spectra were taken in photon energy steps of 0.005 eV with a lock-in time constant of 2 seconds. An initial delay of 10 seconds after each step of the monochromator was introduced to allow the system to settle down. In addition, a

dark laboratory environment as well as stabilised electric power supply and judicious choice of arc lamp was used to reduce noise.

3.2 Photocurrent experiment

3.2.1 Device Fabrication

For the production and filtering of PPY solutions see section 3.1.1 ÜBER. Different concentrations and spinning conditions were used to produce films of thickness ranging from 50 to 250 nm as determined with an α-step thickness meter. Films were spun onto indium-tin-oxide coated glass substrates (ITO-glass) with the ITO-layer partly etched as shown in Figure 3. 3 to allow the deposition of overlapping metal electrodes as typically used for fabrication of polymer light emitting diodes. In a vacuum evaporator, 25 nm thick semitransparent metal electrodes of about 2 mm^2 were evaporated on top of the film.

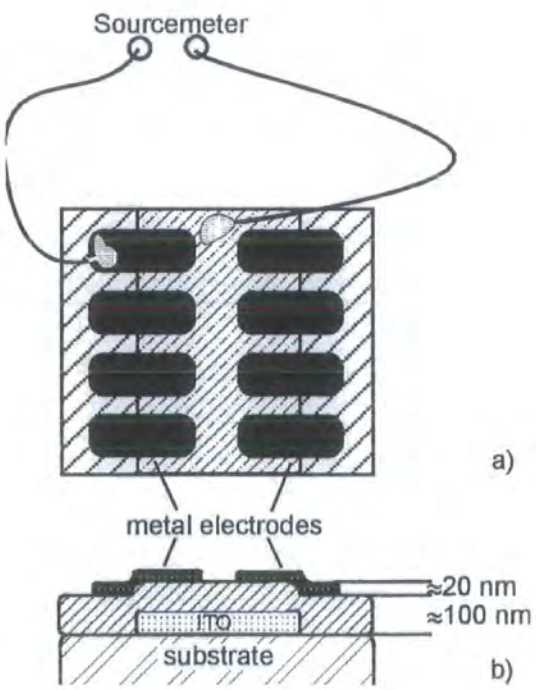

Figure 3. 3 Structure of samples used in photocurrent measurements; a) semitransparent metal electrodes and connection, b) sample cross-section; Structure and preparation equal those of typical organic devices.

For the photocurrent spectra gold was used as electrode material, which showed high transparency combined with good conductive properties, while the field dependence was measured using aluminium contacts to ensure the stability of the devices in the region of higher applied fields. To connect to the electric circuit thin copper wires were attached to the electrodes using conductive silver paint.

3.2.2 Experimental Set-up

The samples were mounted into a closed loop helium cryostat to hold it under vacuum and at constant temperatures, as low as 10K during the measurement.

Samples were illuminated by an ultra quiet 150 W Xe-arc lamp, which was passed through a monochromator equipped with two gratings and appropriate order sorting filters allow measurements over the spectral range 1 eV – 5 eV. A lens focused the beam in order to achieve optimal illumination of the sample. A bias was applied by a Keithley 2400 source-meter, which simultaneously measured the current across the sample. During spectral acquisition the monochromator was stepped to each wavelength and the system then waited several seconds for the photocurrent to settle down, then 10 readings were taken and averaged to reduce noise. The whole procedure to take the spectrum was controlled by PC. To correct the spectra for a constant incident photon flux a spectrum was taken using a calibrated photodiode placed at the position of the sample (including an ITO-coated window in front of the diode to correct the spectra taken under illumination through ITO).

4 Results and Discussion

4.1 Electroabsorption Measurements on Spin-cast PPY

In order to test the experimental set-up and to gain experience in the acquisition of the electroabsorption measurements the EA spectrum of MEH-PPV was recorded and the result is depicted in Figure 4. 1 (inset shows the repeat unit of MEH-PPV).

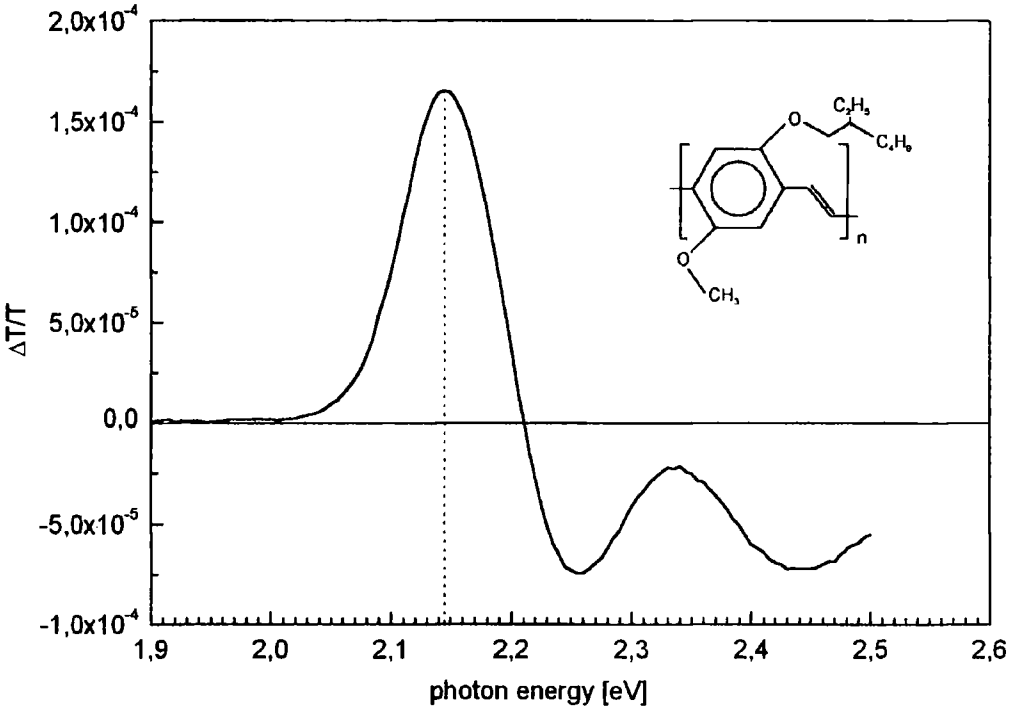

Figure 4. 1 Electroabsorption spectrum of MEH-PPV. The inset shows the repeat unit of the polymer.

Line shape and peak position of the curve as well as the magnitude of the signal is in good agreement with results reported in literature.[49,50] Since MEH-PPV is a soluble and therefore easy to process derivative of PPV the electroabsorption spectrum of this polymer is thoroughly studied.[49,51,52]

4.1.1 Spectral Dependence

The absorption spectrum of PPY was measured in the range from 2 eV to 6.7 eV using a Lambda 19 double beam absorption spectrometer. The sample was placed in the helium cryostat, which was mounted in the spectrometer to allow the measurement of absorption under the same conditions as the electroabsorption spectrum was taken, i. e. at 10 K and in vacuum. Figure 4. 2 shows the obtained linear absorption spectra consisting of two main features one at 3.2 eV and the other at 6.3 eV, which are assigned to the transitions $1A_g \rightarrow 1B_u$ and either $1A_g \rightarrow mB_u$ or a localised transition on the pyridine moiety, respectively.

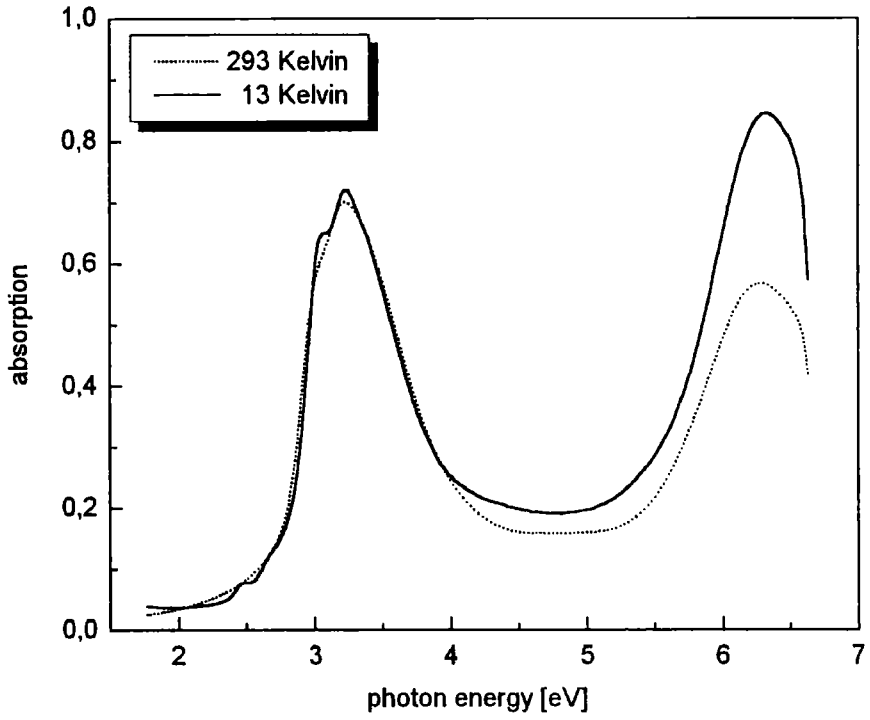

Figure 4. 2 Absorption spectrum of PPY under vacuum at room temperature (dotted line) and at 10 K (solid line)

Two shoulders can be clearly identified on both sides of the low energy peak, which become less resolved at room temperature. These have been ascribed to vibronic components.[36] As expected from a rigid-rod polymer, apart from the sharpening of the vibronics no considerable changes in the absorption spectrum could

be found when cooling down the sample. The high-energy peak is not within the energy range of the electroabsorption spectrometer, and so is not considered further.

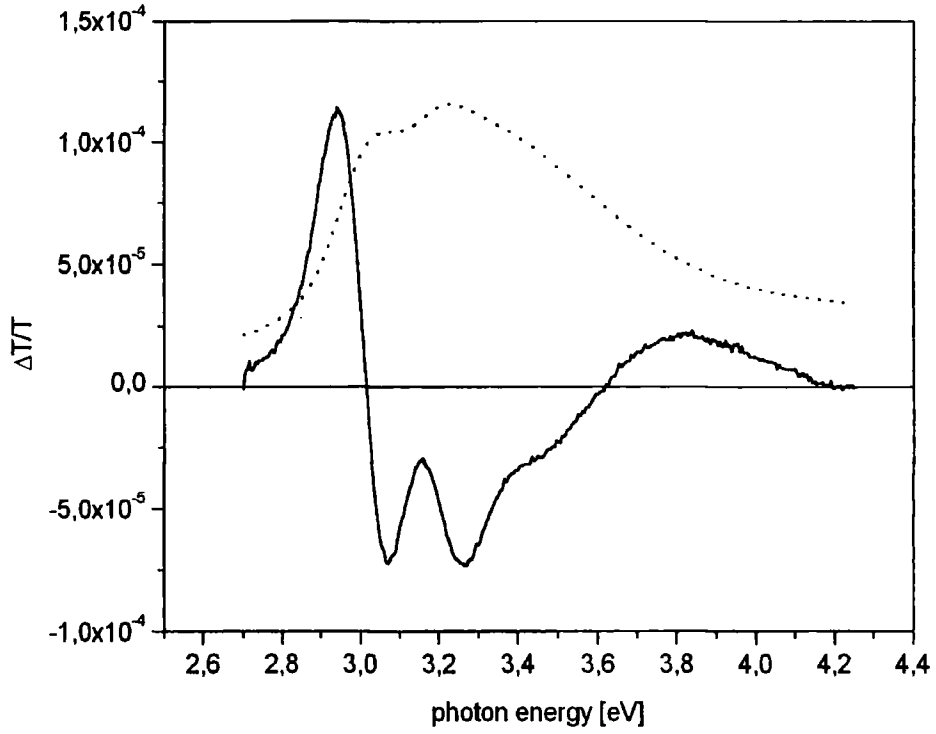

Figure 4. 3 Electroabsorption spectrum (solid line) and absorption spectrum (dotted line) of spin cast PPY at an applied electric field of 63 kV/cm.

Figure 4. 3 shows the electroabsorption spectrum of PPY measured in the energy range from 2.7 eV to 4.3 eV. The spectrum is dominated by the double feature peaking at 2.94 eV and 3.07 eV, respectively, followed by another negative peak at 3.26 eV. After passing the zero line at 3.62 eV a third clearly resolvable positive feature is seen, peaked at 3.82 eV. For comparison the low temperature absorption spectrum is shown as well.

4.1.2 Voltage Dependence

The electroabsorption spectrum of PPY was measured using various values of the applied electric field and results are depicted in Figure 4. 4. All features show increasing absolute values of $\Delta T / T$ with increasing electric field.

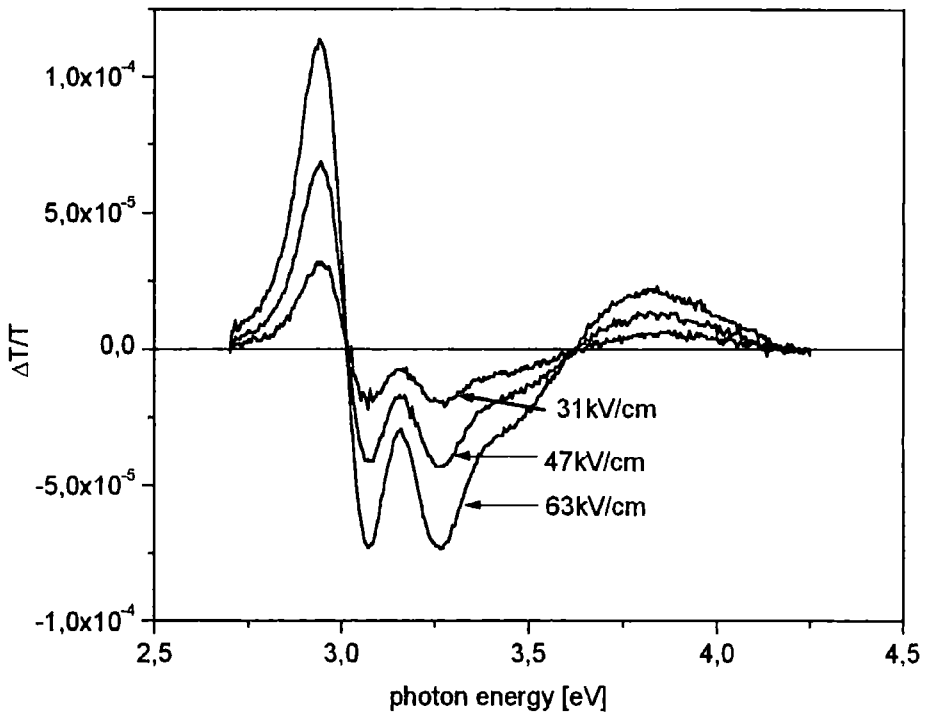

Figure 4. 4 Electroabsorption spectrum of spin cast PPY at various applied electric field.

Figure 4. 5 shows a plot of the absolute electroabsorption signal for the four peaks of the spectrum versus the square of the applied electric field. Straight lines are obtained for every peak, which corresponds to a quadratic voltage dependence of the EA signal confirming its field induced origin (see eq. 2. 2).

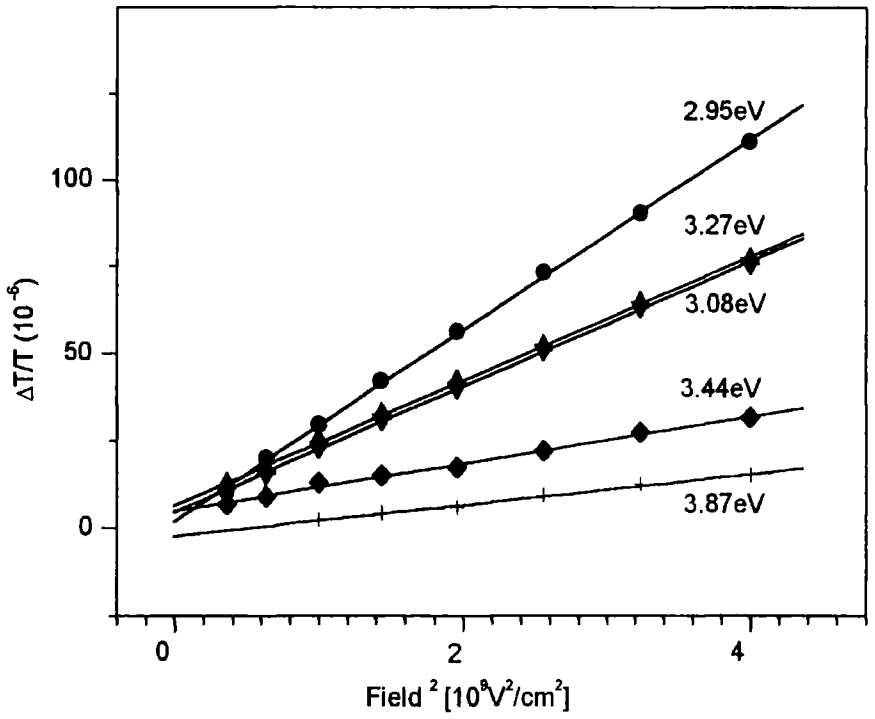

Figure 4. 5 Absolute electroabsorption signal versus the square of the applied electric field. Solid lines represent a linear fit.

4.1.3 Polarisation Dependence

In spin-cast films of rigid-rod-like polymer the chains lie parallel to the substrate surface but are randomly orientated[53] with respect to the other two directions. Therefore such films show an anisotropic absorption spectrum, i. e. the absorption coefficient is independent of the polarisation of the incident light as long as it hits the film under normal incident (perpendicular to the surface). On the other hand, if an electric field is applied in the plane of the film then the change of absorption due to this field is likely to be dependent on the angle between the applied field and the electric field vector of the light.

Figure 4. 6 shows the electroabsorption spectrum of PPY measured with the incident light being polarised parallel or perpendicular to the applied electric field.

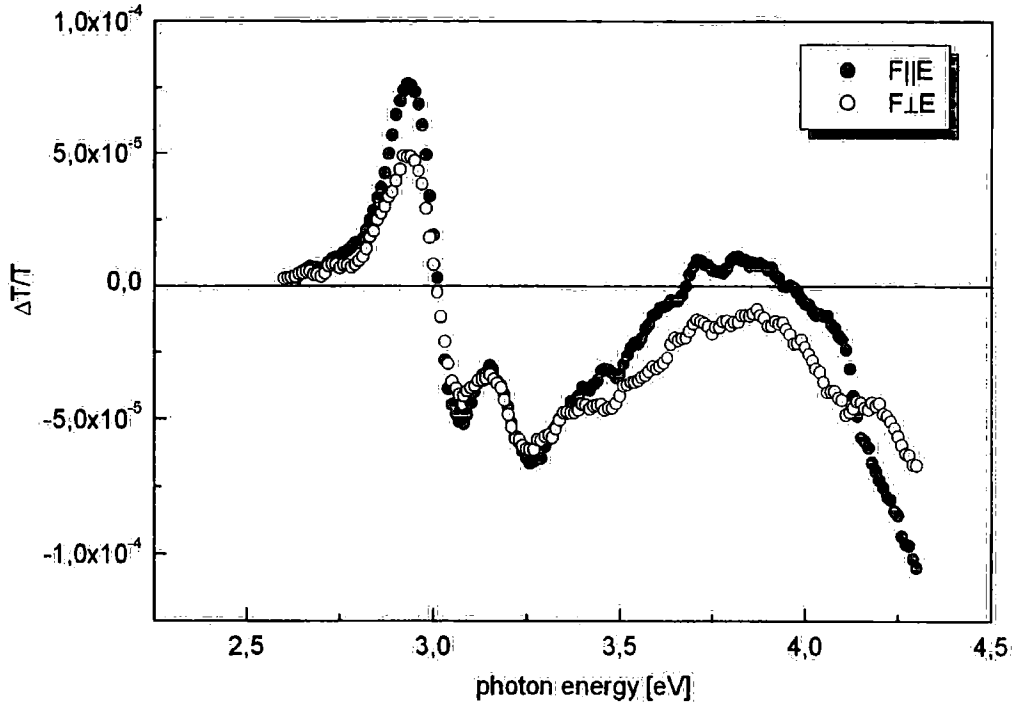

Figure 4. 6 Polarisation dependence of the electroabsorption signal in PPY. The light was polarised parallel (filled circles) or perpendicular (open circles) to the applied electric field, which was 63 kV/cm.

The main feature at 2.94 eV shows an anisotropy ratio of about 1.6, while the ratio is steadily reduced for the features at 3.07 eV and 3.26 eV. For the high-energy feature at 3.8 eV the anisotropy ratio does not follow this trend but is determined to be 2.0 (Table 4. 1).

Feature position	$\Delta\alpha(\parallel)/\Delta\alpha(\perp)$
2.94	1.6
3.07	1.3
3.26	1.1
3.66	2.0

Table 4. 1 Anisotropy ratios of the electroabsorption signal in PPY

4.1.4 Effects of Temperature and Oxygen

Electroabsorption measurements are usually performed in good vacuum and at low temperature to reduce noise. However, to investigate the influence of temperature and oxygen EA-spectra were also recorded at room temperature and in a surrounding of dried air. The room-temperature measurements were performed under high vacuum using an applied voltage of 750 V. At higher voltages the gold electrodes started to evaporate due to the lack of cooling.

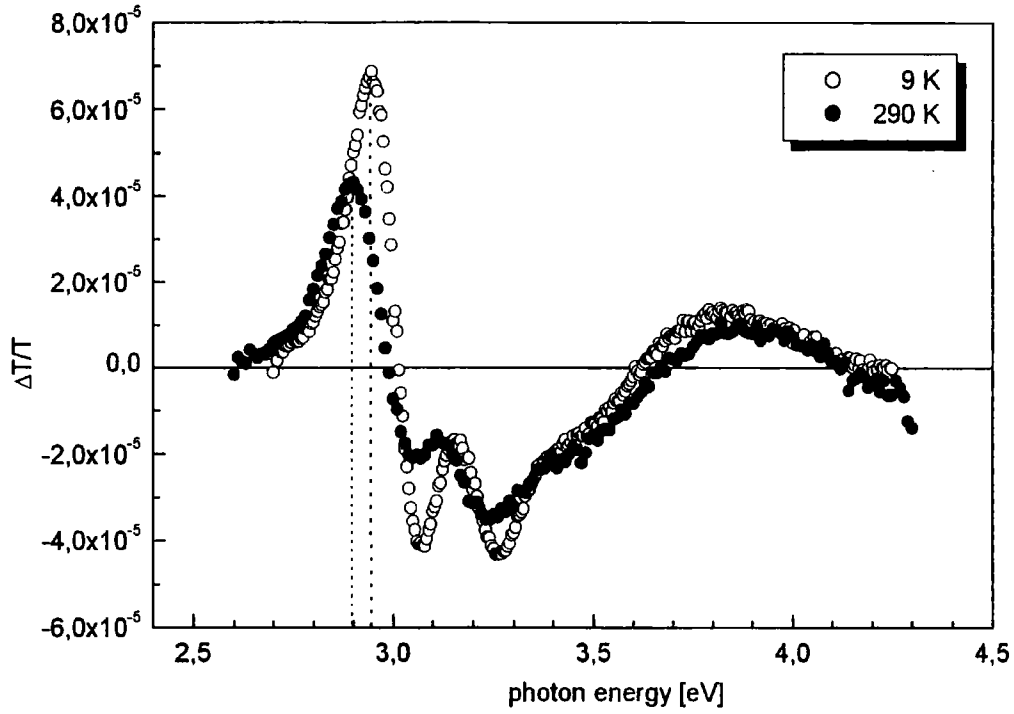

Figure 4. 7 Electroabsorption spectrum of PPY at room temperature (solid line) and at 10 K (dashed line)

Figure 4. 7 shows the EA-spectrum of a PPY film at room temperature and, for comparison, the corresponding low-temperature spectrum using the same value for the applied voltage. The magnitude of the room-temperature spectrum is smaller but the difference decreases with increasing photon energy. In addition, the low energy part of the spectrum (2.5..3.5 eV) is slightly red-shifted by about 50 meV, while the high-energy feature around 3.7 eV seems to remain constant or even blue shifted. Interestingly, the obtained spectrum is smooth and does not exhibit a significantly

higher signal-to-noise-ratio than the low-temperature spectrum. That means that measurements at low temperature do not directly reduce noise but rather they allow the application of higher electric fields, which then results in a higher electroabsorption signal with lower signal-to-noise-ratio.

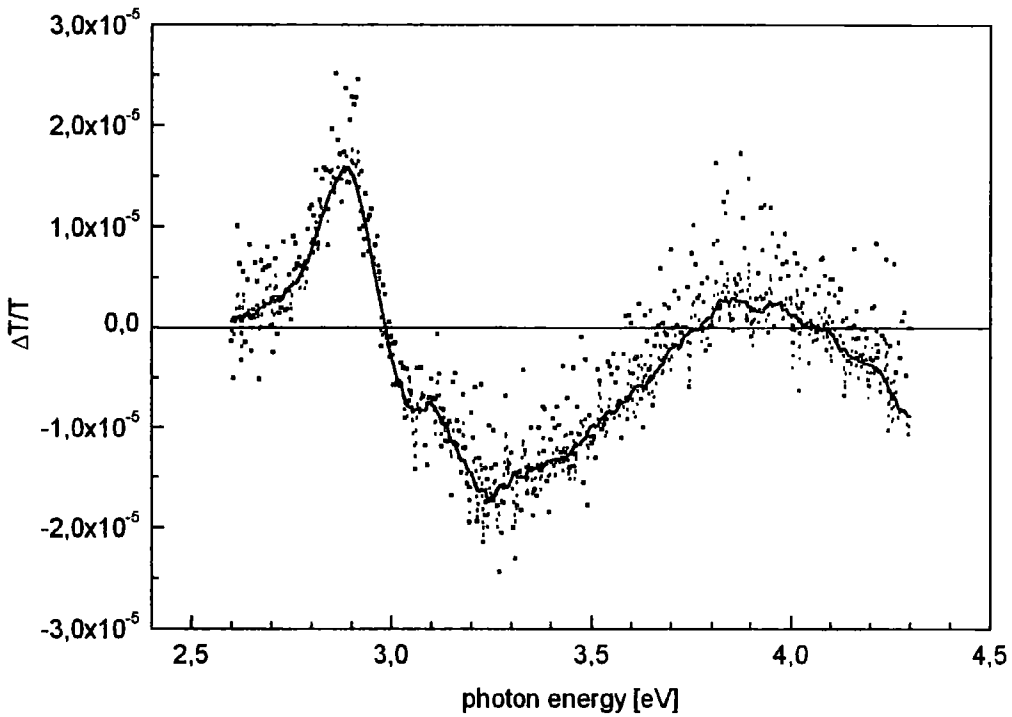

Figure 4. 8 Electroabsorption spectrum of PPY in the surrounding of dried air. Symbols are the measured data, the dotted line shows an accumulation of three spectra under same conditions and the solid line is obtained by smoothing.

The influence of air is more important in this respect. The spectrum depicted in Figure 4. 8 was recorded after the cryostat chamber was ventilated with air that was led through a liquid nitrogen-cooled copper pipe. This technique was used to reduce the amount of water in the air, which otherwise would lead to short circuit connections due to thin films of condensed water on top of the sample. Under this circumstances the maximum value for the applied voltage to ensure stable sample performance was 500 V. It can be seen in Figure 4. 8 that in dried air noise does significantly contribute to the electroabsorption signal (symbols). However, the underlying EA-spectrum is still clearly to recognise, especially after averaging over

three independent spectra recorded at different times on the same sample. This allows comparison with the corresponding low-temperature spectrum (Figure 4. 9). Similar to the behaviour under vacuum the signal drops by about half the value when increasing the temperature from 10 K to room temperature. The same small red-shift of the first three features (2.8..3.5 eV) can be seen, which is therefore likely to originate from the small temperature induced change in of the absorption band (Figure 4. 2).

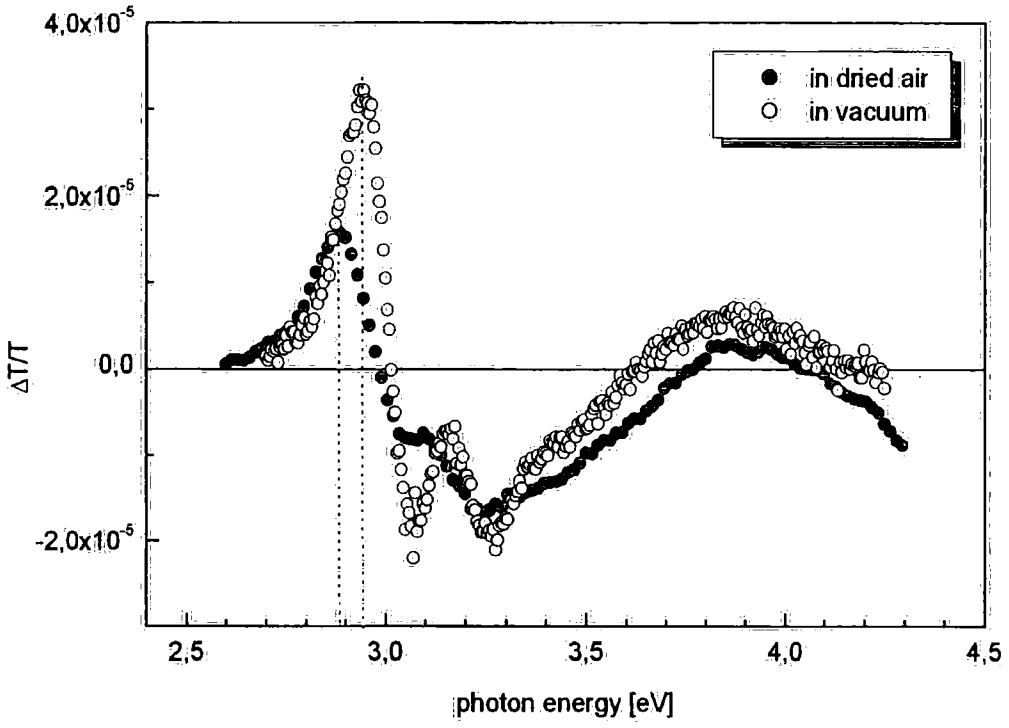

Figure 4. 9 The EA-spectrum recorded under vacuum and at low temperature is depicted as dotted line for comparison.

4.1.5 Analysis and Discussion

The spectrum is dominated by the double feature peaking at 2.94 eV and 3.07 eV, respectively, resulting from the Stark red shift of the main PPY absorption band. This arises through a change of energy of the transition from the ground state to the first excited state $1B_u$ caused by the applied electric field. Accordingly, the signal follows to good first approximation the line-shape of the first derivative of the linear absorption in this part of the EA spectrum. In the energy range from 3.0 eV to 3.5 eV the contribution of the negative absorption signal becomes significant causing the bleaching of the electroabsorption signal of the allowed transition and produces another peak at 3.26 eV. After passing the zero line at 3.62 eV a third clearly resolvable feature is seen, peaked at 3.82 eV.

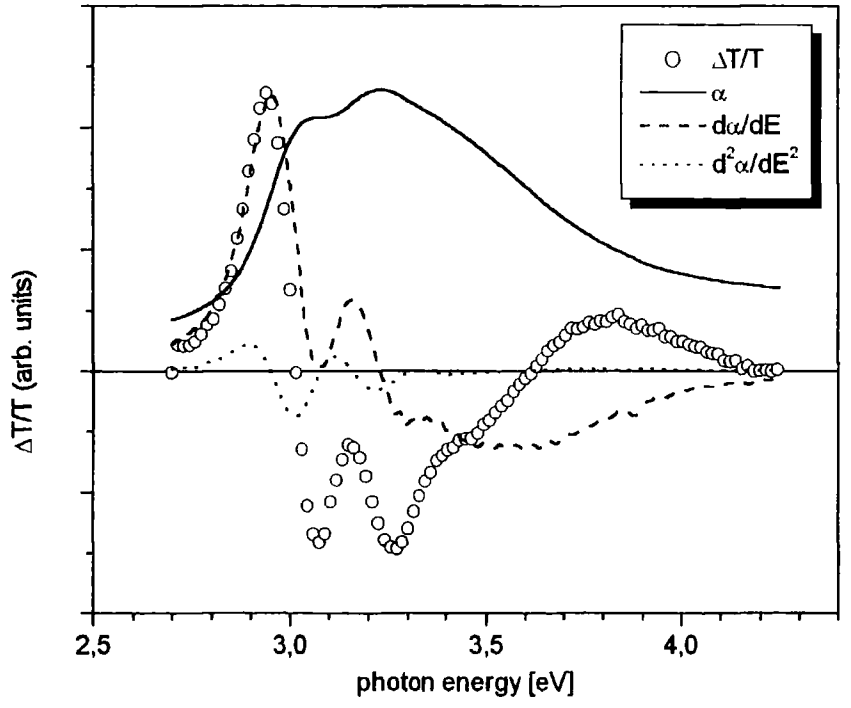

Figure 4. 10 The modelling of the electroabsorption spectrum. Absorption spectrum and its first and second derivative.

As shown in chapter 2.4 the electroabsorption spectrum can under certain circumstances be fitted to the a linear combination of the absorption spectrum (zeroth

derivative) and its first and second derivative according to eq. 2. 3. Figure 4. 10 shows these three derivatives and the experimental EA data arbitrarily scaled. Already in this plot it can be seen that the electroabsorption signal of the main peak at 2.9 eV is well described by $d\alpha/dE$. The next two features at 3.1 eV and 3.3 eV are also first-derivative-like in line-shape, but their negative magnitude is much higher. This can be understood by a negative contribution of the absorption coefficient.

A least squares fitting procedure has been used to exactly fit the spectrum to the linear combination of the absorption spectrum and its first and second derivative (eq. 2. 3). A computer program was written which calculates the three linear coefficients and fit quality parameter for given experimental data. The program allows graphical controlling of the fit and, in particular, the 'online' tuning of the spectral fitting range with simultaneous monitoring of all coefficients and parameters. This makes it possible to fit the low-energy part of the spectrum separately. For details about the program see Appendix I. The following linear coefficients were determined when taking into account the spectral range up to the high-energy feature at about 3.7 eV:

$$\begin{aligned} (k-1) &= -10.7 \cdot 10^{-5} \\ k\Delta E &= 5.10 \cdot 10^{-5}\,eV \\ \frac{k\Delta E^2}{2} &= 2.7 \cdot 10^{-7}(eV)^2 \end{aligned} \qquad (4.\ 1)$$

The model curve with the obtained linear coefficients is shown in Figure 4. 11a. An excellent fit to the electroabsorption spectrum up the about 3.2 eV is found. In the part of the spectrum above 3.2 eV the electroabsorption signal clearly deviates from the fit and must therefore signify a further contribution. This signal is assigned to be the absorption band of a transition to the one photon forbidden energy state $2A_g$, which becomes allowed in the presence of the electric field. This is more clearly seen in the difference spectrum between the electroabsorption signal and the fit, which is depicted in Figure 4. 11b.

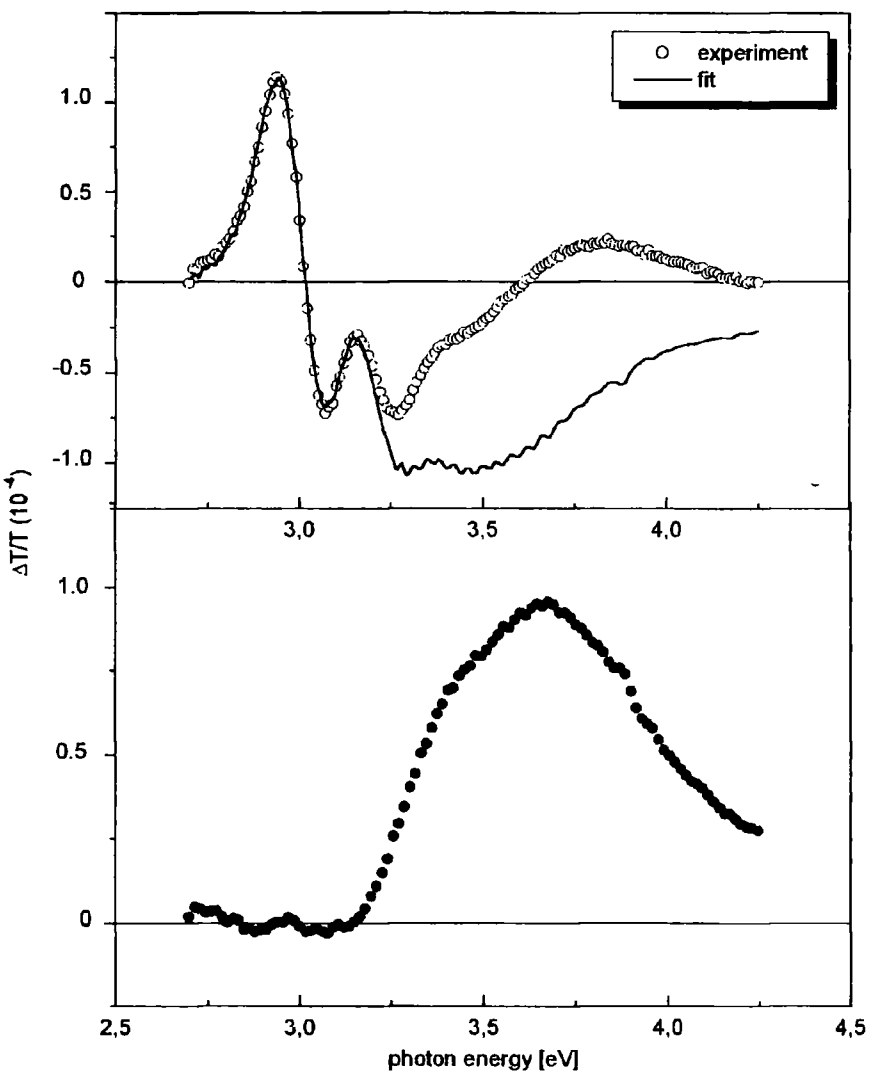

Figure 4. 11 a) Modelling of the electroabsorption spectrum (open circles) with a curve obtained by the linear combination of the absorption and its first and second derivative (solid line) according to eq 2. 3 with the linear coefficients obtained from a least square fitting procedure. b) Difference spectrum between the electroabsorption spectrum and the fit.

The width and shape of the obtained feature is very similar to that of the $1A_g \rightarrow 1B_u$ absorption band at 3.23 eV (Figure 4. 2) and the exact peak position can now be determined to be 3.66 eV with onset at 3.2 eV. Consistent with the emergence of the new transition a strong contribution of the linear absorption signal is seen in the fit to the electroabsorption spectrum indicating bleaching of the $1A_g \rightarrow 1B_u$ transition and a shift of oscillator strength to the nearby $1A_g \rightarrow 2A_g$

transition. This demonstrates the internal consistency of the model leading to the energy level scheme depicted in Figure 4. 12.

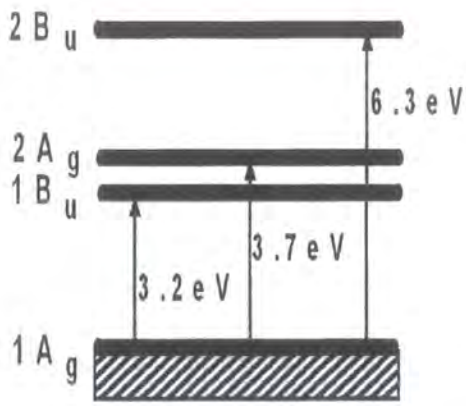

Figure 4. 12 Possible energy levels of the singlet states in PPY

From the results of the fit (eq. 4. 1) the average value of the difference between the ground state and excited state dipole moment $\langle \Delta \mathbf{p} \rangle$ as well as the average change of the components of the polarisibility tensor $\langle \Delta \ddot{\alpha} \rangle$ can be calculated. To do this eq. 2. 2 is substituted into the linear coefficients and expanded up to second order in electric field, assuming the terms which are linear in $\Delta \mathbf{p}$ to vanish because of the isotropic orientation of the polymer chains in the plane of the substrate. This yields the following relations for the coefficients of the first and second derivative of the absorption:

$$k\Delta E = \frac{kF^2}{2} \langle \Delta \ddot{\alpha} \rangle$$

$$\frac{k(\Delta E)^2}{2} = \frac{kF^2}{2} \langle \Delta \mathbf{p} \rangle^2$$

Using the experimental results for $k\Delta E$ $\langle \Delta \ddot{\alpha} \rangle = 4.18 \times 10^{-37}$ Cm/(V/m) is found, which is intermediate between the values obtained for PPV[54] and MEH-PPV[51] and about one or two orders of magnitude larger then that of other polymers (Table 4. 2). This indicates a high degree of delocalisation of the excited state in PPY, which is comparable with that of PPV-based polymers.

The average value of the difference between ground and excited state dipole moment was determined to be $\langle \Delta \mathbf{p} \rangle = 1.9 \times 10^{-29}$ Cm $= 5.7$D. When compared with the values for polymers whose EA-spectrum is dominated by the influence of charge transfer excitons (second derivative line-shape),[23,55] it can be seen that in PPY this effect plays a secondary role (Table 4. 3).

Polymer	$\langle \Delta\ddot{\alpha} \rangle / 10^{-38} Cm/Vm^{-1}$	Band gap ΔE [eV]	References
PPY	41.8	3.2	This work
PPV	71	2.8	54
MEH-PPV	10.6	2.4	49
PPPV*)	2.1	3.1	56
PPI*)	1.7	2.8	54
PPA*)	1.3	2.6	64
Tetracene	0.19	2.4	23
Pentacene	0.19	1.8	23

Table 4. 2 Average change of the components of the polarisibility tensor $\langle \Delta\ddot{\alpha} \rangle$ for PPY and other conjugated polymers

*) PPPV: poly-(phenylphenylenevinylene)
PPI: poly(1,4-phenylene-methylidynenitrilo-1,4-phenylenenitrilomethylidyne)
PPA: poly(phenylene acetylene)

However, the value obtained allows a rough estimate of the displacement of the excited electron (from its correlated hole) assuming one electron transfer[23] to be about of 3 Å. This is consistent with the typical distance between polymer chains and, together with the analysis of the polarisation data, suggests the observed CT-transition to be an interchain $n \rightarrow \pi^*$ transition.

Polymer	$\langle \Delta p \rangle$	$r/Å$	References
PPY	5.7D	1.7	This work
4-BCMU*)	48D	9.9	56
PDES*)	24D	4.9	64
EB-Polyaniline*)	19D	3.9	48
PPV	7.6D	1.6	54
Pentacene	2.5D	0.5	23

Table 4. 3 Average value of the difference between the ground state and excited state dipole moment $\langle \Delta p \rangle$

*)4-BCMU: 4-butoxy-carbonyl-methyl-urethane
PDES: poly(diethynyl silane)
EB-Polyaniline: Emeraldine base polyaniline

This suggestion is supported by the results of the polarised electroabsorption measurements. The value 3:1 has been reported for a variety of other polymers, for example 4-BCMU[56] and PPPV,[57] which was assigned to the alignment of the relevant transition dipole moments parallel to the polymer backbone.[56] However, deviations from this ratio are common in the literature.[58,59] The anisotropy ratio of 3:2 found for

PPY could then indicate a contribution of a transition nonparallel to the polymer backbone.

Finally, the third order non-linear susceptibility $\chi^3(-\omega;0,0,\omega)$ of PPY can be calculated from the electroabsorption spectrum. For this the field-induced change of the real and imaginary part of the complex refractive index is derived from the field-induced change of absorption via the Kramers-Kronig-relation[60]

$$\Delta n(\omega) = \frac{2}{\pi} P \int_0^{+\infty} \frac{\omega' \Delta\kappa(\omega')}{\omega'^2 - \omega^2} d\omega',$$

where $\Delta n(\omega)$ and $\Delta\kappa(\omega)$ are the real and imaginary part of the field induced change in the complex refractive index $\Delta\tilde{n}(\omega) = \Delta n(\omega) + i\Delta\kappa(\omega)$. Using the relation

$$\Delta\kappa(\omega) = \frac{c}{2\omega}\Delta\alpha(\omega)$$

$\Delta\kappa(\omega)$ is directly given from the field-induced change in absorption (the electroabsorption signal).

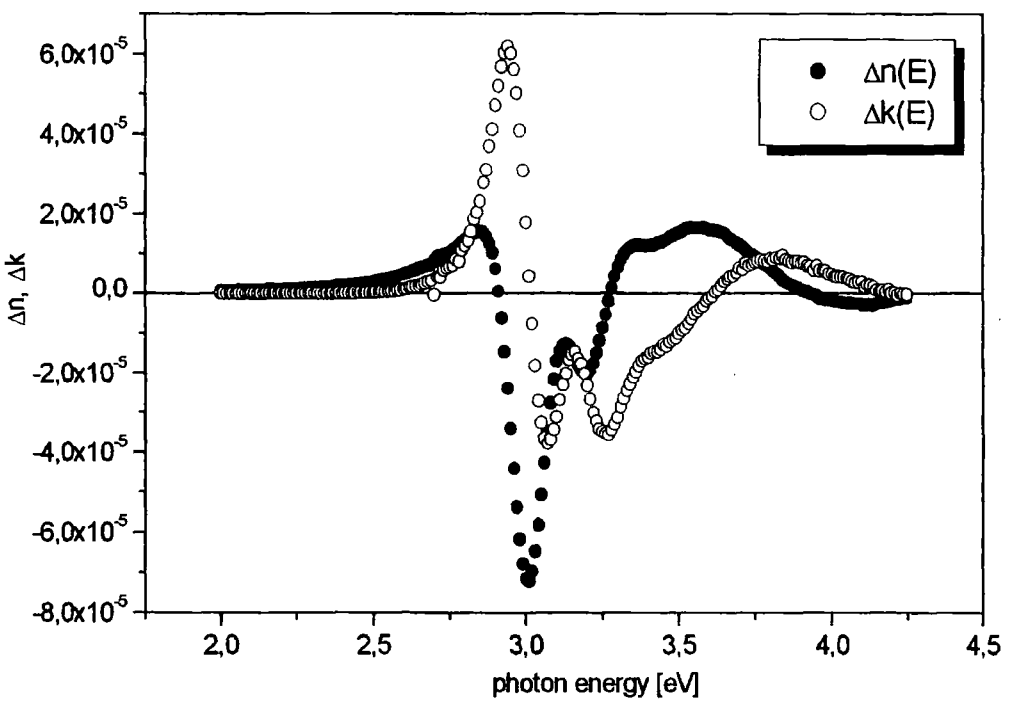

Figure 4. 13 Real and imaginary part of the field induced change in the complex refractive index derived from the electroabsorption spectrum via an Kramers-Kronig-Relation.

To derive the curve $\Delta n(\omega)$ from the EA-spectrum the Kramers-Kronig-integral has to be calculated for every photon energy of the spectrum. To perform this transformation a computer program was written, which uses a simple trapezium method to calculate the principal value of the KK-integral. The obtained curves for $\Delta n(\omega)$ and $\Delta\kappa(\omega)$ are depicted in Figure 4. 13. To derive the third order non-linear susceptibility $\chi^3(-\omega;0,0,\omega)$ the relation[61]

$$\chi^3(-\omega;0,0,\omega) = \frac{\tilde{n}(\omega)\Delta\tilde{n}(\omega)}{2\pi F^2},$$

with F the applied electric field is used.

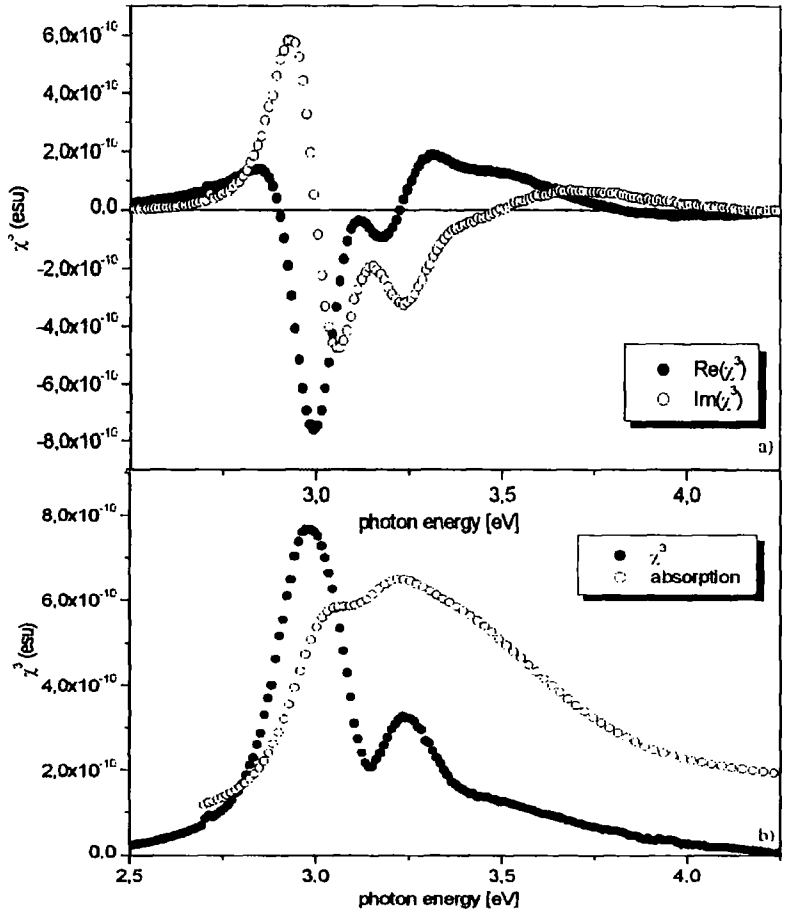

Figure 4. 14 a) Real part (filled circles) and imaginary part (open circles) of the third order non-linear susceptibility $\chi^3_{max}(-\omega;0,0,\omega)$ derived from the electroabsorption spectrum via Kramers-Kronig relation; b) Absolute value of the third order non-linear susceptibility $\chi^3_{max}(-\omega;0,0,\omega)$ (solid circles) and the linear absorption spectrum (open circles) scaled for comparison.

For the real and imaginary part of the refractive index $\tilde{n}(\omega)$ the results of spectroscopic ellipsometry measurements by Monkman *et al.*[38] have been used. Figure 4. 14a shows the real and imaginary part of $\chi^3(-\omega;0,0,\omega)$ while the absolute value $|\chi^3(-\omega;0,0,\omega)|$ is depicted in Figure 4. 14b with the linear absorption signal for comparison. The obtained maximum value $\chi^3{}_{max}(-\omega;0,0,\omega)\approx 6\times10^{-10}$ esu is comparable to the value measured for poly(3- octylthiophene),[62] one or two orders of magnitude smaller than that for poly(2,5-thienylene vinylene)[61] and trans-polyacetylene[58] respectively and one order of magnitude larger then $\chi^3{}_{max}(-\omega;0,0,\omega)$ measured for polyaniline.[63]

The magnitudes of the optical constants obtained from the electroabsorption spectrum as well as the line-shapes and positions of the features of the EA-spectrum itself provide detailed characterisation of the electronic transitions occurring within the conjugated π-electron system as described above. The similarity of the results obtained for PPY compared with other conjugated polymers[19,22,23,51,55,64] and the good fit of the EA-spectrum to the absorption spectrum and its first and second derivative leads to the conclusion that the one photon allowed excited states in PPY are excitonic in nature and not principally different than those of other conjugated polymers. Previously, it has been thought that excimer formation occurred in PPY.[37] This view had been shown to be incorrect[41,36] a conclusion that these EA results further confirm.

4.2 Electroabsorption in Stretched Oriented PPY and in Sandwich Configuration

Conductivity and luminescence, the electrical and optical properties of conjugated polymers that make them so important for commercial applications, are all directly or indirectly correlated to their quasi one-dimensional structure. Direction dependent measurement on aligned polymer samples is an essential tool to directly address the correlation between this one-dimensional molecular structure and the conjugated π-electron system. This chapter presents results and discussion of polarised absorption and electroabsorption measurements in stretched oriented films of poly(2,5-pyridinediyl) using different directions for the polarisation of the incident light and the applied electric field with respect to the polymer axis. This allows to separate the in-chain and off-chain components of the ground and excited state electronic wave function. In addition results of electroabsorption measurements on disordered (spin-cast) PPY films in sandwich configuration are presented, which provides information about the alignment of the polymer chains on a substrate.

4.2.1. Experimental Results

To produce oriented films PPY was cast on polyvinyl alcohol films (PVA films), which were stretched under head to stretching ratios between 1:10 and 1:20. After cooling down the PVA-PPY samples could be removed from the stretching device without losing their orientation and the electrodes could be deposited.

Figure 4. 15 shows the absorption spectrum of a stretched oriented film of PPY for polarisation of the incident light parallel and perpendicular to the stretching direction. It can be seen that the absorption drops more then one order of magnitude when light is polarised perpendicular to the chains. At 3.3 eV both spectra reach their maximum absorption, which is 0.9 and 0.07, respectively, yielding an absorption anisotropy ratio of 13. In Figure 4. 16 the angular dependence of the peak absorption at 3.3 eV is depicted. The curve is very symmetric with respect to zero degree indicating well-ordered structure of the stretched films.

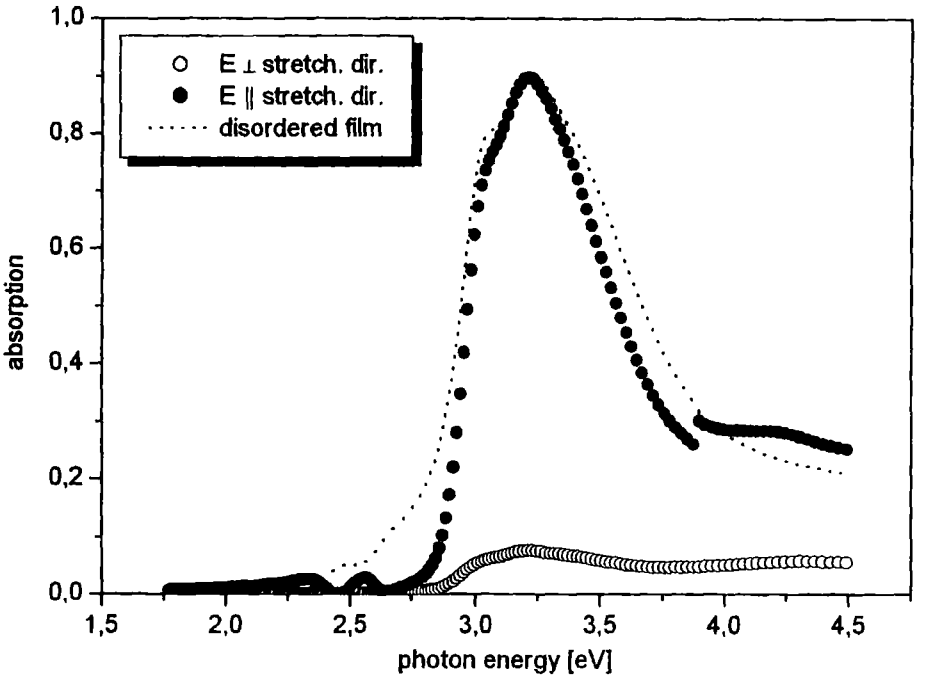

Figure 4. 15 Absorption spectrum of stretched PPY for light polarised parallel (filled circles) and perpendicular (open circles) to the stretching direction. The absorption spectrum of a disordered (spin-cast) film is shown as dotted line. All spectra where recorded at a temperature of 10 K.

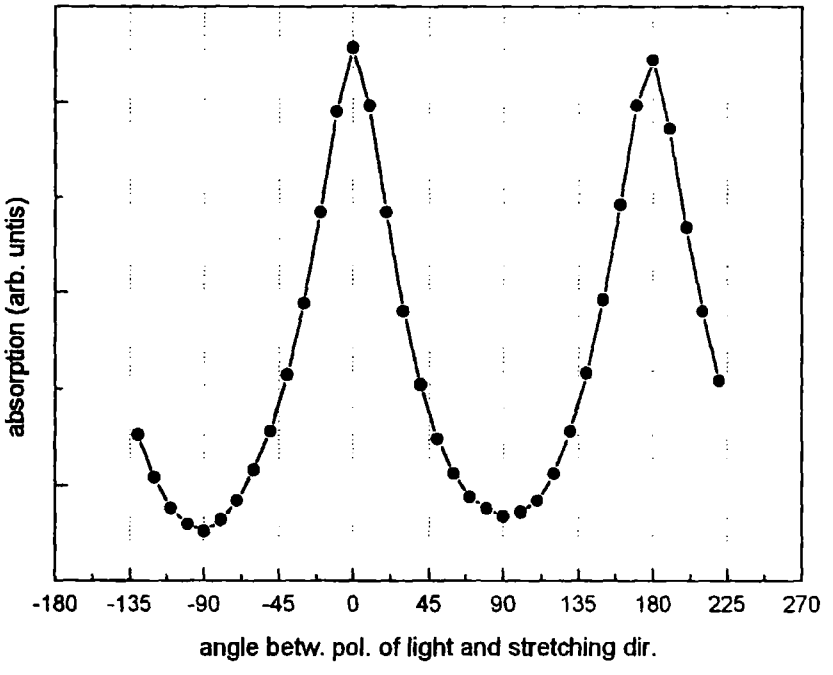

Figure 4. 16 Angular dependence of the maximum absorption at 3.3 eV

To illustrate the effect the increased order in the PPY films has to the line shape of the absorption spectrum Figure 4. 17 shows the scaled spectra for both directions of polarisation. Despite originally having very different magnitudes the two spectra of the stretched film exhibit very similar line shapes with similar distribution of vibronic modes. The deviation in the higher energy part of the spectrum is due to an increasing influence of the absorption of the substrate material. This contribution does not depend on light-polarisation and therefore becomes more apparent in the scaling graph.

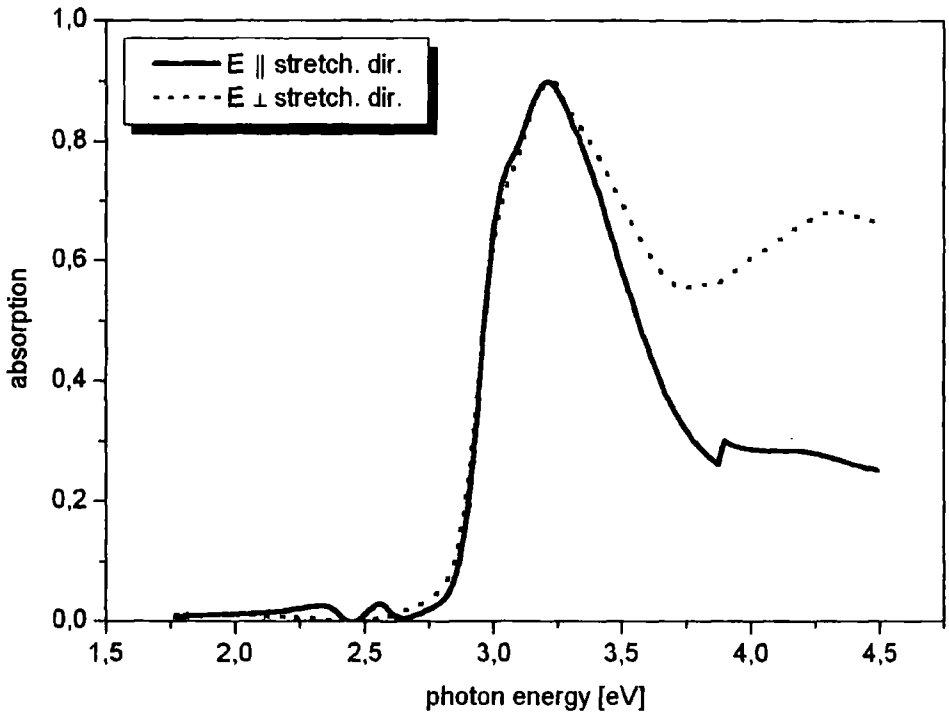

Figure 4. 17 Absorption for light polarised parallel and perpendicular to the stretching direction of an oriented PPY film scaled to demonstrate the constancy in line shape.

An interesting point is the comparison of the absorption spectra of the oriented sample with the non-oriented sample (Figure 4. 15). Clear line narrowing can be observed as a result of the orientation. In particular, the transition-probabilities for transitions in the low energy region of the absorption seem to be significantly

reduced resulting in a sharpening of the onset. On the other hand, the low energy shoulder at about 3 eV does not become more pronounced in the oriented film.

In the electroabsorption experiment there are two vectors that can be rotated with respect to the stretching direction, the externally applied electric field and the electric field vector of the polarised light.

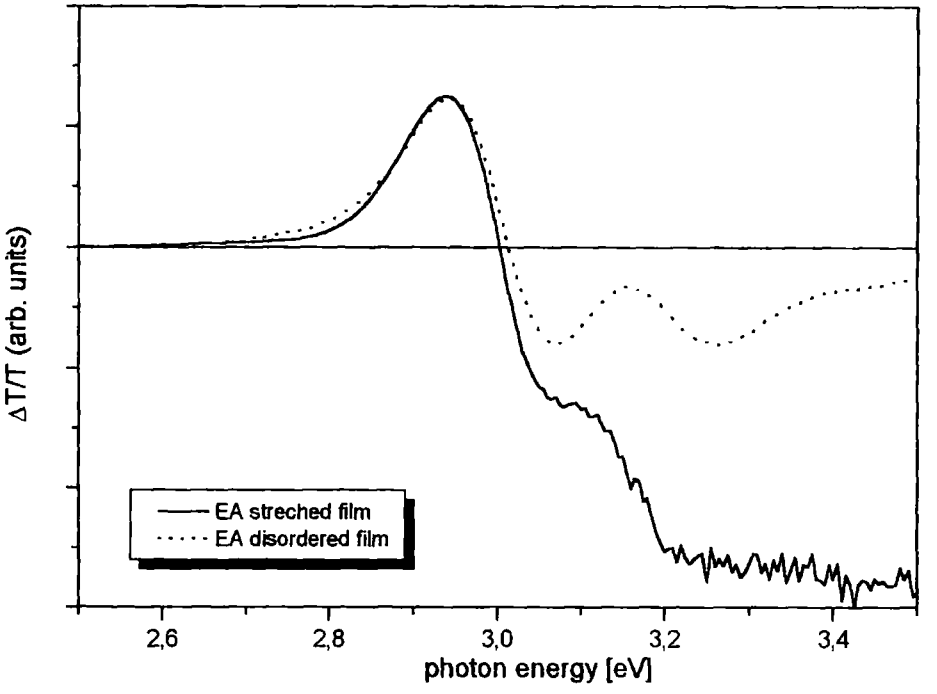

Figure 4. 18 Electroabsorption spectrum of a stretched oriented PPY film with the electric field applied parallel to the stretching direction (solid line). The spectrum and of a disordered film is depicted as dotted line for comparison.

Figure 4. 18 shows the electroabsorption spectrum of a stretched oriented PPY film with both the applied electric field and the polarisation of the light being parallel to the stretching direction. Also depicted is the scaled EA-spectrum of a disordered (spin-cast) film. In the oriented spectra a slightly line narrowing of the main feature around 2.9 eV can be observed. As a result the spectrum of the ordered sample crosses the zero line at a photon energy 10 meV lower than the that of the disordered sample. Apart from this sharpening the line shapes of both spectra look almost

identical, indicating a common origin of the EA response for the ordered and the disordered system. In the high-energy part, again, the stretching material contributes increasingly to the signal.

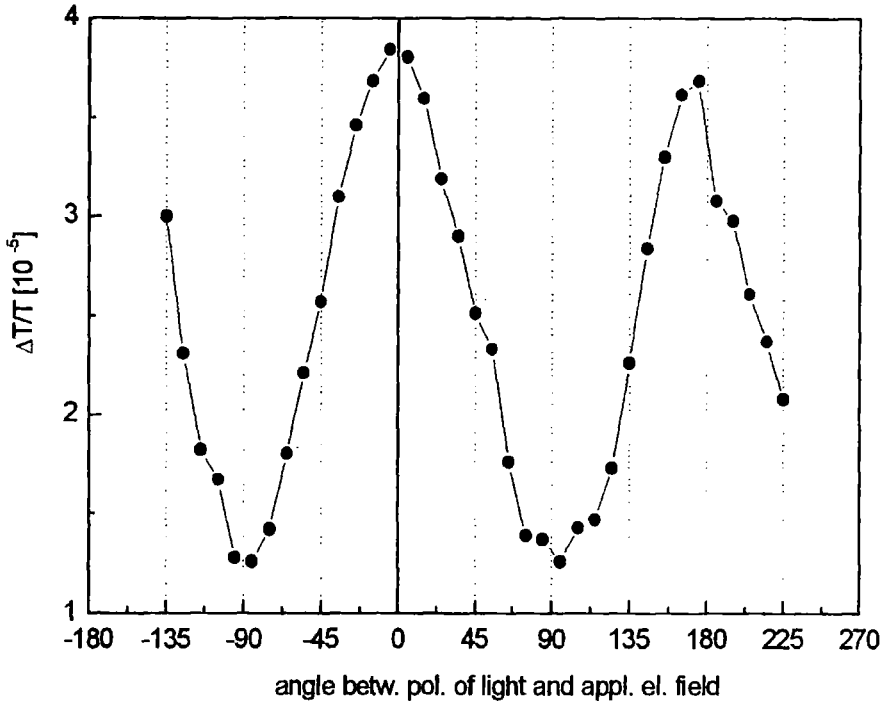

Figure 4. 19 Angular dependence of the Electroabsorption signal at 2.9 eV

If the polarisation of the light is rotated out of the parallel direction while keeping the electric field applied along the chains, the electroabsorption signal is found to decrease. In Figure 4. 19 the angular dependence of $\Delta T/T$ is depicted. Again, the signal is symmetrically with respect to zero degree and reaches its minimum when the light is polarised perpendicular to the chain direction. However the electroabsorption anisotropy ratio $\Delta\alpha(\|)/\Delta\alpha(\perp)$ is determined to be only 3. This is more than four times lower than the obtained linear absorption anisotropy of 13.

To measure the electroabsorption for the applied electric field not parallel to the polymer chains two methods were used. First the electrodes were evaporated with the shadow mask rotated under a certain angle to the stretching direction.

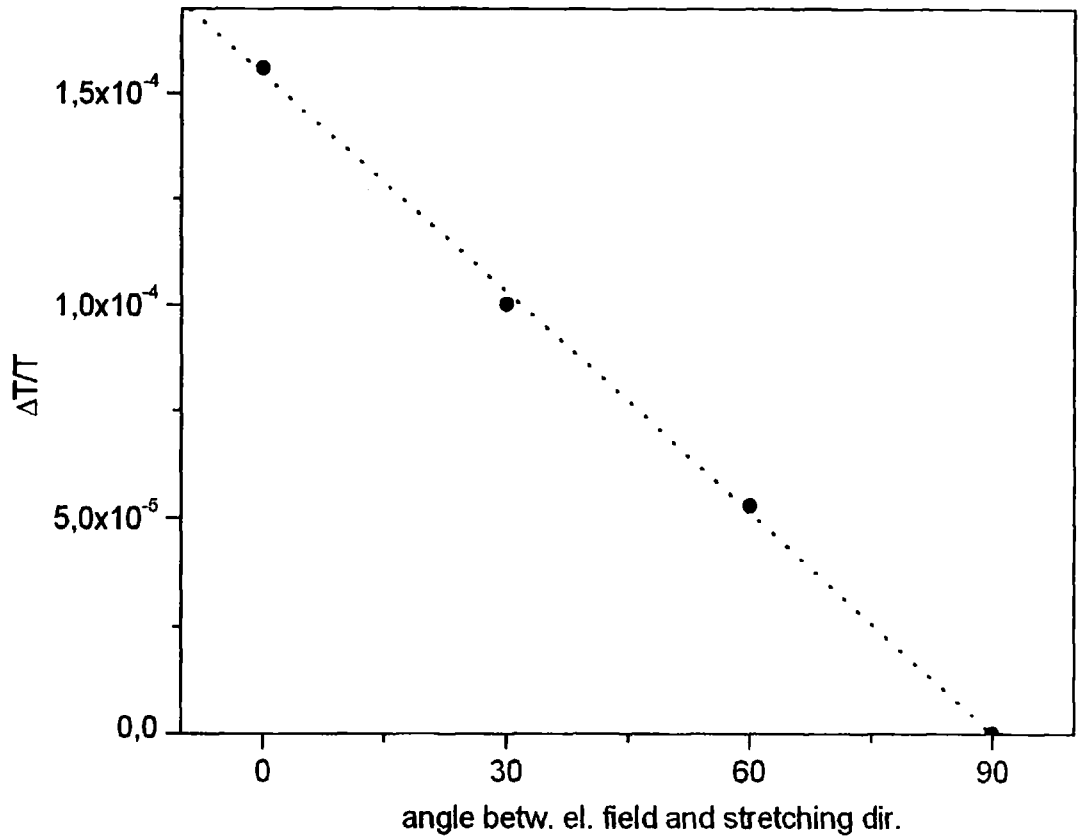

Figure 4. 20 The decreasing of the EA-signal for the stretched oriented film using different angles for the applied electric field with respect to the chain orientation.

The maximum EA-signal measured at a photon energy of 2.9 eV is depicted in Figure 4. 20 for different directions of the applied electric field. The incident light was polarised in the chain direction, which was always found to produce the largest signal. The signal decreases constantly and no electroabsorption signal was detectable when the field was applied perpendicular to the stretching direction.

In a second arrangement a thin (ca. 100 nm) spin-cast PPY film was sandwiched between ITO and semitransparent aluminium equally to the configuration of a light emitting diode. This allows the application of relatively high electric fields. At a field of 500 kV/cm, which is ten times higher than in the planar configuration using the interdigitated electrodes, the magnitude of the sandwich cell EA at 2.9 eV is less than a third of the planar EA. Taking into account the quadratic voltage dependence of the electroabsorption signal in PPY[65] this indicates an EA anisotropy of 100 to 1000 with respect to the direction of the applied electric field.

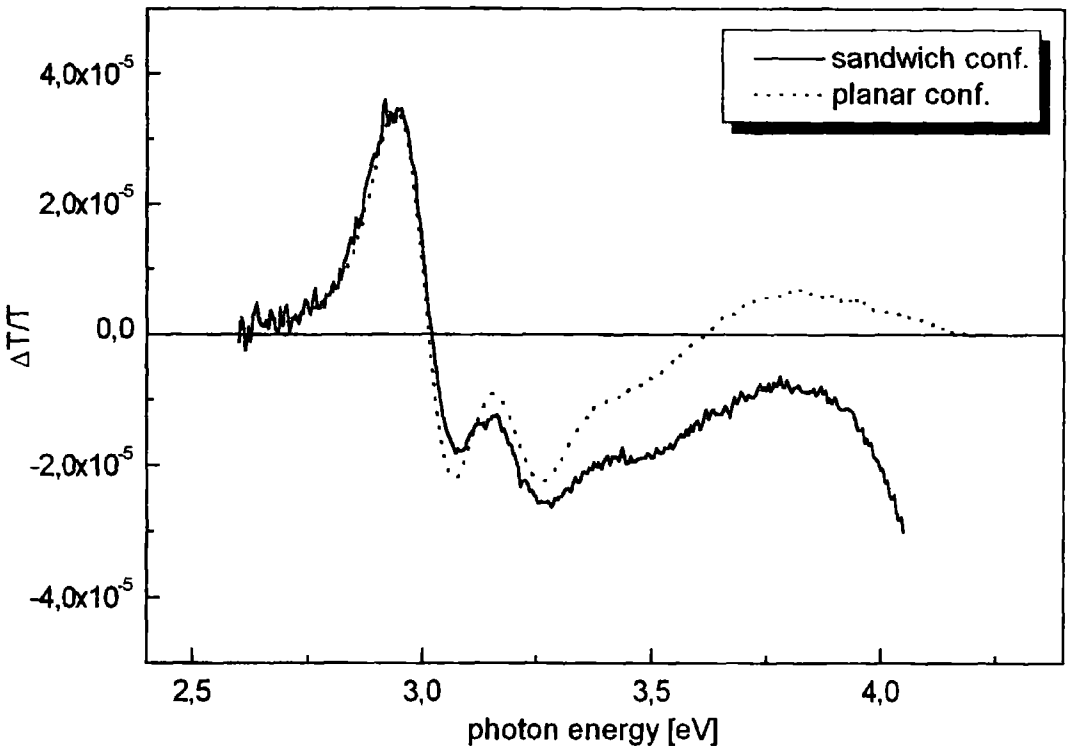

Figure 4. 21 Electroabsorption of a disordered PPY film in a sandwich configuration between ITO and Al.

Figure 4. 21 shows the EA spectrum for a sandwich cell and compares it with the scaled spectrum of a PPY film measured in planar configuration using the interdigitated electrodes. It is remarkable that, despite the huge difference in magnitude of the signal and the distinct electrode arrangements in the two configurations, both spectra exhibit almost identical line shape. This in conjunction with the angular dependence on the stretched films suggests that the electric field component parallel to the chain direction always interacts with the same excited species.

4.2.2. Discussion

The line narrowing of the first allowed transition in the absorption spectrum is expected for a sample with increased order. Similar effects were observed in oriented samples of other conjugated polymers[66,67]. In the poly(phenylenevinylene) derivative MEH-PPV[68] reduced disorder gave rise to a steeper onset of the absorption and to an

improved resolution of the vibronic features. This sharpening of the absorption edge is also observed in the spectrum of the oriented PPY films and indicates that the low energy shoulder of the absorption band at about 3.0 eV corresponds to the lowest, i.e. the vibronically relaxed energy state. In contrast to all other conjugated polymers the energetic position of the absorption maximum and its shoulder are independent of both stretching and the polarisation of the incident light (Figure 4. 17). In poly(octylthiophene), for example, the absorption peak blue-shifts by almost 0.5 eV when changing the light polarisation from parallel to perpendicular and the stretching itself causes an energy shift of 0.1 eV.[66,67] The authors explained this behaviour with an increase of the conjugation length upon stretching. Although the stretched-oriented PPY films exhibit a far larger absorption anisotropy ratio (Figure 4. 16), no shift or significant redistribution of the vibronic components can be observed. This can be explained by the rigid-rod-like nature of the PPY chains. The high degree of crystallinity, which was revealed in X-ray powder diffraction measurements by Monkman *et al.*[38], implies strong interchain interactions between the polymer chains. Therefore even in disordered (spin-cast) films of PPY there is high degree of order in the neighbourhood of each chain. Since this microscopic order and the rigidity of the polymer chains are both unaffected by stretching the conjugated π-electron system does not experience a change of its energy levels.

The electroabsorption response of disordered films of PPY was studied in detail in the last section. Therein the strong low energy feature around 2.9 eV was recognised to arise from a non-linear Stark shift of the first allowed optical transition due to a change in polarisibility between the ground and the excited state. A fit of the EA-spectrum to a linear combination of the absorption signal and its first and second energy derivative allowed the exact determination of the shift by separating the effects involved:

$$\Delta\alpha\ (E) = (k-1)\alpha(E) + k\Delta E\frac{d\alpha(E)}{dE} + \frac{k\Delta E^2}{2}\frac{d^2\alpha(E)}{dE^2} \qquad (4.2)$$

Thus, using the linear coefficient of the first derivative the calculation of the average change in polarisibility upon transition from the ground state to the excited state $\langle\Delta\tilde{\alpha}\rangle$ was possible[22,23]:

$$k\Delta E = \frac{kF^2}{2}\langle \Delta\tilde{\alpha} \rangle \qquad (4.3)$$

With the results of the electroabsorption anisotropy of the stretched sample the average change in polarisibility can now be separated into its two components, parallel and perpendicular to the polymer chains. Thereby it is important to note that the line-shape and peak positions of the electroabsorption spectrum does not change upon stretching (Figure 4. 18) and that the linear Stark effect is still negligible. Therefore eq. 4. 2 and 4. 3 can be applied to the EA-data for polarisation of the incident light parallel and perpendicular to the polymer chains. Then one obtains

$$\langle \Delta\tilde{\alpha} \rangle_{\parallel} = 5.4 \times 10^{-37}\ \mathrm{Cm/(V/m)},$$
$$\langle \Delta\tilde{\alpha} \rangle_{\perp} = 25 \times 10^{-37}\ \mathrm{Cm/(V/m)}.$$

The polarisibility of an energy state denotes the capability of an electron system to redistribute its charges under the influence of an external electric field forming an electric dipole. The values obtained for $\langle \Delta\tilde{\alpha} \rangle_{\parallel}$ and $\langle \Delta\tilde{\alpha} \rangle_{\perp}$ mean that for excited states generated by light polarised perpendicularly to the chains the *change* of this capability upon excitation is about four times larger. Thus the question arises whether these perpendicularly generated excited states are created at the few chains that could not be oriented by the stretching or are they a part of the excited state of the oriented chains. The first alternative can be excluded since this corresponds to the configuration where the electric field is applied perpendicular and the light polarised parallel to the stretching direction. This was seen to show no electroabsorption signal within the accuracy range of the experiment (Figure 4. 20) although far more chains are addressed. Therefore, the relatively high EA-signal for light polarised perpendicularly and electric field parallel to the chain direction is assigned to be a perpendicular component with low oscillator strength ($\alpha(\parallel)/\alpha(\perp)=13$) but very high polarisibility in the chain direction. This - together with the fact that CT excitons in the oriented film are still neglegdible (no significant contribution of the second absorption derivative to the EA signal) - suggests the creation of Wannier-like excitons in the following way: A photon with polarisation perpendicular to the chains leads to the transfer of an electron to a neighbouring chain. This supports the separation of the electron from its correlated hole since the influence of the hole is

reduced when the electron is located in the surrounding of a different chain. The same electric field could then separate electron and hole to a larger extend then in an intrachain exciton, which would explain the high polarisibility of these states. This interpretation would also mean that the small absorption for light polarised perpendicular to the stretching direction originates from such interchain transitions rather then from imperfections of the alignment.

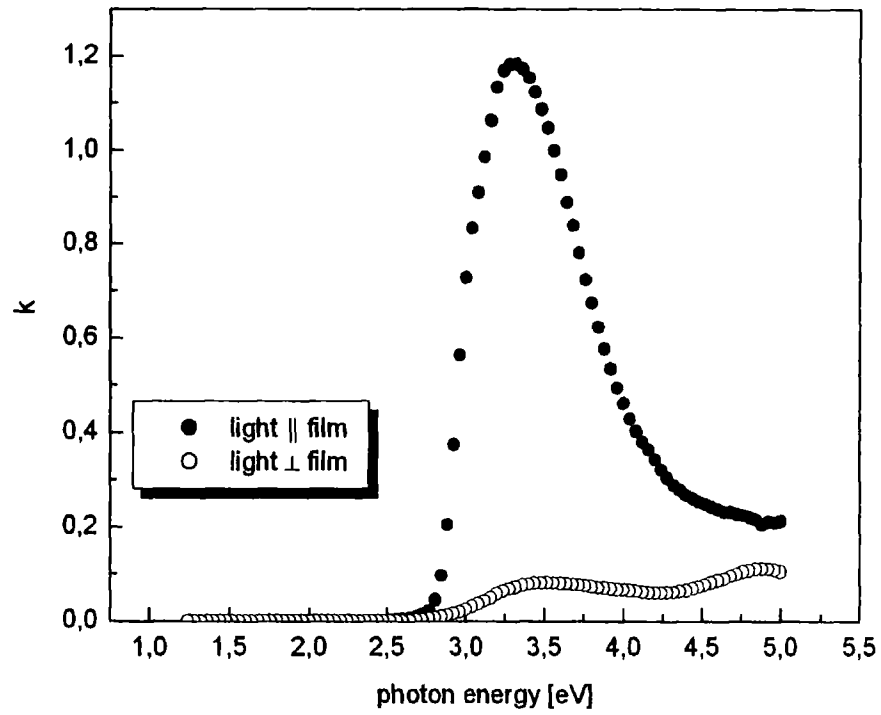

Figure 4. 22 The imaginary part (proportional to the absorption coefficient) of the complex refractive index measured in a thin disordered film of PPY with the polarisation of the incident light in the plane of the substrate (filled circle) or perpendicular to it (open circle). After Monkman *et al.* (Ref[38])

When the electric field was applied perpendicular to the polymer chains very low electroabsorption was measured for the either polarisation directions of the incident light. In the stretched sample no signal at all could be detected (Figure 4. 20) and in the sandwich cell experiment, where far higher electric fields were used, the EA-response was 100 to 1000 times smaller then in the normal configuration. This allows two conclusions: First, the off axis component of the excited state polarisibility is very small or, more exactly, does not differ from the ground state

polarisibility. This is consistent with the general picture that the displacement of charges along the chains is much easier then perpendicular to it. The second conclusion becomes obvious when one remembers that the sandwich cells are produced by simple spin-casting of PPY in formic acid solution. The very high EA-anisotropy then indicates a perfect alignment of the polymer chains in the plane of the substrate. This agrees with the high crystallinity and rigid-rod like nature of the PPY chains as well as with the results of ellipsometry measurements by Monkman *et al.*[38] In these measurements the absorption coefficient of thin disordered (spin-cast) films of PPY for light polarised parallel and perpendicular to the plane of the film could be determined. The spectra obtained for $\kappa(E)$, the imaginary part of the complex refractive index, which is proportional to the absorption coefficient ($\Delta\kappa(\omega) = c/2\omega\,\Delta\alpha(\omega)$), are depicted in Figure 4. 22. An anisotropy coefficient of 15 can be determined confirming the very good alignment parallel to the substrate.

4.3 Photocurrent Measurements on PPY

As a starting point, again, the poly(phenylenevinylene) derivative MEH-PPV was used to reproduce published results as a test of the experimental apparatus. Figure 4. 23 shows the spectra obtained for a gold/MEH-PPV/ITO structure under forward and reverse bias. The spectra are in good agreement with results of Harrison and Gruner[32], for example.

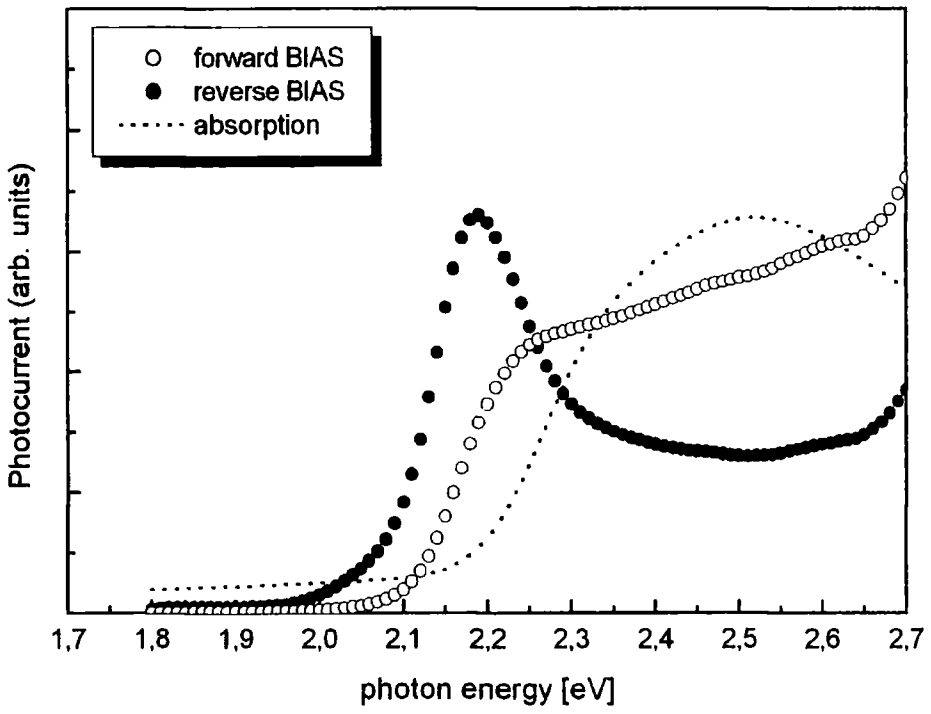

Figure 4. 23 Photocurrent spectrum of MEH-PPV under forward bias (open circles) and reverse bias (filled circles) and the absorption spectrum (dotted line), recorded to reproduce published data.

4.3.1 Experimental Results

Figure 4. 24 shows a typical time dependence of the photocurrent in a 200 nm PPY film under 0.1 V forward bias and illumination at 3.0 eV. About 2 seconds after

starting the recording the light beam was switched on (shutter removed) and the sample was illuminated over a time of about 100 seconds using constant intensity and wavelength. It can be seen that the current increases rapidly after removing the beam shutter and remains nearly constant over a long time. Therefore, when recording the spectra a settling time of 1 second before reading a data point was considered to be sufficient. For higher electric fields or (interestingly) thicker PPY films the decay was sometimes more significant and a longer settling time was chosen.

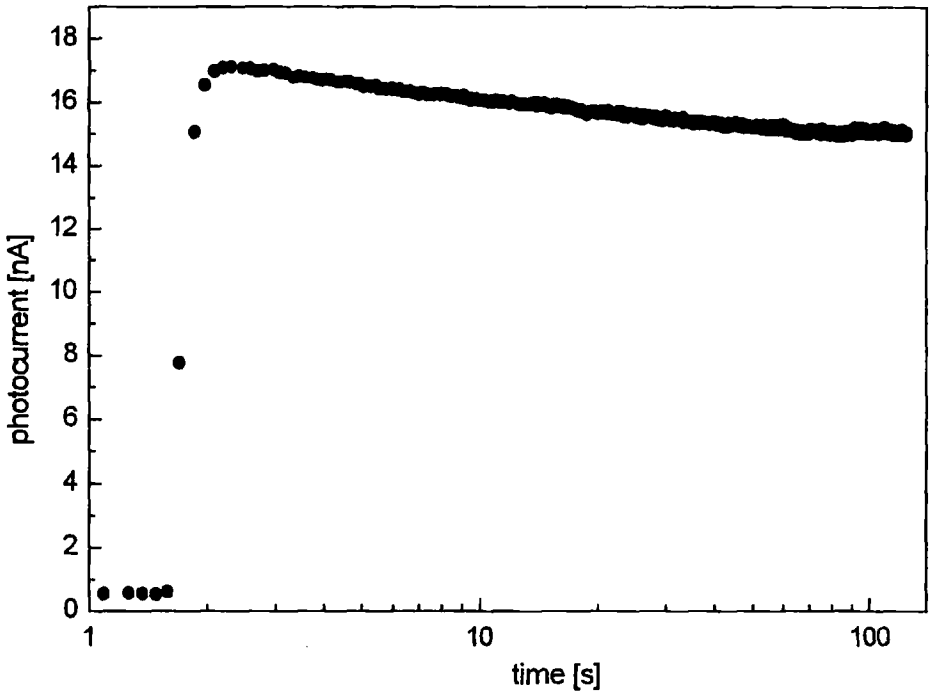

Figure 4. 24 The decay of the photocurrent in a typical Au/PPY/ITO sandwich cell under 0.1 V forward bias measured at a photon energy of 3.0 eV.

Figure 4. 25 and Figure 4. 26 show the photocurrent spectra of a 200 nm PPY film using the four possible directions for illumination and the applied bias. All spectra were darkcurrent corrected, normalised for a constant incident photon flux and scaled for better visibility. First the behaviour for photon energies in the region of the first allowed optical transition ($h\nu<4$ eV) is considered. In Figure 4. 25 the sample was biased in forward direction referring to a positively biased ITO electrode.

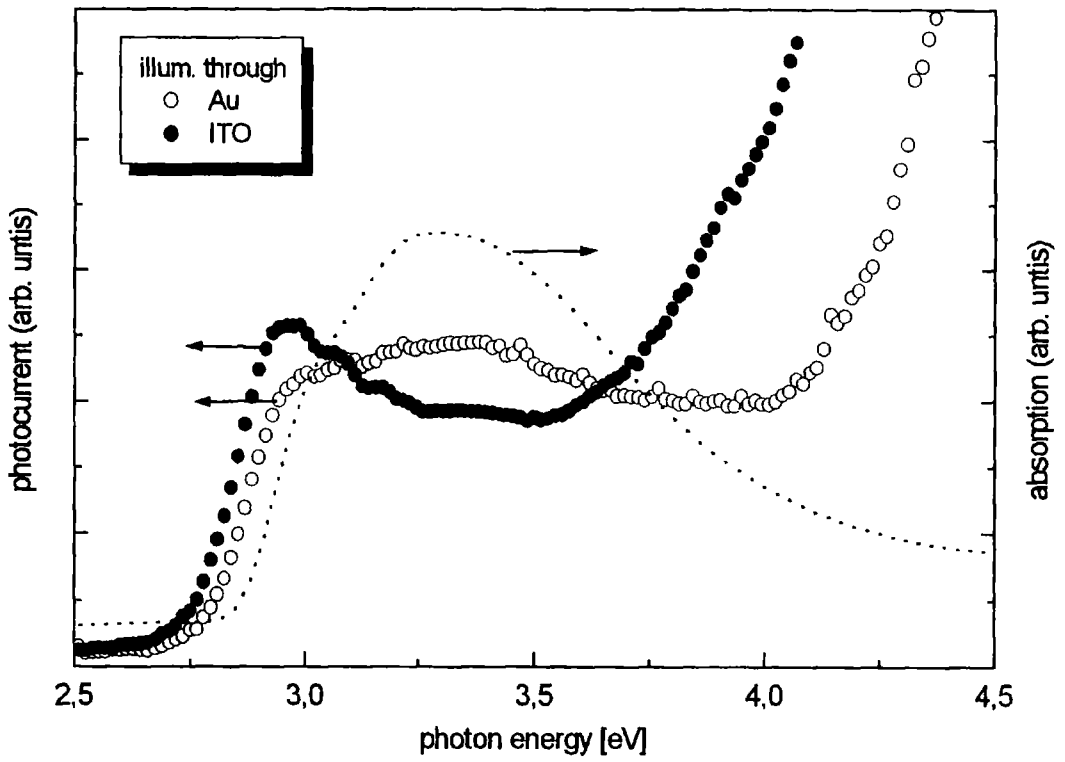

Figure 4. 25 Photocurrent spectra of a 200nm PPY film under forward bias. Illumination was through the ITO contact (filled circles) or through the semitransparent Au contact (open circles). The sample was measured under vacuum at a temperature of 295K. The spectra are darkcurrent corrected, normalised to constant incident photon flux and scaled for better visibility. The incident photon flux at 3 eV was $2x10^{15}$ photons/(cm^2s).

The difference in line-shape between the two spectra obtained from different illumination directions can be described by their relation to the absorption spectrum. When the cell is illuminated through the semitransparent gold electrode the photocurrent spectrum follows the absorption signal (symbatic response), while illumination through the ITO contact results in a narrow peak in the low energy tail of the absorption band at 2.9 eV (antibatic response). In contrast, when the bias is reversed (Figure 4. 26) the symbatic behaviour is observed when illumination is through the ITO electrode, while illumination through the semiconducting gold electrode results in an antibatic response.

Under both forward and reverse bias the absolute value of the photocurrent at the maximum of the antibatic peak at 2.9 eV was smaller then the photocurrent of the corresponding symbatic spectrum at the same photon energy. This is already an indication for the antibatic response to be due to a suppression of the signal in the

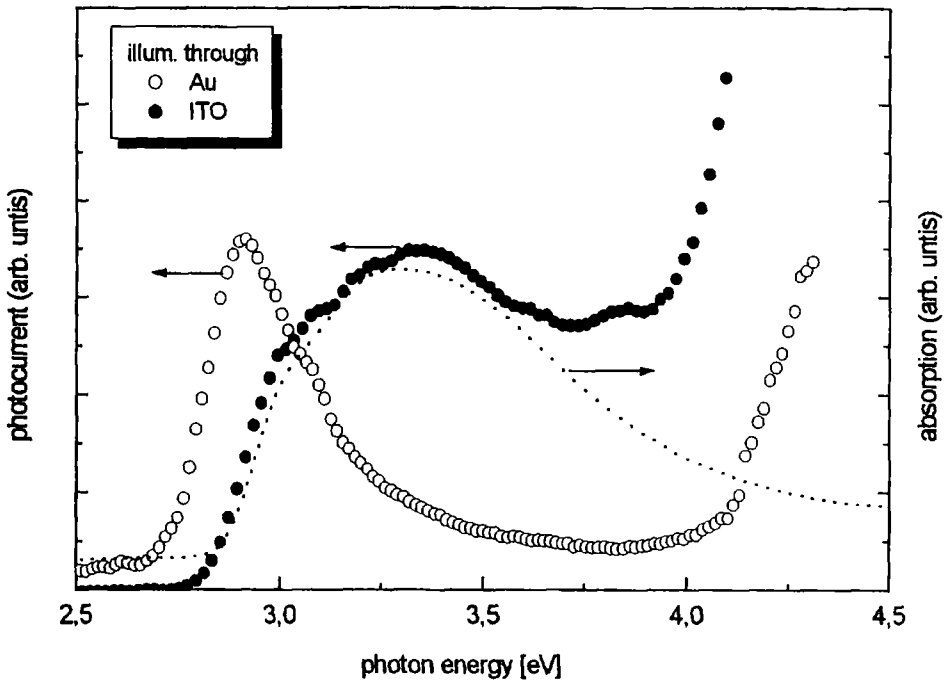

Figure 4. 26 Photocurrent spectra of a 200nm PPY film under reverse bias. Illumination was through the ITO contact (filled circles) or through the semitransparent Au contact (open circles). Sample and conditions like in Figure 4. 25.

region of high absorption. The transmittance of the sample was measured with a calibrated photodiode and the total amount of light passing the film at the position of the absorption peak maximum (3.3 eV) was determined to be only 10 percent of the amount of light being transmitted where the antibatic peak (2.9 eV) was observed (Figure 4. 27).

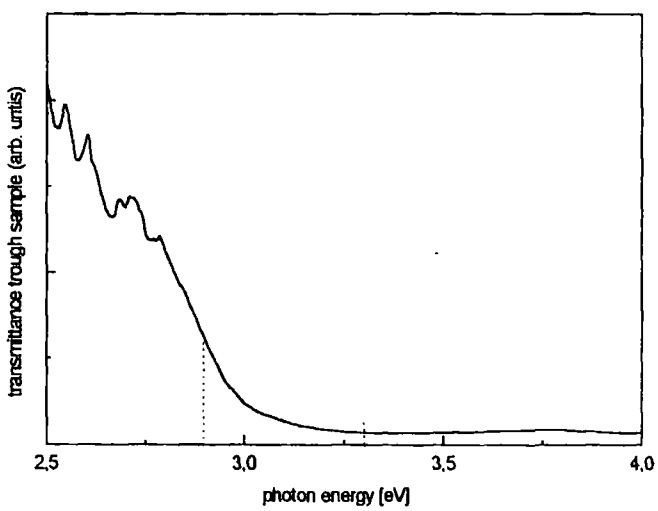

Figure 4. 27 Transmittence of a typical Au/PPY/ITO sandwich cell, measured with a calibrated silicon photodiode.

In the high-energy part of the photocurrent spectra a strong rise can be seen with onset at about 4eV (Figure 4. 25 and Figure 4. 26). The data, which are considered reliable in the range shown in the graph, indicate a far bigger photocurrent in the ultraviolet when compared to the feature around the absorption peak. For both bias directions the photon energy of the onset of the high-energy response is about 0.2 eV lower for illumination through the ITO electrode than for illumination through the semitransparent gold electrode.

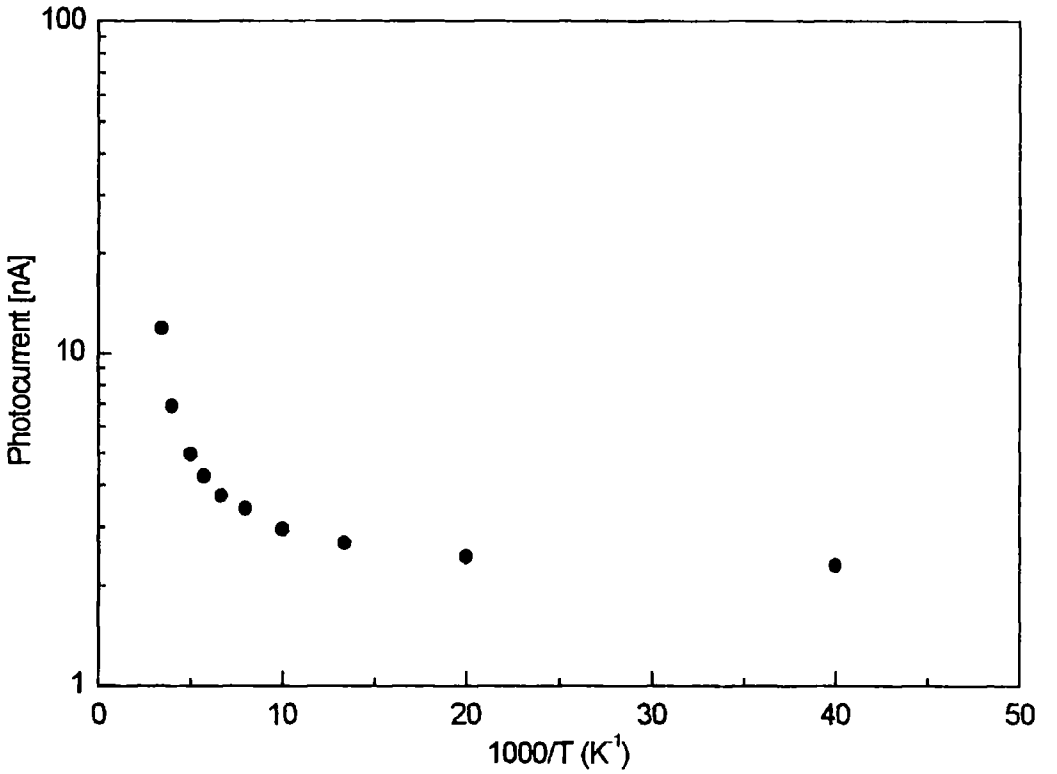

Figure 4. 28 Arrhenius-plot for the temperature dependence of the photocurrent in a 200nm PPY film. Illumination was through the ITO contact using a photon energy of 3.0 eV.

Figure 4. 28 shows the temperature dependence of the photocurrent in a typical PPY sandwich cell. The whole spectrum was measured for selected temperatures to ensure that the temperature dependence is not due to a shift in peak position (Figure 4. 29). Over the entire temperature region from 295 K down to 10 K the photocurrent decreases by a factor of about five only and does not follow an Arrhenius law of a temperature activated process.

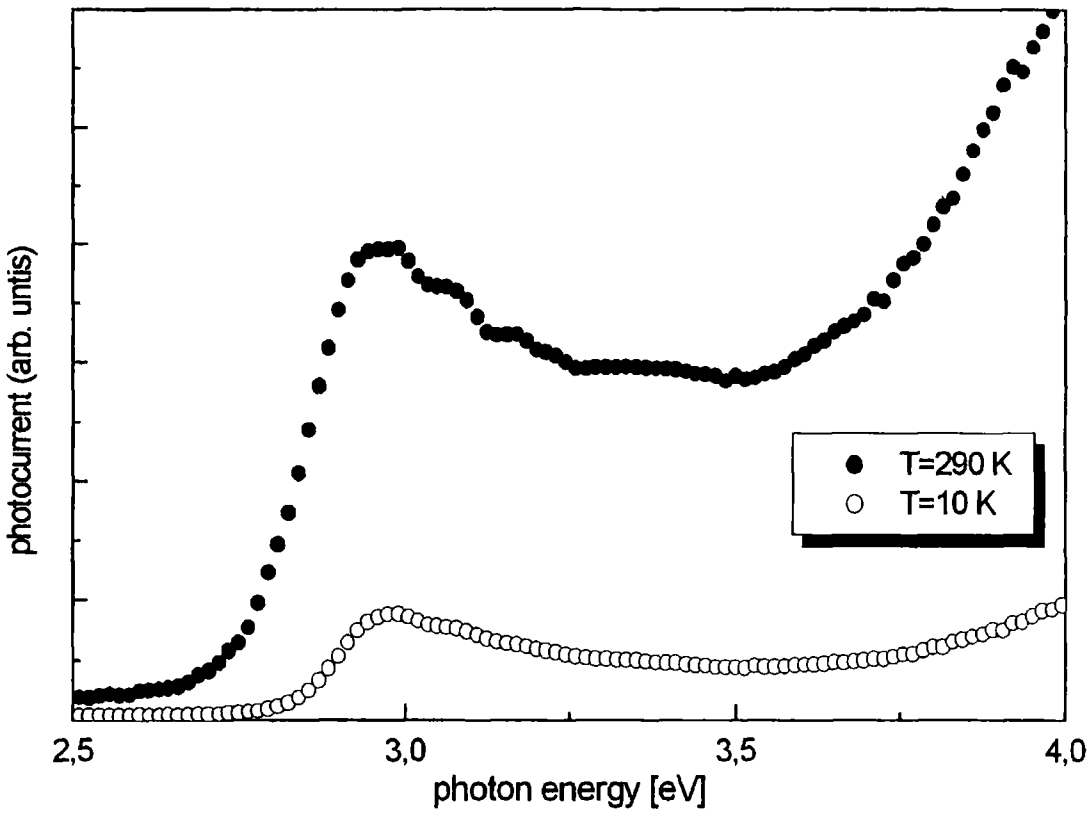

Figure 4. 29 The photocurrent spectra of a 200nm PPY film at 10 K (open circles) and at room temperature (filled circles). Illumination was through the ITO contact using a photon energy of 3.0 eV.

In Figure 4. 30 the photocurrent-voltage characteristics is depicted for three PPY films of different thickness under illumination through the ITO electrode using a photon energy of 3 eV. The photocurrent vanishes at 0.74 V irrespective of the film thickness. Taking this into account the photocurrent shows symmetric behaviour with respect to the polarity of the effective bias (bias minus 0.74 V) since the influence of the internal filter effect is weak at this photon energy. In addition, a strong dependence on the thickness of the PPY film is found. The photocurrent drops by three orders of magnitude when increasing the film thickness from 130 nm to 450 nm, which clearly deviates from Ohms law.

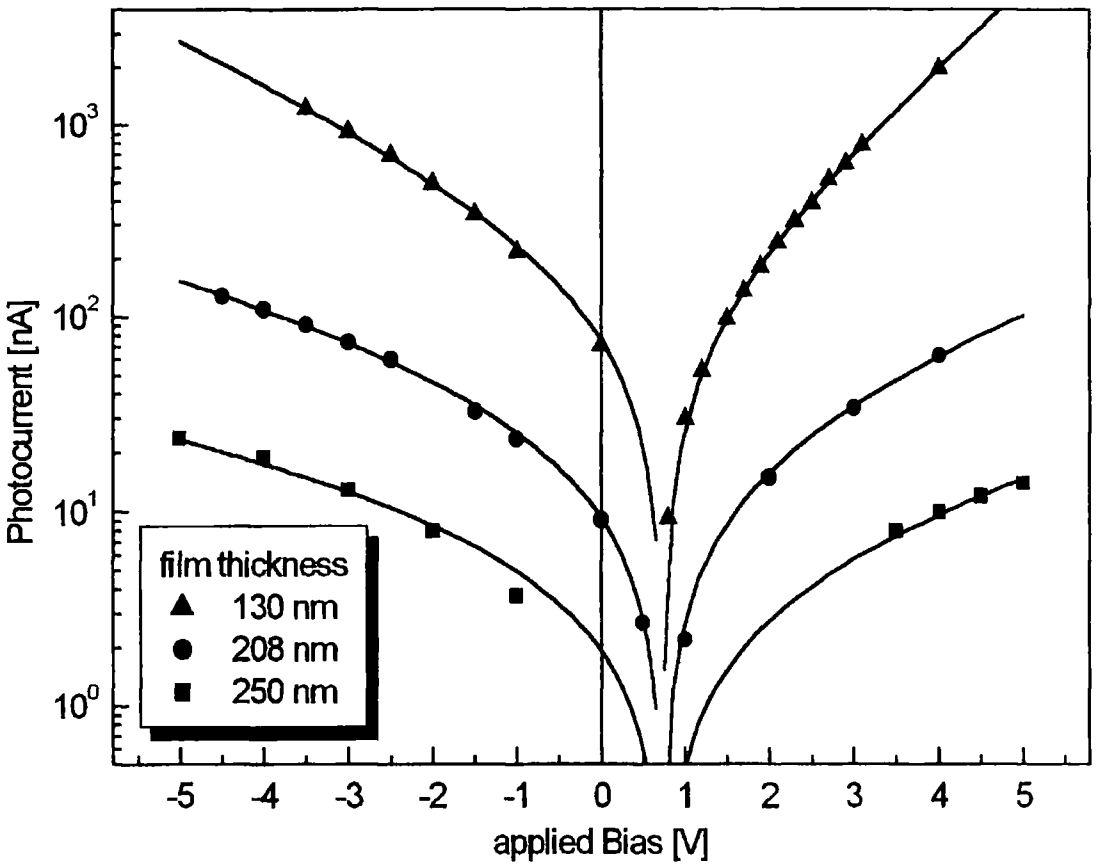

Figure 4. 30 Bias dependence of the photocurrent in three PPY films of different thickness. PPY was sandwiched between ITO and semitransparent aluminium. The solid lines are a guide for the eye, obtained from an exponential fit, taking into account more high voltage data points than depicted. Illumination was through the ITO contact using a photon energy of 3.0 eV.

4.3.2 Discussion

Comparing the four photocurrent spectra in Figure 4. 25 and Figure 4. 26 obtained from using different directions for illumination and applied bias, it can be seen that illumination trough the negative electrode (cathode) results in a photocurrent response that follows the absorption spectrum as expected for photogeneration of charger carriers inside the polymer. When illumination is through the anode it appears that only the light that can pass through the bulk of the material without being significantly absorbed is able to generate a current. This effect, known as the internal filter effect, is responsible for the antibatic response. This is supported by the transmittence measurements, which show that little light with photon energy

near the absorption maximum reaches the polymer regions at the back electrode. Note that the maximum of the antibatic peak was still smaller than the symbatic photocurrent at the same photon energy. It is assumed for the moment that no carrier injection from the electrodes occurs, which will be shown later. In this case the spectral behaviour of the photocurrent indicates that charge carriers are photogenerated inside the polymer near the cathode. With this result, information about the relative mobilities of the charge carriers in PPY can be found. Figure 4. 31 shows the Fermi levels of the electrodes and the relevant energy levels of PPY obtained from UPS data[39] for ITO(+)/PPY/Au(-) structure under forward bias.

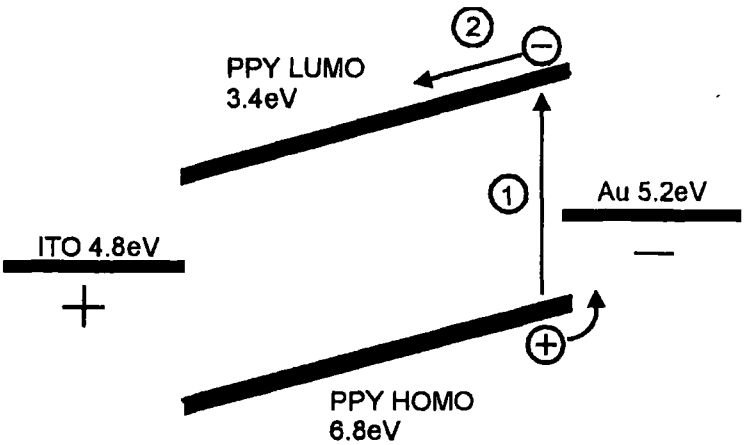

Figure 4. 31 Band structure of an ITO/PPY/Au sandwich cell under forward bias. The energy levels of PPY are estimated from UPS data (Ref.[39]). Process 1 represents the photogeneration of bound electron-hole pairs and process 2 the separation of electron and hole into the conduction and valence band followed by the diffusion of the electron towards the anode.

Charge carriers generated near the cathode (Au) can dissociate with the electron travelling through the bulk of the PPY layer towards the anode (ITO) and the hole being collected by the cathode. On the other hand, carriers generated near the anode can only contribute to a photocurrent if holes are able to move through the bulk of the polymer. The experiment shows this process to be suppressed in PPY, which must be due to a low hole mobility in PPY. The same argument is applicable for the reverse biased cell (Figure 4. 26). In this configuration the photogeneration occurs at the ITO electrode and the symbatic and antibatic response with respect to the illumination direction is reversed. These results, although a mirror image, are consistent with observations of the internal filter effect in p-type conducting

polymers.[69,32] For example, the poly(phenylenevinyline) derivative MEH-PPV, which is believed to be a good hole conductor with low electron mobility, shows symbatic behaviour for illumination through the anode, while illumination through the cathode results in an antibatic response.

The non-Arrhenius-like temperature dependence of the photocurrent is typical for films of some 100 nm thickness only. Following the proposal of Moses *et al.*[33] this weak temperature dependence indicates that the average distance the electrons can travel before becoming trapped is of the order of the film thickness and that therefore the photocurrent in such thin films is not restricted by trapping processes but by the much weaker temperature dependent process of carrier generation. This is consistent with the observation that the photocurrent strongly decreases when using thicker PPY films indicating that electrons are likely to become trapped on their way to the anode. Hence, in thin film it is possible to directly address the charge carrier generation process.

Now, the bias dependence of the photocurrent is considered. The vanishing of the signal at 0.74 V is due to the compensation of a reverse built-in potential i.e. the difference in work function between the electrode materials ITO and aluminium in agreement with the results of Malliaras *et al.*[70] Defining an effective bias as the sum of the built-in potential and the external applied bias a symmetric behaviour is obtained for the effective forward and reverse bias response. With the different work-functions of ITO and aluminium in mind this is a first indication of the absence of carrier injection from the electrodes over a Schottky barrier or via tunnelling. A fit to a Schockley equation of the type $j \propto \exp(U/nkT)$, with U the applied bias, results in diode quality factors $n = 40...100$, which provides further evidence against carrier injection. In addition, carrier injection processes are known to be temperature activated[24,71], which is in contradiction to the experimental results. A photocurrent determined by the Frenkel-Pool effect, the photoemission of trapped charge carriers, should also show strong temperature dependence[72] and can therefore also ruled out. In the following, a model that was recently proposed by Albrecht, Barth and Bassler[34,9] is applied to explain the field and temperature dependence of the photocurrent in PPY. The model describes the photocurrent as originating from the dissociation of germinate electron hole pairs in a random hopping system under the

influence of an electric field that is composed of the effective external field and the Coulomb fields created by the two charges. Such electron hole pairs arise from thermalised excitons, which are photogenerated by the incident light. Using Monte Carlo simulation techniques, which include the structural disorder that is known to be present in conjugated polymers, Albrecht and Bassler could successfully model the experimental results of photocurrent measurements on thin films. Two main results were pointed out : First, the field dependence of φ_b, the exciton dissociation yield obtained from normalising the photocurrent to the number of absorbed photons, follows the predictions of Onsager's theory. Second, disorder in conjugated polymers aids germinate pair dissociation and leads to a non-Arrhenius-like temperature dependence of φ_b in contradiction to Onsager's theory.

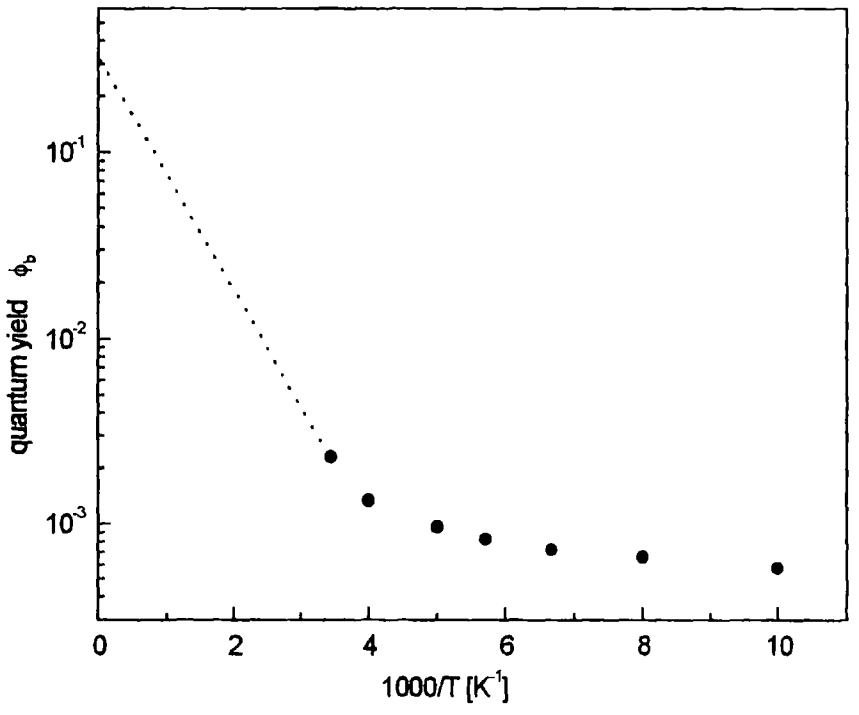

Figure 4. 32 Arrhenius-plot for the temperature dependence of the dissociation quantum yield, which was obtained by normalising the photocurrent to the number of absorbed photons. A PPY film of 200 nm thickness was used. The extrapolation $T \rightarrow \infty$ yields the primary dissociation yield $\varphi_{b,0}$. Illumination was through the ITO contact using a photon energy of 3.0 eV.

The temperature dependence of the exciton dissociation yield φ_b is depicted in Figure 4. 32 φ_b and can be understood as the product of the primary dissociation yield $\varphi_{b,0}$ and the quantum yield φ_{esc}, which describes the probability of the generated electron hole pair to escape germinate recombination. In the limit $T \to \infty$ the escape quantum yield is assumed to become unity, which means $\varphi_b(T \to \infty) = \varphi_{b,0}$. The experimental data for PPY yield a primary dissociation yield of $\varphi_{b,0} = 0.2$, upper and lower bound being 0.1 and 0.4, respectively. The high error level indicates that the accurate determination of the high temperature asymptote is rather difficult, however, the accuracy of $\varphi_{b,0}$ only weakly effects the further analysis. Taking $\varphi_{b,0} = 0.2$ the escape quantum yield $\varphi_{esc} = \varphi_b/\varphi_{b,0}$ can be derived and its field dependence is depicted in Fig. 7 in a log-log plot.

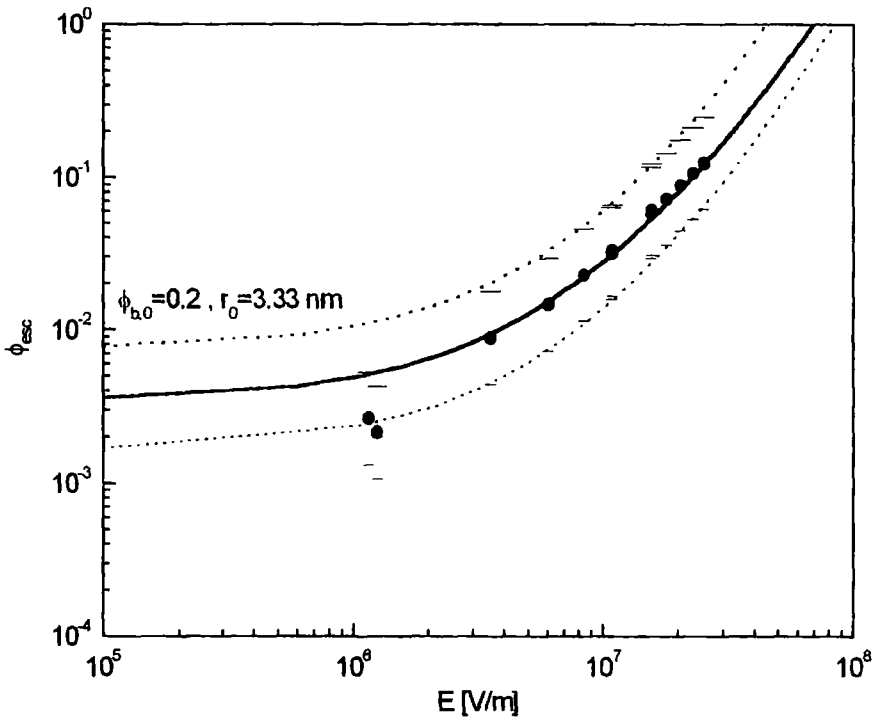

Figure 4. 33 Field dependence of the escape quantum yield ϕ_{esc} including upper and lower error levels. The solid line represents Onsager's theory after the application of an approximation by Pai and Enck (Ref.[35]) using an initial pair distance r_0=3.33 nm and ε=3. Dotted lines represent Onsager's theory corresponding to the upper and lower error levels yielding r_0=3.86 nm and 2.94 nm, respectively.

In order to compare the results with Onsager's theory of germinate pair dissociation an approximation by Pai and Enck[35] is used, which allows the calculation of φ_{esc} as a function of applied electric field for a given initial electron-hole distance r_0. Using ε=2.5 from ellipsometry measurements[38] the experimental data for PPY are found to fit to such a curve if r_0=3.33 nm is chosen. Following the proposal of Barth and Bassler this initial intra-pair distance translates into an apparent exciton binding of $E_b = 0.14\,eV \pm 0.02\,eV$. For the maximum possible value $\varphi_{b,0} = 1$ one still obtains E_b=0.19 eV. The measurements have been carried out at photon energies in the low energy tail of the absorption (2.9eV) so that corrections due to the wavelength dependence of the quantum yield should not significantly effect the results. Note that the fit of the experimental data for φ_{esc} to the theoretical Onsager curve is more accurate than one might first think. Since line-shape *and* absolute value of φ_{esc} depend on only one parameter, r_0, a good fit to such a curve provides strong indication that the underlying mechanism can be satisfactorily described by this theory. The obtained value for E_b might still be an underestimation of the real exciton binding energy because the charge generation zone is found to be confined to a zone near the cathode, which can possibly further assist exciton dissociation by collecting holes. However, the value E_b=0.14 eV is about one order of magnitude higher the kT at room temperature, which favours the exciton model of correlated electron-hole pairs as a description of the first allowed excited state. The exciton binding energy found for PPY compares well with recent results of poly(p-phenylenevinylene) derivatives. A combination of electroabsorption and internal photoemission measurements carried out by Campbell *et al.*[10] reports an exciton binding energy of 0.2 eV and values of 0.3-0.4 eV have been obtained applying Onsager's theory[9] and by Scanning Tunnelling Microscopy[14]. On the other hand, values below kT at room temperature (25 meV) were concluded from picosecond transient photoconductivity measurements[12] and from measurements on light emitting electrochemical cells[73], which is in contrast to the results of PPY. Also, exciton binding energies near 1 eV can be found in the literature,[50,13] one magnitude higher then the value obtained for PPY.

The strong increase of the photocurrent in the high-energy part of the spectrum can not be correlated to a feature in the absorption spectra of PPY. Such behaviour of the photocurrent in the UV has also been observed in poly(p-phenylene vinylene) (PPV) and its derivative MEH-PPV by Koehler and co-workers[74,75]. These authors assigned the large UV photocurrent to originate from transitions from delocalised occupied molecular orbitals to localised unoccupied molecular orbitals or vice versa. However, the large photocurrent peaks are observed at photon energies where the polymers have small absorption peaks, whilst no feature is visible in the absorption spectrum of PPY in the region of the photocurrent rise. A possible explanation for the strong increase of the photocurrent in the high-energy part of the spectrum is the dissociation of unrelaxed excited states. Such hot excitons could be responsible for the unsymmetrical broadening of the absorption spectrum at photon energies of about 4 eV and should have a far smaller exciton binding energy. As a result a threshold-like photocurrent can be found corresponding to an interband transition from the valence to the conduction band of the polymer. Further experimental work in the field and temperature dependence of the UV-photocurrent is necessary to obtain more information about this component.

4.4 Electroabsorption and Photocurrent in some PPY derivatives

4.4.1 Absorption and Electroabsorption in CSW 25.2

The polymers with the name CSW were synthesised by Dr. C. S. Wang[76] and have induced some interest because of their luminescent properties. These polymers are easy to process since they are soluble in formic acid or chloroform, which allow deposition on suitable substrates by spin-coating.

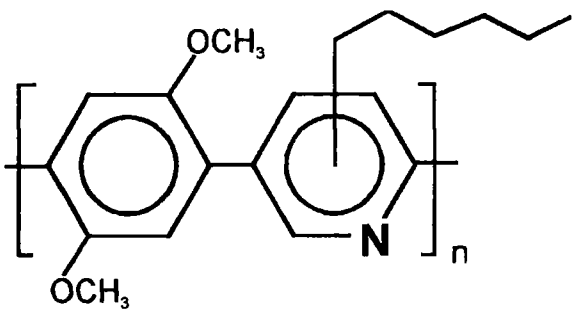

Figure 4. 34 CSW 25.2

The chemical structure of CSW 25.2 is depicted in Figure 4. 34, it was dissolved in formic acid using a concentration of 20 mg per ml, for example, and spun onto quartz substrates with a spin velocity of 2000 rpm. The absorption spectrum was measured in region from the visible blue into the deep UV and the result is depicted in Figure 4. 35. The spectrum consists of three clearly pronounced peaks at 3.57 eV, 4.38 eV and 6.08 eV. At the moment little is know about this polymer, but when compared with the absorption spectrum of PPY one might suppose that the first two peaks refer to one-photon allowed transition to different electronic states, which arise from the two aromatic rings of the repeat unit. In the low energy tale of the last peak another feature can be observed at about 5.1 eV.

Figure 4. 35 shows also the low-temperature absorption spectrum and compares it with the curve recorded at room temperature. Similar to the results of PPY no significant change of height, width or energy position of the peaks is found. However, there is a small difference between the two curves, which must be attributed to the less accurate corrections, since the reference beam is not available when the spectrometer is used with the cryostat mounted inside.

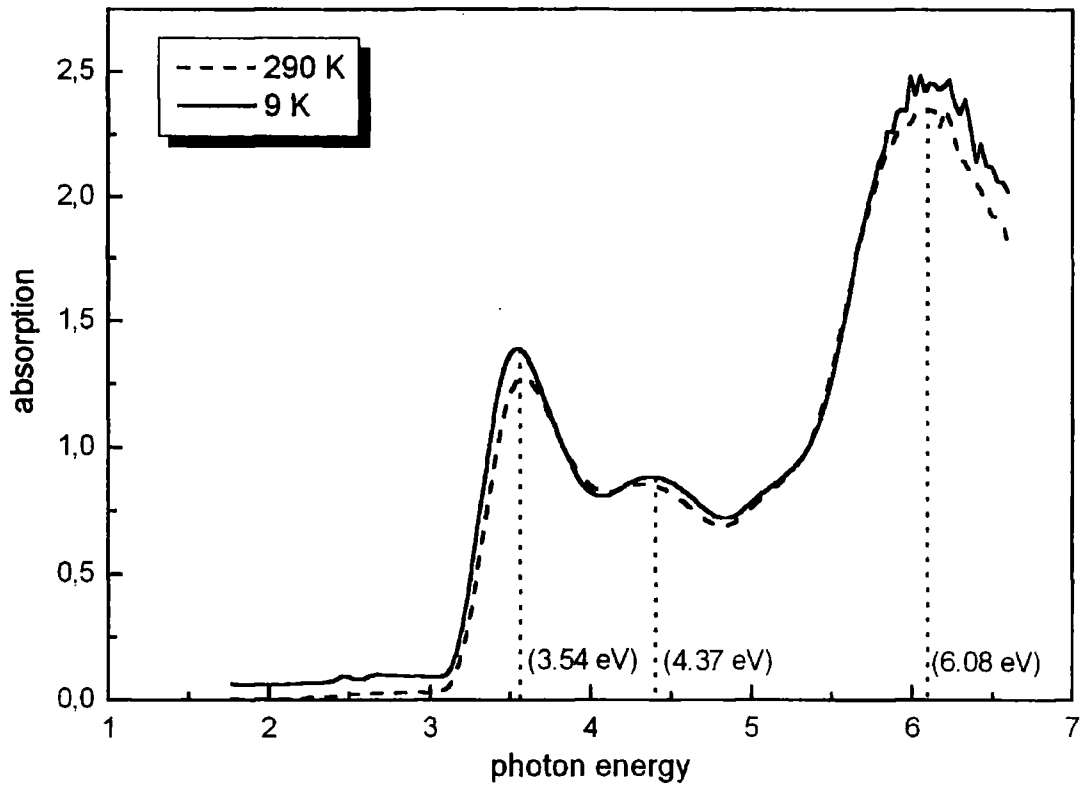

Figure 4. 35 Absorption spectrum of a thin film of CSW 25.2 at a temperature of 10K (solid line) and at room temperature (dotted line).

The electroabsorption signal of CSW25.2 was found to be one order of magnitude smaller then in PPY. Therefore a sufficiently long lock-in time constant (10 seconds) in combination with a settling time of 40 seconds was used to obtain reliable data points. Figure 4. 36 shows the electroabsorption spectrum of CSW25.2 in the region of the first two optical allowed transitions. In first approximation the curve resembles a sinusoidal function with a maximum at 3.32 eV, a minimum at 3.72 eV and a further maximum at 4.25 eV. Thereby the first two features are symmetric with respect to $\Delta T / T = 0$, which is different from the PPY results. With the least square fitting program (see Appendix I) the electroabsorption spectrum was fitted to a linear combination of the absorption spectrum and its first and second energy derivative according to eq. 2. 3. As it can be seen in Figure 4. 36 the EA-signal is very well described by such a linear combination over the whole spectral range of the experiment and the following fitting equation was determined:

$$\Delta\alpha\ (E) = -3.12\times10^{-6}\alpha(E) + 3.07\times10^{-6}\frac{d\alpha(E)}{dE} + 1.20\times10^{-8}\frac{d^2\alpha(E)}{dE^2}.$$

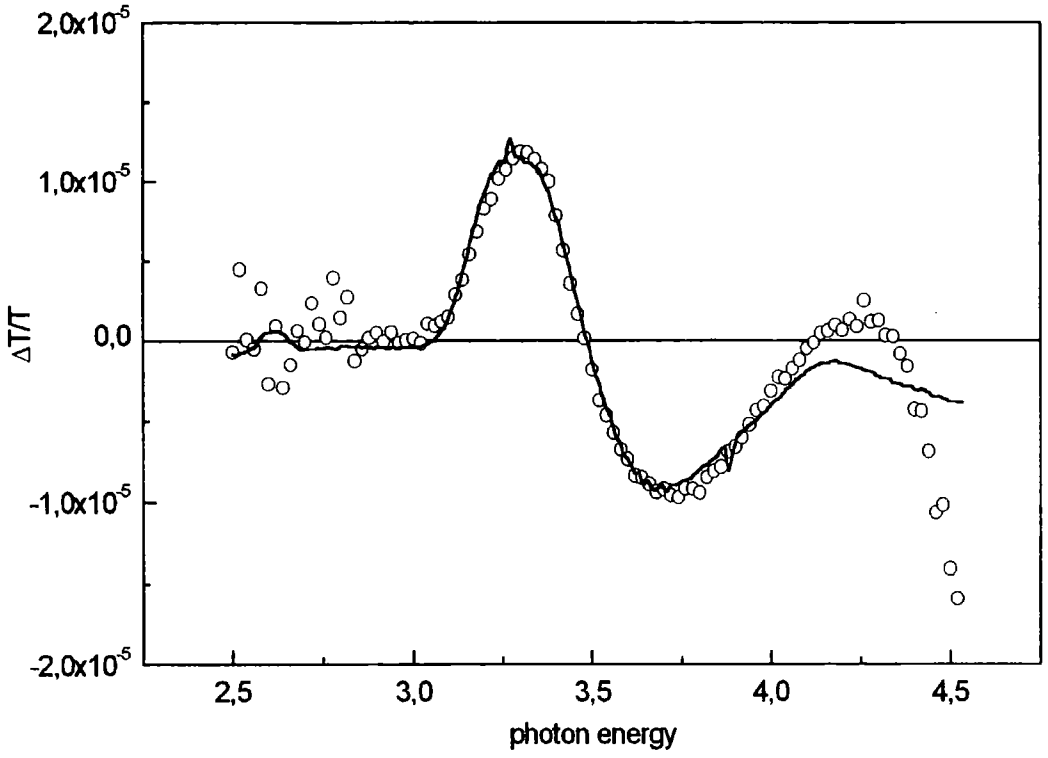

Figure 4. 36 Electroabsorption spectrum of CSW25.2 in planar configuration (circles) measured with an applied electric field of 62.5 kV/cm. The sample was kept under vacuum and at a temperature of 10 K. The solid line represents a fit with a linearcombination of the absorption spectrum and its first and second derivative.

From this equation and from Figure 4. 36 it is obvious that, again, the EA-spectrum is mainly described by the first derivative of the absorption spectrum indicating a non-linear Stark shift. There is also a very small contribution of the second derivative suggesting the presence of charge transfer excitons as described for PPY in section 4.1.5. The contribution of the zeroth derivative was considered to arise from the shift of oscillator strength to a one-photon forbidden energy state that becomes allowed in the presence of the symmetry breaking electric field. While for PPY such a new transition emerged in the high-energy part of the EA-spectrum indicated by a deviation of the experimental curve from the fit, no such feature can be observed in the CSW spectrum. The transition is therefore expected to be at a photon energy above 4.5 eV, outside the range of the experiment. However, the obtained linear

coefficients allow the calculation of the average change in polarisibility upon transition from the ground state to the excited state $\langle \Delta\tilde{\alpha} \rangle$ and the difference between ground and excited state dipole moment $\langle \Delta \mathbf{p} \rangle$ as specific constants characterising the excited state in CSW25.2:

$$\langle \Delta\tilde{\alpha} \rangle = 0.25 \times 10^{-37}\ \mathrm{Cm/(V/m)}$$
$$\langle \Delta \mathbf{p} \rangle = 0.4 \times 10^{-29}\ \mathrm{Cm} = 1.2\mathrm{D}$$

Both values are significantly lower then the corresponding values found for PPY, which suggest that the excited state in CSW25.2 is less delocalised. This would imply a shorter conjugation length in this derivative, which is consistent with the observation that the absorption bands of the first allowed optical transitions occurs at higher photon energies then in PPY.

4.4.2 Absorption and Electroabsorption in CSW67

The chemical structure of CSW67 is depicted in Figure 4. 37. The polymer can not be considered as a derivative of PPY but has also attracted some interest for possible applications in multi-layer light emitting diodes. This is mainly induced by its strong photoluminescence in the visible blue[77] in conjunction with good processing possibilities (soluble in chloroform and processible in air).

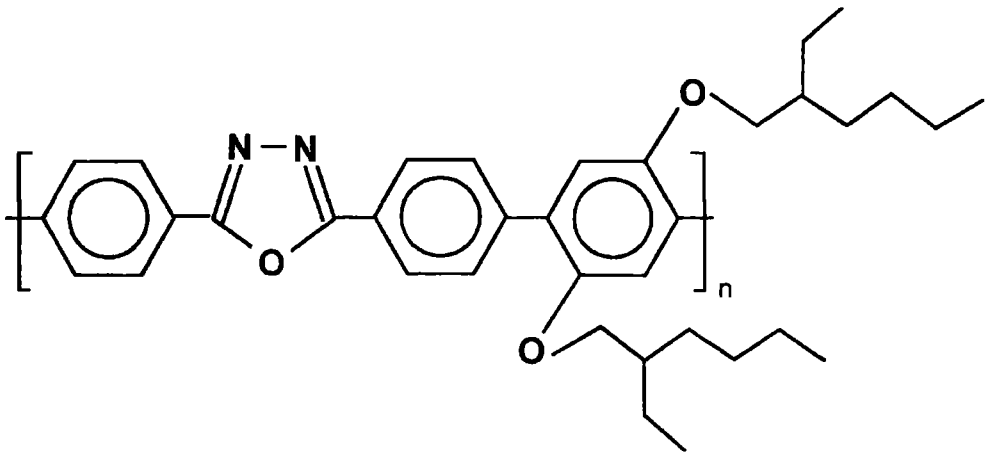

Figure 4. 37 Chemical structure of CSW67.

The repeat unit of CSW67 consists of an 1,3,4 oxadiazole ring situated between two benzene rings and another benzene ring, which is linked to two polyacetylene fragments (Figure 4. 37). The oxadiazole is considered to be responsible for the luminescence properties of CSW67 - this five-membered ring is well know as the fluorescent component in textiles and other artificial materials.[78]

Thin films were processed on quartz substrates by spin-casting from a chloroform solution. Using different concentrations (10 to 20 mg/ml) and spinning conditions (1000 to 2000 rpm) four films of different thickness were produced. To obtain the absorption coefficient and its spectral dependence the absorption of the four films was measured with the lambda19 absorption spectrometer and the α-step thickness meter was used to determine their thickness (Inset of Figure 4. 38).

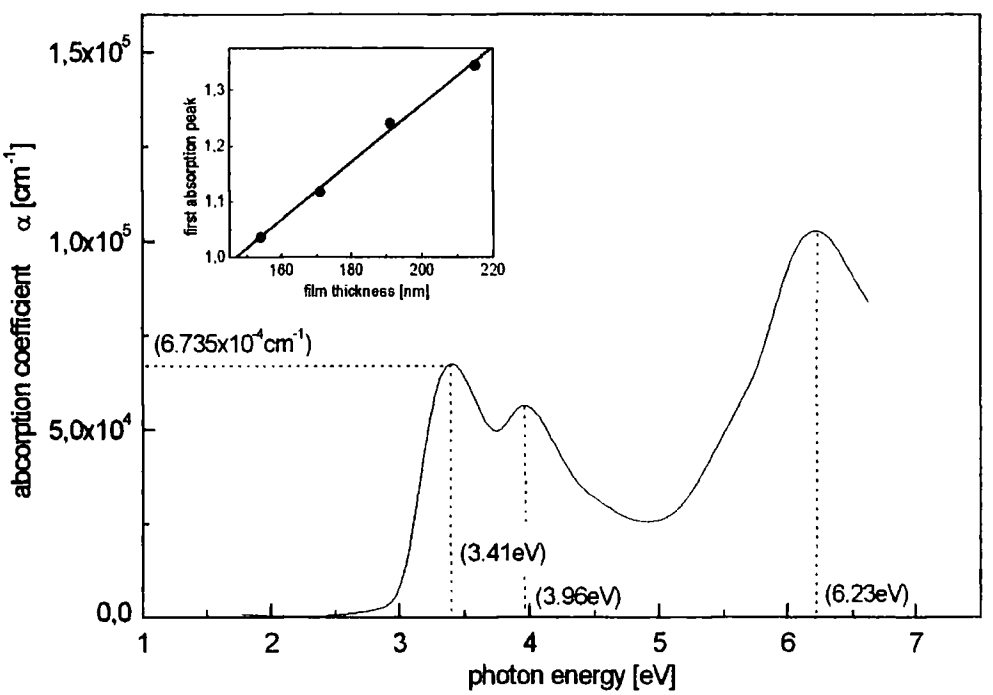

Figure 4. 38 Spectral dependence of the absorption coefficient valid for CSW67 films with absorption in the region of about 1. The inset shows the absorption of four films of CSW67 versus their thickness. The incident light had a photon energy of 3.4 eV

A linear fit yields:

$$d \cdot \alpha = 0.25 + \left(5.13 \times 10^{-3}\,\mathrm{nm}^{-1}\right) \cdot d,$$

where d denotes the film thickness. The equation contains an offset, which means that there must be a deviation from the linear behaviour in thinner films, since $\alpha=0$ for $d=0$ must be obeyed. However, for films with an absorption of about 1 the absorption coefficient depicted in Figure 4. 38 can be assumed.

Similar to the spectrum of CSW25.2 the absorption of CSW67 shows a double feature in the low-energy region (3.41 eV and 3.96 eV) and comes to another peak in the deep UV (6.23 eV), which interestingly coincides with the absorption peak of isolated oxadiazole molecules.[78] At the maximum of the first peak the absorption coefficient is $6.7 \times 10^{-4} cm^{-1}$.

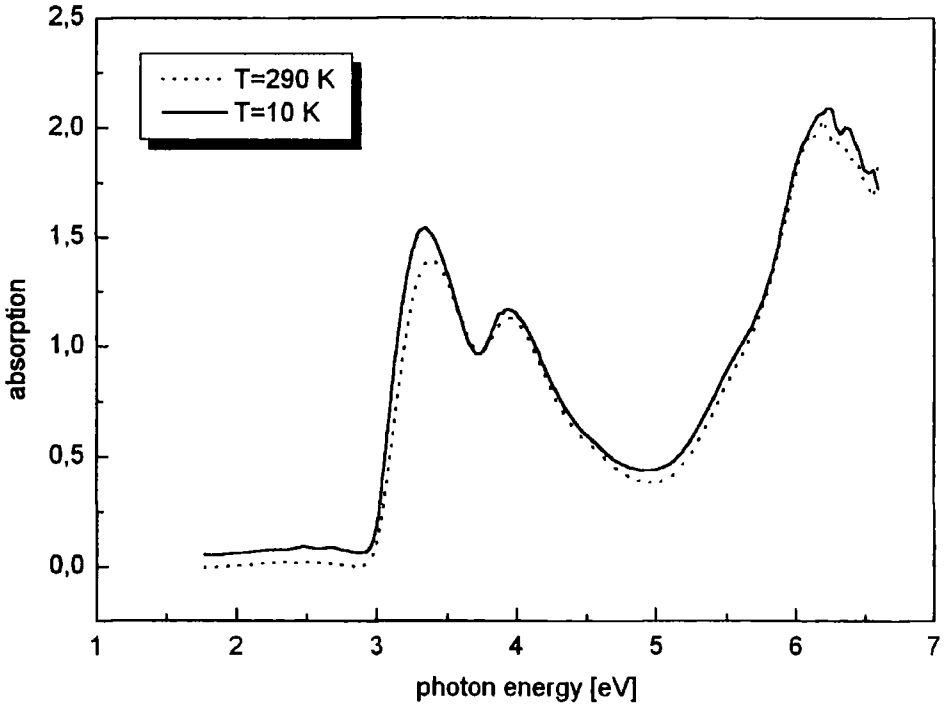

Figure 4. 39 Temperature dependence of the absorption spectrum of CSW67.

Figure 4. 39 shows the low energy absorption spectrum of CSW67 recorded at 10K. Again, no significant change can be observed indicating the stability of the electronic states with respect to temperature similar to the results of PPY and CSW25.5.

The electroabsorption spectrum is depicted as symbols in Figure 4. 40 for an CSW67 film of about 200 nm thickness. The curve performs nearly two complete oscillations symmetric to $\Delta T/T = 0$ with decreasing amplitude in the order of magnitude of the EA-signal in PPY. When compared to the absorption spectrum

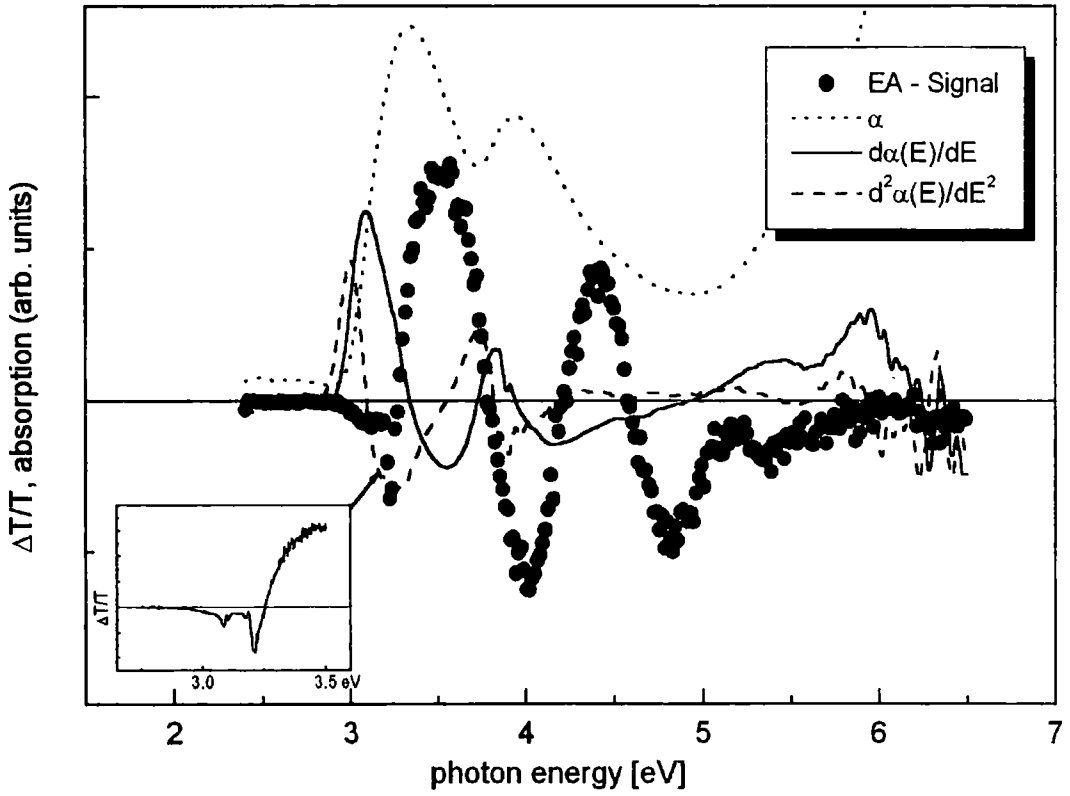

Figure 4. 40 Electroabsorption spectrum of CSW67 (circles) and the absorption spectrum (dotted line) with the first (solid line) and second (dashed line) derivative.

and its first and second derivative (dashed lines in Figure 4. 40) CSW67 shows an intriguing behaviour: None of the three curves resembles the line-shape of the EA-signal and the least square fitting program is not able to provide an acceptable approximation either. Bearing in mind the apparent universality of the Fourier development in eq. 2. 3 it must be admitted that the electroabsorption behaviour of CSW67 is completely unclear at the moment. Another interesting feature of unknown origin in the EA-spectrum is the small, negative peak at 3.2 eV, which is confirmed in a later experiment with very high spectral resolution and time constants (inset of Figure 4. 40).

4.4.3 Photocurrent in CSW67

Photocurrent measurements were performed on ITO/CSW67/Al sandwich cells. First a very thin film (<100 nm) was used, which was processed by spinning from a 14 mg/ml solution with 1500 rpm. The absorption of this film at the first allowed transition was below 0.6, which means that the layer was well illuminated for every photon energy and no internal filter effect is expected. Consequently the photocurrent spectrum shows symbatic behaviour regardless which direction for the applied bias was chosen (Figure 4. 41).

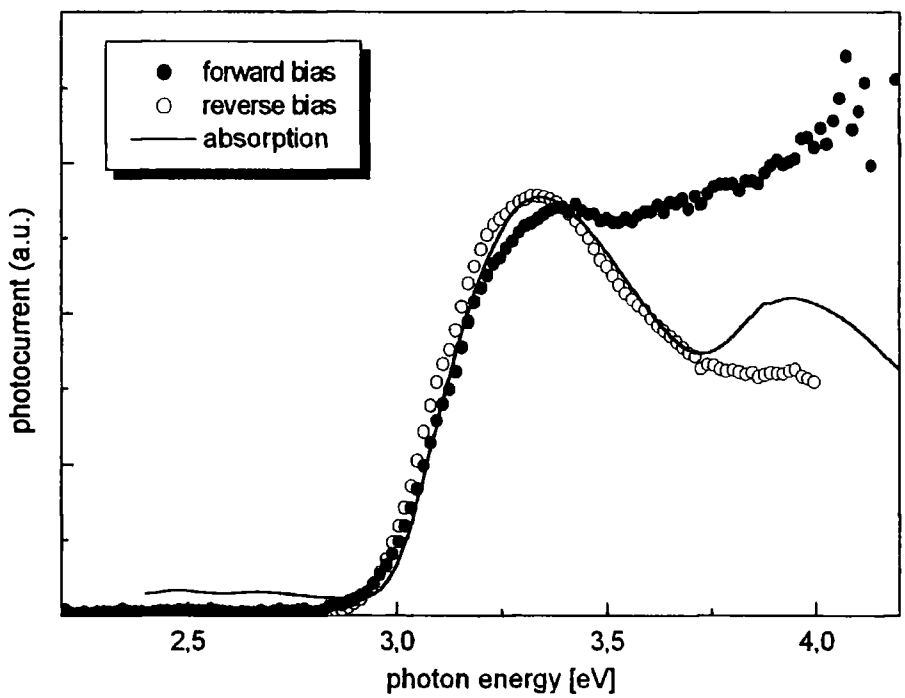

Figure 4. 41 Photocurrent spectrum of a thin film (<100 nm) of CSW67 sandwiched between ITO and aluminum measured with an applied bias of at +1.2 V and –1 V, respectively.

Forward and reverse spectra closely match the absorption signal and especially for reverse bias the curves are almost identical. This favours homogeneous bulk photogeneration with a wavelength independent generation yield. To provide further support for this interpretation the photocurrent was measured using a CSW67-layer of about 200 nm thickness with an absorption in the region of 2 at the first allowed

transition. Figure 4. 42 shows the four spectra that were recorded using the different directions for the incident light and the applied bias. The four curves all show the same antibatic peak at 3.0 eV, which is clearly different to the PPY results.

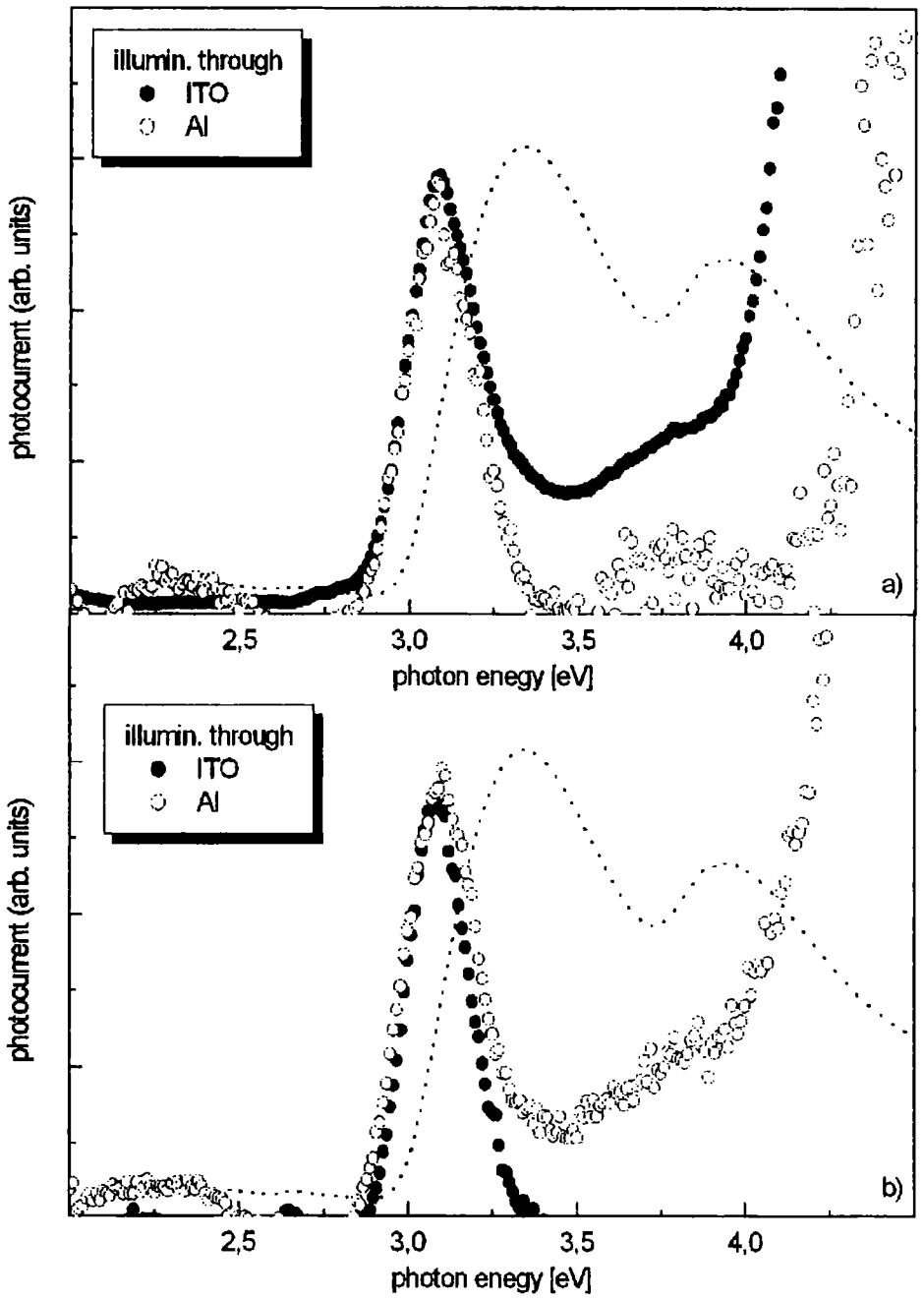

Figure 4. 42 Photocurrent spectra of ITO/CSW67/Al sandwich cells under a) forward bias and b) reverse bias. Illumination was through the ITO (filled circles) or through the semitransparent aluminium electrode (open circles).

The identity of all the spectra with respect to light and bias direction rules out any effects of charge carrier injection from the electrodes since even if both electrodes would have the same injection behaviour a symbatic response would be expected for all curves. In agreement with the results of the thin films the photocurrent in CSW67 is therefore attributed to bulk photogeneration. Analogous to the approach for PPY (section 4. 3) this high absorption of the 200 nm film at 3.3 eV leads to an absorption of such light in the first 10 to 50 nanometer of the film, which means that only a narrow zone close to the front electrode can serve as origin for the photogeneration of charge carriers. Therefore at the maximum of the absorption, at about 3.3 eV the photocurrent is strongly reduced leaving a well-pronounced antibatic peak at 3.0 eV, where the absorption is small enough to ensure illumination of the hole layer.

As an important conclusion information about the mobility of the charge carriers in CSW67 can be obtained. If one type of carrier, i.e. either electrons or holes, posses significantly higher mobility the photogeneration must occur at the electrode, which attracts the less mobile type. In conjunction with an internal filter effect this would imply characteristic symbatic and antibatic features depending on the direction of light and applied bias (see section 4. 3). The consequent antibatic behaviour of the photocurrent in CSW67 is therefore considered as an indication that electron mobility and hole mobility are rather similar in this polymer.

5 Conclusions and Prospects

This work reports the results and analysis of the first electroabsorption and photocurrent measurements on poly(2,5-pyridinediyl), a conjugated, luminescence polymer. Although both experimental methods are usually considered separately, motivation to compare their results is obvious since they investigate the same physical phenomenon, the excited electronic states of a material. *In both experiments the excited states are exposed to an electric field and the response of these states to the field is investigated.* While the electroabsorption determines the nonlinear optical response, the photoconductivity is a result of direct and indirect generation of free charges from the excited states. In particular, in the electroabsorption experiment it could be found that in the presence of an electric field the oscillator strength (the intensity) of the transition to the first excited state is reduced in favour of a new transition that becomes weakly allowed. In addition, it was revealed that a shift of the energy of the first excited state occurs in PPY, which is mainly due to a change in polarisibility compared to the ground state. The quantitative analysis of the EA-data led to the picture, that the first excited state can be described as a neutral Frenkel exciton. On the other hand, in the photocurrent experiment the electric field was found to lead to a dissociation of the excited states into free charge carriers, electrons and holes, which give rise to a current across a normally insulating PPY-film. The application of Onsager's theory provided a good fit to the experimental data demonstrating again that these original excited states are bound excitons. The formation of Frenkel excitons as the dominating excited species is therefore confirmed in both experiments. Bearing in mind the simple chemical structure of PPY a presentable degree of universality for conjugated polymers in general can be expected from this as well as from most of the other results obtained.

However, PPY posses some unique properties that promise some good opportunities for the application of this polymer in the field of PLED's. In this respect this work gave conclusive evidence for the electron transporting,

semiconducting properties of PPY and confirmed its rigid-rod-like and high crystalline nature by a different experimental approach.

This theses has presented a comprehensive investigation into the absorption-, electroabsorption- and photocurrent behaviour of the first excited states in poly(2,5-pyridinediyl). In other conjugated polymers, which show similar optical excitation spectra these states are believed to be responsible for most of the electro-optical properties like luminescence and photocurrent. On the other hand, another energy state of very high oscillator strength is clearly recognised (see absorption spectra) in the deep UV at 6.3 eV. Moreover, in the photocurrent spectra strong increase of the signal in the UV was found and there were also inklings of additional UV-features in the electroabsorption spectra[79]. An extension of the spectrometer to enable measurements at very high photon energies is therefore expected to provide crucial insigth into the nature of the high-energy state. Since similar UV-states and their behaviour were also reported for other important conjugated polymers with still controversial interpretations of their origin, such investigations could be a further valuable contribution for a better understanding of the photophysics of these materials.

6 Appendix – Details of the Created Software

6.1 EAfit.pas: Analysis of Electroabsorption Data

The Turbo Pascal program Eafit.pas was created to fit an electroabsorption spectrum to a linear combination of the corresponding absorption spectrum and its first and second derivative according to eq. 2. 3, which has the form:

$$\Delta\alpha(E) = l_1\alpha(E) + l_2\alpha'(E) + l_3\alpha''(E)$$

The experimental data for $\Delta\alpha(E), \alpha(E), \alpha'(E)$ and $\Delta\alpha''(E)$ must be provided in four single ASC-files, which must contain two columns, the first for the energy and the second for the corresponding value. The two data points in each line of the files have to be separated by a tabulator character and the files must not have a header. All four files must be identical with respect to the energy column, i.e. all curves must have the same start and end energy and the same constant energy step.

To find the linear coefficients l_1, l_2, and l_3 the program solves the following system of equations[80]:

$$\int \Delta\alpha\alpha dE = l_1 \int \alpha^2 dE + l_2 \int \alpha\alpha' dE + l_3 \int \alpha\alpha'' dE$$
$$\int \Delta\alpha\alpha' dE = l_1 \int \alpha\alpha' dE + l_2 \int \alpha'^2 dE + l_3 \int \alpha'\alpha'' dE$$
$$\int \Delta\alpha\alpha'' dE = l_1 \int \alpha\alpha'' dE + l_2 \int \alpha'\alpha'' dE + l_3 \int \alpha''^2 dE$$

where the integrals refer to the summation over the whole spectral range. The system has the form of a matrix equation $\mathbf{b} = \mathbf{A} \circ \mathbf{l}$, with $\mathbf{l} = (l_1, l_2, l_3)$ the vector of the linear coefficients and this vector can by calculated by inversion of the matrix **A**: $\mathbf{l} = \mathbf{A}^{-1} \circ \mathbf{b}$.

During the execution of the program the experimental data and the fitting curve are displayed along with the linear coefficients, the variance and the number of data points currently taken into account. Using the arrow keys the latter number can be increased, while the program instantly displays the results on the screen. The program can be finished by pressing the 'escape'-key.

6.2 Kramers.pas: Kramer-Kronig Transformation of Electroabsorption Data

The program Kramers.pas derives the field-induced change of the real part of the complex refractive index from the field-induced change of absorption via a Kramers-Kronig-relation (see section 4.1.5). For that the integral

$$\Delta n(\omega) = \frac{c}{\pi} P \int_0^{\infty} \frac{\Delta\alpha(\omega')}{\omega'^2 - \omega^2} d\omega'$$

is calculated for every $\omega = E/\hbar$. The electroabsorption spectrum must be supplied as a tab-spaced, two-column ASC-file without header and with the photon energy (not ω) in the first column and the EA-data in the second column. The calculated curve for $n(\omega)$ will be stored in a different file of the same format.

6.3 Photo.pas: Device Controlling and Data Recording in the Photocurrent Experiment

The program Photo.pas was written to control the data transfer between the electronic components of the photocurrent experiment and the PC. The devices were connected using the IEEE standard interface and the computer was equipped with an IEEE card plus Pascal unit to provide the interface between the hardware and the programming language. Another unit, tm300.tpu, was adopted, which declares the commands *gotowv* and *slit* to operate the monochromator.

The main menu allows four choices, *Manual measurement, DC photocurrent spectrum, Time resolved Photocurrent* and *Exit program.* A friendly graphical enviroment includes easy movement between all objects using arrow keys and changing of options by highlighting and <Enter>-pressing. The part *Manual measurement* is used to set up the experiment, to find the optimal experimental conditions and to do all current-measurements that can not be done with one of the other program points. It continuously reads and displays the current that flows across the sample and allows the online-change of photon energy, light intensity (slit width)

and applied bias. The part *DC photocurrent spectrum* records the photocurrent spectrum and it starts with a form wherein the following parameter can be set up :

BIAS	applied Bias in Volts
Start energy	start photon energy of the spectrum in eV
End energy	end photon energy of the spectrum in eV
Energy step	energy step in eV
Settling time	time waited after setting each energy step before data are read (in ms)
Numb. of readings	number of readings at every energy to average for noise reduction
Time betw. readings	time between the noise reduction readings in ms
Entrance slit width	
Filename of spectrum	max. 8 characters, no file extension

After selecting *run spectrum* the user is asked to block the beam to allow the measurement of the darkcurrent. Then the spectrum is recorded and the read data are displayed graphically and as numbers at any time during the measurement. Thereby the plot is rescaled automatically whenever necessary to ensure good visibility. This sophisticated output of the contemporary readings is of obvious advantage for such time-consuming measurement on very sensitive and sometimes unstable samples.

In the last part of the program the time behaviour of the photocurrent can be investigated. Since the time steps are generated by the computer the minimum interval is 1 millisecond. The program is therefore not able detect a prospective fast component of a photocurrent but allows an estimate of the stability of a steady state signal. The parameter that can be changed for the time resolved measurement have the same meaning as in the program point *DC photocurrent spectrum*, apart from the option *number of readings*, which refers to serial readings with an time interval of *time betw. readings*

7 Acknowledgements

The work contained in this thesis has been performed since 1st of October 1998 in the Organic Electric Materials group at the Department of Physics, University Durham. At this point I want to thank all the people who have supported me during my time in Durham and who have made this work possible. My thanks therefore go to

- my supervisor, Dr. Andy P. Monkman, for organizing my MSc course, for his guidance and encouragement and for his understanding concerning my extended stays in Germany,
- my wife Cornelia for unlimited love and support and for understanding at some lonely evenings, which I had to spend with the spectrometer rather then with her,
- my parents for great support in every kind and throughout my education making our stay in Durham possible at all and my parents in law and the rest of our family for love, support and help,
- my relatives Mr. and Mrs. Pivowarczyk for their big support helping to make sure that we had everything we need in England,
- my foundation, the Dr.-Carl-Duisberg-Stiftung, Bayer AG, Leverkusen, Germany, for granting my study and covering my tuition fees,
- Lockhard E. Horsburgh and Chang S. Wang for providing high-quality polymers,
- Anna K. Sheridan and John Lupton for practical introductions and many help with the techniques of the production of polymer films and devices, for providing results of photoluminescence and transport measurements, for many useful discussions and for helping me to quickly find my way about in a foreign country.
- Phil Wood for help with least-square problems and very reliable computer knowledge,
- all the other members of our group as well as Dr. I. D. W. Samuel and all members of the Journal Club for useful discussions and stimulations and for contributing to a pleasant and relaxed atmosphere,
- Norman Thompson, David Patterson and all workers of the workshops for reliable and uncomplicated help with all technical things.

September 1999, Frank Feller

8 References

Publications arising from work presented in this thesis :

- *Electroabsorption Spectroscopy on Poly(2,5-pyridinediyl)*
  F. Feller and A. P. Monkman, *Physical Review B* **60**, 8111 (1999)

- *Photocurrent in an Electron Transporting Luminescent Polymer*
  F. Feller and A. P. Monkman, Applied Physics Letters (accepted for publication)

- *Photoconductivity in Poly(2,5-pyridinediyl)*
  F. Feller, C. W. Sitch and A. P. Monkman, (submitted)

- *Absorption and Electroabsorption on an Oriented Film of a Conjugated Polymer*
  F. Feller and A. P. Monkman, (in progress)

- *Optical Excitations in Novel Luminescent Conjugated Polymer*
  F. Feller, C. S. Wang and A. P. Monkman, (in progress)

---

[1] J. H. Burroughes, D. D. C. Bradley, A. R. Brown, R. N. Marks, K. Mackay, R. H. Friend, P. L. Burns, and A. B. Holmes, *Nature* **347**, 539-541 (1990).
[2] R. Scharf, *Physikalische Blaetter* **55**, 37 (1999)
[3] a) B. E. Kohler and I. D. W. Samuel, *Journal of Chemical Physics* **103**, 5248 (1995); b) M. L. Shand, R. R. Chance, M. L. Postollec and M. Schott, *Physical Review B* **25**, 4431 (1982); c) H. Meier, U. Stalmach and H. Kolshorn, *Acta Polymer* **48**, 379 (1997)
[4] W. P. Su, J. R. Schrieffer and A. J. Heeger, *Physical Review Letters* **42**, 1698 (1979)
[5] S. R. Peierls, *Quantum Theory of Solids*, (1955)
[6] W. P. Su in *Handbook of Conducting Polymers*, T. A. Skotheim, Marcel Dekker Inc., New York, 1986, pg. 757
[7] R. R. Chance in *Handbook of Conducting Polymers*, T. A. Skotheim, Marcel Dekker Inc., New York, 1986, pg. 852
[8] M. Pope and C. E. Swenberg, *Electronic Processes in Organic Crystals*, New York, 1982, pg. 71
[9] S. Barth and H. Bassler, *Physical Review Letters* **79**, 4445-4448 (1997).
[10] I. H. Campbell, T. W. Hagler, D. L. Smith, and J. P. Ferraris, *Physical Review Letters* **76**, 1900-1903 (1996)
[11] Z. Shuai, S. K. Pati, W. P. Su, J. L. Bredas, and S. Ramasesha, *Physical Review B* **55**, 15368-15371 (1997)
[12] C. H. Lee, G. Yu, D. Moses and A. J. Heeger, *Physical Review B* **49**, 2396 (1994)
[13] J. M. Leng, S. Jeglinski, X. Wei, R. E. Benner and Z. V. Vardeny, *Physical Review Letters* **72**, 156 (1994)
[14] S. F. Alvarado, P. F. Seidler, D. G. Lidzey, and D. D. C. Bradley, *Physical Review Letters* **81**, 1082-1085 (1998)
[15] P. Gomes da Costa and E. M. Conwell, *Physical Review B* **48**, 1993 (1993)
[16] H. Haken and H. C. Wolf, *Molecular Physics and Elements of Quantum Chemistry*, Springer-Verlag Berlin Heidelberg, 1992, pg. 252
[17] F. Engelke, *Aufbau der Moleküle*, Teubner Studienbücher : Chemie, Stuttgart, 1985

[18] A. P. Monkman in *Molecular Electronics*, Taunton, Somerset: Research Studies Press New York, Wiley, 1992, Fig. 7.11
[19] G. Weiser and A. Horvath, *Chemical Physics* **227** 153 (1997)
[20] M. Liess, S. Jeglinski, Z. V. Vardeny, M. Ozaki, K. Yoshino, Y. Ding, and T. Barton, *Physical Review B* **56**, 15712 (1997)
[21] Guo, S. Mazumdar, S. N. Dixit, F. Kajzar, F. Jarka, Y. Kawabe, and N. Peyghambarian, *Physical Review B* **48**, 1433 (1993)
[22] F. Rohlfing and D. D. C. Bradley, *Chemical Physics* **227**, 133 (1998)
[23] L. Sebastian, G. Weiser, and H. Bassler, *Chemical Physics* **61**, 447 (1981)
[24] S. Barth, H. Bassler, H. Rost, and H. H. Horhold, *Physical Review B* **56**, 3844-3851 (1997)
[25] H. Bleier, S. Roth, Y. Q. Shen, D. Schäfer-Siebert and G. Leising, *Physical Review B* **38**, 6031 (1988)
[26] A. J. Campbell, M. S. Weaver, D. G. Lidzey and D. D. C. Bradley, *Journal of Applied Physics* **84**, 6737 (1998)
[27] J. J. M. Halls, K. Pichler, R. H. Friend, and S. C. Moratti, *Synthetic Metals* **77**, 277-280 (1996)
[28] B. Dulieu, J. Wery, S. Lefrant, and J. Bullot, *Physical Review B* **57**, 9118-9127 (1998)
[29] I. D. Parker, Journal *Of Applied Physics* **75**, 1656-1666 (1994)
[30] D. Braun and A. J. Heeger, *Applied Physics Letters* **58**, 1982 (1991)
[31] L. Onsager, *Physical Review B* **54**, 554 (1938)
[32] M. G. Harrison, J. Gruner, and G. C. W. Spencer, *Physical Review B* **55**, 7831-7849 (1997)
[33] D. Moses, J. Wang, G. Yu, and A. J. Heeger, *Physical Review Letters* **80**, 2685-2688 (1998)
[34] U. Albrecht and H. Bassler, *Chemical Physics Letters* **235**, 389-393 (1995)
[35] D. M. Pai and R. C. Enck, *Physical Review B* **11**, 5163 (1975)
[36] A. P. Monkman, M. Halim, S. Dailey, I. D. W. Samuel, M. Sluch, and L. E. Horsburgh, *SPIE Proceedings* **82**, 3148 (1997)
[37] T. Yamamoto, T. Maruyama, Z. H. Zhou, T. Ito, T. Fukuda, Y. Yoneda, F. Begum, T. Ikeda, S. Sasaki, H. Takezoe, A. Fukuda, and K. Kubota, *Journal Of the American Chemical Society* **116**, 4832-4845 (1994)
[38] A. P. Monkman, L. E. Horsburgh, M. E. Vaschetto, P. D. Hatton, H. D. Burrows, W. Brown, and L. Pettersson, *SPIE Proceedings*, 1999 (to be published)
[39] T. Miyamae, D. Yoshimura, H. Ishii, Y. Ouchi, K. Saki, T. Miyazaki, T. Koike, and T. Yamamoto, *Journal Of Chemical Physics* **103**, 2738-2744 (1995)
[40] J. W. Blatchford, S. W. Jessen, L.-B. Lin, T. L. Gustafson, D.-K. Fu, H.-L. Wang, T. M. Swager, A. G. MacDiarmid and A. J. Epstein, *Physical Review B* **54**, 9180 (1996)
[41] J. W. Blatchford, S. W. Jessen, L. B. Lin, J. J. Lih, T. L. Gustafson, A. J. Epstein, D. K. Fu, M. J. Marsella, T. M. Swager, A. G. MacDiarmid, S. Yamaguchi and H. Hamaguchi, *Physical Review Letters* **76**, 1513 (1996)
[42] J. W. Blatchford, T. L. Gustafson, A. J. Epstein, *Journal of Chemical Physics* **105**, 9214 (1996)
[43] L. E. Horsburgh, A. P. Monkman and I. D. W. Samuel , *Synthetic Metals* **101**, 113 (1999)
[44] M. Halim, I. D. W. Samuel, E. Rebourt and A. P. Monkman, *Synthetic Metals* **84**, 951 (1997)
[45] S. Dailey, M. Halim, E. Rebourt, L. E. Horsburgh, I. D. W. Samuel, and A. P. Monkman, *Journal of Physics-Condensed Matter* **10**, 5171-5178 (1998)
[46] D. D. Gebler, Y. Z. Wang, J. W. Blatchford, S. W. Jessen, L. B. Lin, T. L. Gustafson, H. L. Wang, T. M. Swager, A. G. Macdiarmid and A. J. Epstein, *Journal of Applied Physics* **78**, 4264 (1995)
[47] A. P. Monkman, M. Halim, I. D. W. Samuel, and L. E. Horsburgh, *Journal of Chemical Physics* **109**, 10372 (1998)
[48] S. Pomfret, *PhD Thesis University Durham*, 1998
[49] M. Liess, S. Jeglinski, Z. V. Vardeny, M. Ozaki, K. Yoshino, Y. Ding, and T. Barton, *Physical Review B* **56**, 15712-15724 (1997)
[50] S. J. Martin, H. Mellor, D. D. C. Bradley, and P. L. Burn, *Optical Materials* **9**, 88-93 (1998)
[51] S. J. Martin, D. D. C. Bradley, P. A. Lane, H. Mellor and P. L. Burn, *Physical Review B* **59**, 15133 (1999)
[52] T. W. Hagler, K. Pakbaz and A. J. Heeger, *Physical Review B* **51**, 14199 (1995)

[53] latest results of the OEM-group of the University Durham show a small degree of radial order of the PPY chains in spin cast films. However, this order is only weakly pronounced and the comparable large electrode area accumulates any possible direction of the individual chains.
[54] F. Rohlfing and D. D. C. Bradley, *Chemical Physics* **227**, 133-151 (1998)
[55] S. J. Pomfret, A. P. Monkman and E. E. Havinga *Synthetic Metals* **78**, 285 (1996)
[56] A. Horvath, G. Weiser, G. L. Baker, and S. Etemad, *Physical Review B* 51, 2751(1995)
[57] A. Horvath, H. Bassler, and G. Weiser, *Phys. Status Solidi B* 173, 755 (1992)
[58] S. D. Philips, R. Worland, G. Yu, T. Hagler, R.Freedman, Y. Cao, V. Yoon, J.Chiang, W. C. Walker, and A. J. Heeger, *Physical Review B*, 40, 9751 (1989)
[59] C. Botta, G. Zhuo, O. M. Gelsen, D. D. C. Bradley, and A. Musco, *Synth. Met.* 55-57, 85-90 (1993)
[60] G. Leising, *Physical Review B* **38**, 10313 (1988)
[61] O. M. Gelsen, D. D. C. Bradley, H. Murata, N. Takada, T. Tsutsui, and S. Saito, *Journal Of Applied Physics* **71**, 1064-1069 (1992)
[62] S. J. Martin, O. M. Gelsen, D. D. C. Bradley, and C. Botta, *Mol. Cryst. Liq. Cryst.* **256**, 591 (1994)
[63] S. J. Pomfret, E. Rebourt, L. Abell, and A. P. Monkman, *Synth. Met.* **84**, 729 (1997)
[64] S. Jeglinski, Z. V. Vardeny, Y. Ding, and T. Barton, *Mol. Cryst. Liq. Cryst.* **256**, 87 (1994)
[65] F. Feller and A. P. Monkman, *Physical Review B* **60**, 8111 (1999)
[66] T. Danno, J. Kürti and H. Kuzmany, *Physical Review B* **43**, 4809 (1991)
[67] S. Luzzati, P. Elmino and A. Bolognesi, *Synthetic Metals* **76**, 23 (1996)
[68] T. W. Hagler, K. Pakbaz, K. F. Voss, and A. J. Heeger, *Physical Review B* **44**, 8652-8666 (1991)
[69] A. Kohler, H. F. Wittmann, R. H. Friend, and M. I. Khan, *Synthetic Metals* **67**, 245-249 (1994)
[70] G. G. Malliaras, J. R. Salem, P. J. Brock, and J. C. Scott, *Journal Of Applied Physics* **84**, 1583-1587 (1998)
[71] M. S. Roy, G. D. Sharma and S. G. Sangodkar, *Synthetic Metals* **81**, 15 (1996)
[72] D. Ghosh, S. Hazra, P. Pal, and T. N. Misra, *Journal Of Materials Science* **27**, 4184-4188 (1992)
[73] G. Yu, Y. Yang, Y. Cao, Q. Pei, C. Zhang, and A. J. Heeger, *Chemical Physics Letters* **259**, 465-468 (1996)
[74] A. Kohler, D. A. DosSantos, D. Beljonne, Z. Shuai, J. L. Bredas, R. H. Friend, S. C. Moratti, and A. B. Holmes, *Synthetic Metals* **84**, 675-676 (1997)
[75] A. Kohler, D. A. dosSantos, D. Beljonne, Z. Shuai, J. L. Bredas, A. B. Holmes, A. Kraus, K. Mullen, and R. H. Friend, *Nature* **392**, 903-906 (1998)
[76] C. S. Wang *et al.*, *Advanced Materials* (to be published)
[77] thanks to A. K. Sheridan, Department of Physics, University Durham, for providing results of photoluminescence measurements on CSW67
[78] A. R. Katritzky, *Comprehensive Heterocyclic Chemistry* Vol 3, Pergamon Press, 1984, chapter 4. 3
[79] the electroabsorption behaviour in deep UV is not presented in this theses since a high noise level due to limitations of the spectrometer did not allow reliable statements. However, the observations gave inklings for the presence of at least one further feature.
[80] C. L. Lawson and R. J. Hanson, *Solving Least Square Problems*, SIAM, 1995